Bulletin of the Seismological Society of America

Ground Motion Model for crustal events in Italy by applying the Multi-Source Geographically Weighted Regression (MS-GWR) method

--Manuscript Draft--

Manuscript Number:	BSSA-D-21-00044R3
Article Type:	Article
Section/Category:	Regular Issue
Full Title:	Ground Motion Model for crustal events in Italy by applying the Multi-Source Geographically Weighted Regression (MS-GWR) method
Corresponding Author:	Giovanni Lanzano, Ph.D. Istituto Nazionale di Geofisica e Vulcanologia Milan, ITALY
Corresponding Author's Institution:	Istituto Nazionale di Geofisica e Vulcanologia
Corresponding Author E-Mail:	giovanni.lanzano@ingv.it
Order of Authors:	Giovanni Lanzano, Ph.D.
	Sara Sgobba
	Luca Caramenti
	Alessandra Menafoglio
Abstract:	In this paper, we implement a new approach to calibrate Ground Motion Models (GMMs) characterized by spatially varying coefficients, using the calibration dataset of an existing GMM for crustal events in Italy. The model is developed in the methodological framework of the Multi-Source Geographically-Weighted Regression (MS-GWR, Caramenti et al. 2020), which extends the theory of multiple linear regression to the case where the model coefficients are spatially varying, thus allowing to capture the multiple sources of non-stationarity in ground motion related to event and station locations. In this way, we reach the aim of regionalizing the ground motion in Italy ultimately specializing the model in a non-ergodic framework. Such an attempt of regionalization also addresses the purpose to capture the regional propagation effects in the modelling, which is a need for the Italian country, where attenuation properties vary significantly across space. As the proposed model relies on the ITA18 (Lanzano et al., 2019) dataset and functional form, it could be considered as the ITA18 non-stationary version, thus allowing one to predict peak ground acceleration and velocity, as well as 36 ordinates of the 5%-damped acceleration response spectra in the period interval T=0.01-10s. The resulting MS-GWR model shows an improved ability to predict the ground motion locally, compared to stationary ITA18, leading to a significant reduction of the total variability at all periods, of about 15-20%. The paper also provides scenario-dependent uncertainties associated to the median predictions, to be used as a part of the epistemic uncertainty in the context of probabilistic seismic hazard analyses. Results show that the approach is promising to improve the model predictions especially on densely sampled areas, although further studies are necessary to resolve the observed trade-off inherent to site and path effects, which limits their physical interpretation.
Author Comments:	
Suggested Reviewers:	Carmine Galasso c.galasso@ucl.ac.uk
	Nicolas Kuehn UCLA kuehn@ucla.edu
	Peter Stafford Imperial College London p.stafford@imperial.ac.uk
Opposed Reviewers:	

Response to Reviewers:	
Additional Information:	
Question	**Response**
Key Point #1: <i>Three key points will be printed at the front of your manuscript so readers can get a quick overview. Please provide three COMPLETE sentences addressing the following: 1) state the problem you are addressing in a FULL sentence; 2) state your main conclusion(s) in a FULL sentence; and 3) state the broader implications of your findings in a FULL sentence. Each point must be 110 characters or less (including spaces).	The final goal is to assess an empirical ground motion model with spatially varying coefficients in Italy
Key Point #2:	The spatially varying model is able to more accurately predict the ground motion than a stationary model
Key Point #3:	The proposed model can be used to improve the PSHA estimates and the shaking maps

Ground Motion Model for crustal events in Italy by applying the Multi-Source Geographically Weighted Regression (MS-GWR) method

Authors: *Giovanni Lanzano[1], Sara Sgobba, Luca Caramenti, Alessandra Menafoglio*

[1]corresponding author, email: giovanni.lanzano@ingv.it

The authors acknowledge there are no conflicts of interest recorded.

Abstract:

In this paper, we implement a new approach to calibrate Ground Motion Models (GMMs) characterized by spatially varying coefficients, using the calibration dataset of an existing GMM for crustal events in Italy. The model is developed in the methodological framework of the Multi-Source Geographically-Weighted Regression (MS-GWR, Caramenti et al. 2020), which extends the theory of multiple linear regression to the case where the model coefficients are spatially varying, thus allowing to capture the multiple sources of non-stationarity in ground motion related to event and station locations. In this way, we reach the aim of regionalizing the ground motion in Italy, specializing the model in a non-ergodic framework. Such an attempt of regionalization also addresses the purpose to capture the regional effects in the modelling, which is a need for the Italian country, where ground-motion properties vary significantly across space. As the proposed model relies on the ITA18 (Lanzano et al., 2019) dataset and functional form, it could be considered as the ITA18 non-stationary version, thus allowing one to predict peak ground acceleration and velocity, as well as 36 ordinates of the 5%-damped acceleration response spectra in the period interval T=0.01-10s. The resulting MS-GWR model shows an improved ability to predict the ground motion locally, compared to stationary ITA18, leading to a significant reduction of the total variability at all periods, of about 15-20%. The paper also provides scenario-dependent uncertainties associated to the median predictions, to be used as a part of the epistemic uncertainty in the context of probabilistic seismic hazard analyses. Results show that the approach is promising to improve the model predictions especially on densely sampled areas, although further studies are necessary to resolve the observed trade-off inherent to site and path effects, which limits their physical interpretation.

1. Introduction

Ground Motion Models (GMM) are basic tools for the prediction of the seismic parameters adopted in many applications in engineering and seismology fields, such as the assessment of probabilistic and deterministic seismic hazard analysis and the definition of shaking scenarios. Basically, GMMs estimate the conditional distribution of the ground-motion parameters (median and associated standard deviation) given some explanatory variables, such as magnitude, distance, fault mechanism, proxies for site effects and other parameters. GMMs are commonly defined through closed-form and reproducible prediction equations, where several coefficients are derived by empirical regressions of strong motion parameters computed from datasets of recordings.

Before the 2000s, GMMs were mainly derived for relatively small areas where sufficient seismic records were available, such as California and Japan (see *Data and Resources* for the list of GMMs; a critical review of empirical GMMs can be found in Douglas & Edwards, 2016). These models were generally calibrated on datasets composed mainly of analog records of strong events. Although they often showed relatively small standard deviations, some strong motion parameters, such as long-period spectral acceleration ordinates, were poorly predicted, especially wherever suffering from waveforms filtering at low frequencies (Boore and Bommer, 2005). In Italy, the first GMM of Sabetta & Pugliese (1987,1996) represented the basis of the Italian seismic hazard map published in 2004 (MPS04, Stucchi et al. 2011).

Later on, the general trend in engineering seismology was to calibrate global GMMs encompassing very large areas over the continents, such as the pan-European GMMs (*e.g.*, Bindi et al. 2014; Akkar et al. 2014). These global GMMs are typically based on the hypothesis of ergodicity, meaning that the distribution of ground motions over time at a given site is the same as their spatial distribution over all sites for the same magnitude, distance, and site condition (Anderson and Brune, 1999). Ergodic models thus provide shaking predictions even in areas where data are scarcely available, allowing the development of seismic hazard maps for vast areas (*e.g.,* SHARE model, Woessner et al. 2015).

However, such an attempt to model the ground motion globally, caused a general increment of the standard deviations, as a result of the inclusion of earthquakes originating from different shallow active crustal regions, even from lower seismicity areas. Moreover, the absence of a proper regionalization in some models, results in predictions strongly influenced by the most sampled regions, *e.g.,* the model by Cauzzi et al. (2015) which is Japan-biased and the model by Bindi et al. (2014) which is Italy-biased.

The regionalization was introduced for the first time in the NGA-West2 project (Bozorgnia et al. 2014), where several global GMMs included regional corrective factors for site effects, mainly in terms of scaling with the shear-wave velocity, averaged in the uppermost 30 meters ($V_{S,30}$), and anelastic attenuation in California, Taiwan, Japan, China and Italy (Abrahamson et al. 2014; Boore et al. 2014; Chiou and Youngs, 2014). Similar approaches were also carried out in Europe and Middle-East by Kotha et al. (2016, 2020), by including the regional dependence of apparent anelastic attenuation terms.

More recently, site-specific seismic hazard analyses for critical infrastructures (*e.g.,* the PEGASOS study: Probabilistic Seismic Hazard Analysis for Swiss Nuclear Power Plant Sites) also showed that the ergodic approach leads to particularly severe estimates of the design spectral amplitudes, especially for longer return periods that are strongly affected by the standard deviation of the model (Cramer, 2003; Bazzurro and Cornell, 2004). To allow more accurate predictions of seismic motion and to reduce the associated variability, some methods have been introduced to move ergodic models into partially or totally non-ergodic models (Al Atik et al. 2010). In the practice, this goal is achieved by decomposing the model residuals into event and site terms (Rodriguez-Marek et al. 2011; Luzi et al. 2014), and more rarely also in source and path terms (Lin et al. 2011; Villani and Abrahamson, 2015; Lanzano et al. 2017), through the application of mixed-effects regression techniques (Stafford, 2014). In this way, the systematic sources of ground motion variability are recognized and accounted for as epistemic uncertainties, while reducing the aleatory component. Nevertheless, such corrections and the resulting reduction in variability are only beneficial for sites where seismic stations are installed, or for sources where significant earthquakes occurred.

In the last years, several efforts have been made to introduce the concepts of the geo-statistics into seismology with the aim to properly regionalize the ground motion and extend the benefits of the non-ergodic approach to sites where no records are available (Kuehn & Abrahamson, 2020; Schiappapietra & Douglas, 2020; Sgobba et al. 2019, 2021). The spatial regionalization is generally introduced in the ground motion modelling by means of two different approaches: 1) the first one consists in the calibration of spatial correlation models of the within-event residuals (Park et al., 2007; Goda and Atkinson, 2010; Esposito and Iervolino, 2012; Sokolov and Wenzel, 2011) and the repeatable site- and path- corrective terms (Anderson and Uchiyama, 2011; Sahakian et al., 2019; Kuehn and Abrahamson, 2020; Sgobba et al. 2019, 2021; Chao et al. 2020) to generate multiple realizations of ground-motion random fields; 2) the second way requires calibrating a model with spatially-variable regression coefficients, which provide a prediction model that is inherently non-ergodic (Landwehr et al., 2016). Considering that both the proposed approaches allow one to remove (fully or partially) the ergodic assumption, type #1 partially ignore regional variability of the median response while accounting for spatial correlation in the residuals; conversely type #2 accounts for regional variabilities of the median response while neglecting the possible correlation in its residuals.

In this paper, we propose a novel methodology to calibrate an empirical GMM of type #2, in which some coefficients of the model vary smoothly with geographical location, adopting an approach similar to that proposed by Landwehr et al. (2016). The method we apply is the Multi-Source Mixed Geographically Weighted Regression (MS-GWR), developed *ad-hoc* by Caramenti et al. (2020) for the Italian context. MS-GWR provides a methodological framework allowing one to effectively estimate and perform inference (testing, model selection) on a regression model characterized by spatially varying coefficients – the variability being induced by multiple sources of non-stationarity (site- and event- effects in the case of GMMs). Unlike the modeling approach of Landwehr et al (2016), MS-GWR does not require any strong distributional assumption on the model' residuals (e.g., Gaussianity), either for estimation or testing. The model is developed for shallow crustal events in Italy, employing the same dataset used by Lanzano et al. (2019) to calibrate a partially non-ergodic model (namely ITA18) with fixed coefficients (*i.e.*, spatial-stationarity).

In the following, the MS-GWR method and the GMM calibration are outlined, then some tests and application examples are reported to show performance and application potential of the proposed approach.

2. Dataset and functional form

The calibration dataset is the same originally derived by Lanzano et al. (2019) to calibrate the ground motion model ITA18 for shallow crustal earthquakes in Italy. Differently from the original dataset, we select only the data from Italy and neighboring countries (France, Swiss and Slovenia). This because the few data (14%) selected from other regions (Japan, California, Turkey, Greece, etc.), used by Lanzano et al. (2019) to extend the maximum magnitude of model validity, cannot be used for the application of the MS-GWR method in Italy. In total, the dataset is composed by 4,784 observations of 137 events from 925 stations, recorded between 1976 and 2016, with magnitudes ranging from 3.5 to 6.9. Additional details on the dataset selection are provided in Lanzano et al. (2019).

Figure 1a shows the source-to-station paths of the observations used for model calibration, pointing out that some areas are not well-sampled due to their lower seismicity, such as the western Lombardy, the eastern Piedmont, the Trentino and southern Tyrol region, the coastal area of Tuscany, the Salento peninsula and the south-western area of the Sicily. The magnitude–distance distribution is shown in Figure 1b: the number of near-source records with distances lower than 10 km is about 300, which is still relevant w.r.t. ITA18 original dataset.

The functional form presented by Lanzano et al. (2019) for ITA18 is:

$$log_{10}Y = a + b_1(M_w - M_h)\mathbb{I}(M_w \le M_h) + b_2(M_w - M_h)\mathbb{I}(M_w > M_h) + \left[c_1\left(M_w - M_{ref}\right) + c_2\right]log_{10}\sqrt{R_{JB}^2 + h^2} + c_3\sqrt{R_{JB}^2 + h^2} + k\left[log_{10}\left(\frac{V_{S,30}}{800}\right)\mathbb{I}\left(V_{S,30} \le 1500\right) + log_{10}\left(\frac{1500}{800}\right)\mathbb{I}\left(V_{S,30} > 1500\right)\right] + f_{SS}SoF_{SS} + f_{TF}SoF_{TF} + \varepsilon \qquad [1]$$

where, Y is the observed IM (Intensity Measures), *i.e.,* the peak ground acceleration and velocity (PGA and PGV) and 36 ordinates of acceleration response spectra at 5% damping (SA) in the period (T) range 0.01–10s. The prediction is valid for RotD50, which is the median of the distribution of the IMs, obtained from the combination of the two horizontal components across all non-redundant azimuths (Boore, 2010). The explanatory variables are the moment magnitude (M_W), the Joyner and Boore source-to-site distance (R_{JB}), the average seismic shear-wave velocity from the surface to 30 m ($V_{S,30}$) and the styles of faulting (SoF) which are dummy variables, introduced to specify strike-slip (SS) and reverse fault (TF), while for normal fault types (NF), the coefficient is zero (f_{NF}=0). The term ε is the remaining residual, *i.e.,* the logarithmic difference between observations and predictions.

In this analysis, we modify the original functional form in Eq. [1], by introducing some spatially varying coefficients:

$$log_{10}Y = a + b_1(M_w - M_h)\mathbb{I}(M_w \le M_h) + b_2(M_w - M_h)\mathbb{I}(M_w > M_h) + \left[c_1\left(M_w - M_{ref}\right) + c_2(t_e)\right]log_{10}\sqrt{R_{JB}^2 + h^2} + c_3(t_e)\sqrt{R_{JB}^2 + h^2} + k(t_s)\left[log_{10}\left(\frac{V_{S,30}}{800}\right)\mathbb{I}\left(V_{S,30} \le 1500\right) + log_{10}\left(\frac{1500}{800}\right)\mathbb{I}\left(V_{S,30} > 1500\right)\right] + f_1 SoF_1 + f_2 SoF_2 + \varepsilon \qquad [2]$$

where the ground-motion model is calibrated for the same IMs as in Lanzano et al. (2019). The coefficients for geometric spreading c_2 and anelastic attenuation c_3 are assumed dependent on the coordinates of the event t_e; the coefficient k of the linear scaling with $V_{S,30}$ is instead function of station coordinates, t_s. In the calibration of the MS-GWR model, we decide to model the spatial dependencies in the same way as done by Landwehr et al. (2016), so as not to overly modify the original functional form of ITA18. As a matter of fact, a better modeling of path effects through the coefficients c_2 and c_3 should include a dependence on both event and site coordinates. However, calibration of a local model depending on the four-dimensional vector of coordinates (t_e, t_s) would be hardly doable in practice, because this would require calibrating the model for all the local neighborhoods of (t_e, t_s) – *i.e.,* it would require a reasonably high amount of data around any combination of event- and site- coordinates (*i.e.*, curse of dimensionality).

Differently from the study of Landwehr et al. (2016), the offset is not modeled by introducing the spatial dependence on event and station locations, because MS-GWR was shown to be ineffective in assessing spatially varying offset (Caramenti et al., 2020). This issue may indirectly be solved through a random effect modeling (similarly as done in ITA18); however, regionalized regression models based on MS-GWR are yet to be developed and this will thus be the scope of future work.

In the next Section 3, we describe the general model and the estimation method used to calibrate model [2].

3. Method

The method we consider to calibrate model in Eq. [2] lies in the framework of Geographically Weighted Regression (GWR, Brunsdon et al., 1998), which extends the theory of multiple linear regression to the case where the model coefficients are spatially varying. Denoting by z_i the i-th observation of the response variable (the logarithm of the IM being considered when Eq. [2] is concerned) and by x_{ij}, $i = 1,2, \ldots$, the set of regressors relative to the i-th observation, the general model we aim to estimate is:

$$Z_i = \sum_{j \in C} \beta_{jC} x_{ij} + \sum_{j \in E} \beta_{jE}(t_{e,i}) x_{ij} + \sum_{j \in S} \beta_{jS}(t_{s,i}) x_{ij} + \epsilon_i \qquad [3]$$

where ϵ_i is a zero-mean random error (not necessarily Gaussian) with variance σ^2, $t_{e,i} = (u_{ei}, v_{ei})$, $t_{s,i} = (u_{si}, v_{si})$ denote the event- and site- coordinates, respectively, associated with the i-th observation, while *C,E* and *S* denote the set of regressors associated with the stationary coefficients (*C*), and the non-stationary coefficients (*E* and *S*), depending on event-coordinates (*E*) or site-coordinates (*S*). The difference between the model in Eq. [3] and that estimated by a standard GWR (Fotheringham et al., 2002) is twofold: (1) a set of coefficients (β_{jC}) is allowed to be spatially stationary, and (2) two different sources of spatial non-stationarity are allowed – *i.e.,* those induced by the spatial indexes t_e and t_s characterizing the sets *E* and *S* of regressors. The key differences between the model in Eq. [3] and that of Landwehr et al (2016) rely in (1) the parametric (Gaussian) assumptions made by these authors on the term ϵ_i, which is here avoided, and (2) on the nature of the coefficients $\beta's$. The latter are here assumed deterministic (and unknown), whereas they are modeled as Gaussian processes governed by coefficient-specific covariance kernels in Landwehr et al (2016) (consistent with the Bayesian approach there considered).

Following Caramenti et al (2020), to estimate the response Z_0 from MS-GWR model, for a target combination of event and site coordinates $t_{e0} = (\mathrm{u_{e0}}, \mathrm{v_{e0}})$, $t_{s0} = (\mathrm{u_{s0}}, \mathrm{v_{s0}})$ (hereafter named target location), and regressors $\mathrm{x_{0j}}$, we rely on two spatial kernels, $\mathrm{K_E}$ and $\mathrm{K_S}$, whose role is to localize the estimation of the model in a neighborhood of the target location, by down-weighting the contribution of the data observed at locations far apart from the target (resp. in terms of event- or site-coordinates). In this work, we consider as $\mathrm{K_E}$ and $\mathrm{K_S}$ two Gaussian kernels, with bandwidth set via generalized cross-validation (GCV). Any other kernel function could be used instead, with a potential impact on the degree of smoothness of the resulting estimates (the smoother the kernel, the smoother the estimates). It is worth noting that the kernels $\mathrm{K_E}$ and $\mathrm{K_S}$ do not represent coefficient-specific *covariance kernels* (used, *e.g.,* in Landwehr et al. 2016), but they rather determine the degree of locality of the regression model in Eq. [3]. Hereafter, when referring to the regionalized nature of the model we will either use the expression *spatial variability of the coefficients* or *non-stationarity*, precisely referring the non-constant nature of the β's. We will avoid the expression *spatial correlation* instead, to avoid confusion w.r.t. the model of Landwehr et al (2016), because the coefficients are here assumed to be deterministic (although unknown).

From the computational standpoint, given a target location, MS-GWR is based on an iterative procedure which estimates in cascade the three pieces of the model in Eq. [3]. First, the constant part is fitted, obtaining an estimate $\hat{\beta}_{\mathrm{jC}}$ of the coefficients β_{jC}. From this estimate, partial residuals are computed by difference as $\mathrm{Z_i} - \sum_{\mathrm{j \in C}} \hat{\beta}_{\mathrm{jC}} \mathrm{x_{ij}}$, and then used to estimate the second piece of the model, namely the spatially non-stationary term $\hat{\beta}_{\mathrm{jE}}$. This is done through GWR based on the spatial kernel $\mathrm{K_E}$ – which selects the relevant data in the neighborhood of the target event location, $\mathrm{t_{e0}}$. Having obtained $\hat{\beta}_{\mathrm{jE}}$, this is again used to obtain updated partial residuals, which are finally employed to estimate the second set of non-stationary coefficients. This last step is done again through GWR, but in the neighborhood of the site locations (thus using $\mathrm{K_S}$), eventually obtaining $\hat{\beta}_{\mathrm{jS}}$.

As we do not aim here to describe the mathematical and algorithmic details involved in the estimation of MS-GWR model, we limit to mention two key facts. First, from the algorithmic viewpoint, the cascade described above depends on the order chosen for the terms in Eq. [3]. The study of Caramenti et al. (2020) shows that estimating first the offset *a* leads to relevant improvements in terms of estimation accuracy and prediction power, with respect to any other estimation order. No substantial difference is instead implied by different estimation orders for the non-stationary terms. In practice, the evaluation of different choices of the order of estimate, as well as of the hyperparameters of the models (i.e., the kernel bandwidths), can be done via (generalized) cross-validation (GCV). Second, from the mathematical viewpoint, the estimation procedure can be reinterpreted as a linear estimation from the data, which greatly simplifies the estimation of the uncertainty associated with the model. Indeed, one can explicitly quantify the uncertainty in the coefficient estimation, as well as the prediction variance for a target location t_{e0}, t_{s0} and vector of regressors $\mathrm{x}_0 = (\mathrm{x}_{j0}, \mathrm{j} \in \mathrm{C} \cup \mathrm{E} \cup \mathrm{S})$.

The estimated variabilities associated with the regression and error terms can be used to quantify the epistemic and aleatory uncertainty in the model. Indeed, the aleatory variability is represented by the (spatially constant) variance σ^2 of the error term ϵ_{i}, whereas the epistemic uncertainty by the (spatially non-constant) variance of the estimator $\hat{\beta}_{\cdot,0}$. Note that the introduction of non-stationary terms in Eq. [3] allows one to move part of the aleatory variability of the model ITA18 to the regression terms, leading to a decrease in the variance of the error ($\sigma^2 < \sigma^2_{\mathrm{ITA18}}$). This entails an increase in the epistemic uncertainty associated with the model coefficients, due to the increased complexity of the GMM. However, the increase in data availability and knowledge allows for a reduction of this latter uncertainty, thus enabling one to decrease the overall uncertainty in the model.

We finally mention that the MS-GWR framework allows for a non-parametric inference on the model coefficients (in the sense of the distribution of the error term ϵ), based on a permutation approach (see Caramenti et al. (2020) for details and testing of the methods). Such setting enables one to perform model selection through hypothesis testing on the stationarity of the model coefficients (marginally or jointly on set of coefficients), as well as on their statistical significance. In this work, we do not focus on this aspect, as we rely on the results obtained by Caramenti et al. (2020) for PGA, based on the same dataset here considered. These authors run extensive inferential analyses which yielded the selection of model in Eq. [2], which is here calibrated for the 36 vibration periods being considered. The use of the same model for all the vibration periods is a standard practice in seismology (Douglas and Edwards, 2016), as it greatly simplifies the overall interpretability of the calibrated GMMs. Additional analyses run for other periods anyway confirmed that model selection in these cases can be consistently made as for PGA, the p-values (Wasserstein and Lazar, 2016) of the tests being similar to those obtained in Caramenti et al. (2020) (not shown).

4. Calibration results and comparison with ITA18

4.1 Stationary and spatially dependent coefficients

Following the approach proposed by Caramenti et. al (2020) for MS-GWR calibration, the kernel bandwidths were set to $h_E = 25km$ and $h_S = 75km$ for those associated with event and site coordinates, respectively, for periods up to 5s. For periods longer than 5 seconds the bandwidths were set to $h_E = 40km$ and $h_S = 80km$. Although spatially adaptive kernels could we used in principle, we prefer to keep a spatially constant kernel to reduce the number of hyperparameters of the model. The estimation order was set to *S*, *E* and *C*, consistent with GCV results. All the coefficients estimated for model in Eq. [2] are provided in the electronic supplements. In particular, the spatially varying coefficients are computed for an equally-spaced grid of 10km. All the coefficient tables are also available in a GitHub repository (see *Data and Resources*).

Figure 2 compares the stationary coefficient of MS-GWR models with the corresponding ones of ITA18 for the SA ordinates, including PGA (*i.e.,* SA at T=0). The values obtained by calibrating the fixed coefficients of the MS-GWR method are very similar to those obtained for ITA18, over the entire range of periods, except for a slight difference between the values of the b_2 coefficient for periods longer than 5s. The latter coefficient models the scaling with the magnitude for stronger earthquakes ($M>M_h$); in the case of longer periods, the value of M_h is higher (about 6.3 for T>5s, see Lanzano et al. 2019) and the number of data available for very strong earthquakes in this analysis is smaller than ITA18, since the foreign events have been removed from the dataset.

Table 1 reports the comparison of the regression parameter p-Value (Wasserstein and Lazar, 2016) related to ITA18 w.r.t. that obtained for the stationary coefficients of the MS-GWR. A coefficient with a low p-value (marked as <0.05) indicates that the corresponding term is a meaningful addition to the predictive model. This is the case for coefficients *a*, b_1, and c_1 for both the ITA18 and MS-GWR models. On the contrary, f_1 and f_2 coefficients exhibit p-values larger than 0.05 for both models, confirming that this additional variable (*i.e.,* the style of faulting) has a small impact on the model predictions (Bommer et al. 2003).

The maps of the spatially varying coefficients of the distance scaling for two selected ordinates of the acceleration response spectra (T=0.1s and 1s) are given in Figure 3. The values of the coefficient c_2 for the geometrical spreading vary in the interval -1.1 to -1.9 and in the interval -0.9

and -1.7 for SA T=0.1s and 1s, respectively. In both cases, the stationary coefficients derived by ITA18 are included in the interval of the spatially varying coefficients calibrated by MS-GWR.
At short period, the fastest attenuation (*i.e.,* lower c_3 values) is observed in the Campania region, close to the volcanic districts of Vesuvius and Phlegrean fields, while, at long periods in the northern Piedmont region. The values of the coefficient c_3 for the anelastic attenuation is included in the range -0.009 to 0.003 and range -0.005 to 0.005 for the selected parameters. The ITA18 stationary coefficients are still included in the interval of c_3 values of MS-GWR.
From a broad look at the spatial distribution of the coefficients in Figure 3, c_2 and c_3 maps look anti-correlated, because regions with higher c_2 have lower c_3 and vice-versa. This observation suggests that the coefficients for geometric spreading and apparent anelastic attenuation may have a strong trade-off, which has already been frequently observed in the calibration of stationary coefficient models (Boore et al. 2014; Campbell and Bozorgnia, 2014). In fact, the reference model ITA18 already shows a very strong anti-correlation at T=0.1s, assuming values of Pearson's correlation index $\rho_{c2,c3} = -0.99$ (see Table 1 in Lanzano et al. 2019). In order to check this issue, we estimate the spatially varying $\rho_{c2,c3}$ values from the MS-GWR model and plot them in Figure 4 for the two SA ordinates. The coefficients are still strongly anti-correlated and show values below -0.9 in a large portion of the Italian territory, both at 0.1s and 1s. This result shows that, although the prediction is accurate, the interpretation of the spatial trend of the geometric and anelastic attenuation coefficients on the basis of local geology could be tricky.
Another issue, partially connected with the latter, is related to the positive values that the c_3 coefficients assume in some areas: indeed, in such a case, the application of the model to distances above the validity limit (generally 100-200km), leads to unrealistic effects, such as the enhancement of the ground motion from a certain distance onwards. At long-periods, the most practical solution is to remove the anelastic attenuation term from the functional form, as done by Landwehr et al. (2016) for T>1s and by ITA18 for periods longer than 1.4s. On the contrary, the positive values of c_3 at short periods that, for example, occurs in Po river basin (northern Italy) are likely related to wave reflections at Moho interface. As reported in Lanzano et al. (2016), "this phenomenon has been already observed by Douglas et al. (2004) in central Italy and southern Iceland and by Bragato et al. (2011) in northern Italy and is explained as the enhancement of ground motion due to S-wave reflection at the Moho discontinuity (SmS phase)”. In the particular case of the Po Plain, Bragato et al. (2011) and Lanzano et al. (2016) showed that the net effect is precisely an enhancement of PGA and high frequency parameters from a certain distance onwards (> 50km). Placing c_3=0 is a rough simplification that ignores these phenomena. It is necessary to adopt alternative solutions to model this term, as proposed by Lanzano et al. (2016),

which sets a hinge distance (around 70km) and establishes a slope change in attenuation. On the other hand, the beneficial aspect of this spatial modeling is the ability to capture faster anelastic attenuation in Central Italy, which was also observed by several authors comparing predictions with observations (Scasserra et al. 2009; Luzi et al. 2017).

The maps of the k coefficients of the $V_{S,30}$ scaling are instead given in Figure 5 for the same intensity measures of Figure 3. The interval of variation of the k coefficient is quite wide at all periods, but the ITA18 values are still in the range of the MS-GWR values. At short periods, k assumes in several cases slightly positive values in south-eastern Sicily and northern coast of Tuscany, that unrealistically correspond to amplifications of the median prediction as $V_{S,30}$ increases (see Kamai et al. 2014 for the expected $V_{S,30}$ scaling). This unstable behavior is sometimes observed in the GMM regression of FAS ordinates at high frequencies (Bora et al. 2015) and demonstrates that $V_{S,30}$ and site effects are poorly correlated in this range of periods.

However, looking at the spatial distribution of the stations, the positive values in the coastal part of Tuscany could be caused by the fact that there are no stations in this area to constrain the scaling with $V_{S,30}$. In eastern Sicily, 24 recordings from 15 stations are available: the mean site amplification (called $\delta S2S_{ref}$) with respect to reference site predictions ($V_{S,30}$=800m/s) prediction at the spectral period T=0.1s is estimated for each station and reported in Figure 6 as a function of the $V_{S,30}$/800. If we draw a regression line, whose slope approximately describes the scaling with $V_{S,30}$, we observe that the amplification grows as $V_{S,30}$ increases, *i.e.,* k is positive. However, this trend is caused by the scarcity of records available in this area and is particularly conditioned by the value observed by the IT.GEA station. As a matter of fact, if the latter was excluded, one could note an opposite scaling (weakly negative).

4.2 Model variability

The efficiency of the proposed approach for ground motion modelling is evidenced by the significant decrease in total variability (σ) of the MS-GWR w.r.t. ITA18 at all periods (Figure 7a), attaining an average reduction of about 10%. The trend of sigma still presents a bump at T=0.1s, which confirms that such a large variability is due to effects not accounted by this model, *e.g.,* the limited ability of $V_{S,30}$ in capturing the site effect variability at high-frequencies. In any case, the aleatory variability at this period drops from 0.41 to 0.34 $\log_{10}$ units. The electronic supplements (see *Data and Resources*) report the distribution of the total residuals as a function of magnitude, distance and $V_{S,30}$ for the two control periods. The results still confirm the goodness of the calibration, since there are no remarkable biases with the predictor variables

In order to assess which component of the variability is more affected by the introduction of the non-stationarity in the GMM coefficients, we *a-posteriori* decompose the total residual of the MS-GWR model into the event, station, and event- and station- corrected terms and calculate the associated variabilities. As for ITA18, a random-effects approach is used to estimate the repeatable terms more robustly. Figure 7b, c and d show a comparison of the standard deviations obtained from the decomposition of the MS-GWR residuals with those provided by the ITA18 reference model. It is apparent that much of the reduction in total variability relates to the event term (τ), which is reduced across all periods in an amount ranging between 40 and 50%. The reduction in the site-related variability (ϕ_{S2S}) is much smaller, ranging between 5 and 10%. The remaining variability (ϕ_0), on the other hand, would be completely indifferent to the proposed MS-GWR modeling. Assuming no significant trade-off between residual components, this result suggests that the introduced spatial dependencies primarily capture differences between the sources, likely due to differences in mean stress drops. The site effect is limitedly benefited by this ground motion modeling (k dependence on station coordinates). Regional differences in seismic wave propagation, not captured by the starting functional, should be contained in the residual term cleaned of repeatable event and station effects: the fact that it is not reduced suggests that much of such effects are not captured by the introduced spatial dependencies (associated to event location), thus raising the need to introduce different parameterizations of the functional form and spatial dependencies.

Lanzano et al. (2019) also quantified the prediction error of ITA18 by estimating the statistical uncertainty in the median predictions, calculated on the model fit and the data distribution, as in Al-Atik & Youngs (2014). In the case of MS-GWR, the prediction uncertainty is computed by leveraging on the linear form of the estimators to account for the variability of the coefficients' estimators $\hat{\beta}_{\cdot,0}$ (see Caramenti et al., 2020, for further details). The spatial distribution of median predictions $\hat{y}$ and the associated epistemic uncertainty SD ($\hat{y}$) (also denoted as σ_μ), for an example scenario (M_w=6.0, R_{JB}=10km, $V_{S,30}$=300m/s and normal faults) are reported in Figure 8 for the two selected intensity measures.

The median predictions of the SA ordinate at T=0.1s vary from 0.15g to about 1g for the considered scenario, while at T=1s, the SA values are in the range 0.05-0.3g. The associated uncertainty varies from 0 to about 0.2 log10 units, both for short and long periods, with the lowest values in the central Apennines, where sampling is dense, and the highest in central Apulia, coastal areas of Tuscany and some areas in southern Calabria and Sicily, characterized by few and sparse data.

Figure 8 also reports the location of two selected sites (A and B), where we further explore the dependency of σ_μ on the different explanatory variables (Figure 9). The site A (43°N, 13°E) is located in the area with the largest density of records, corresponding to the epicentral area of the 2016-2017 central Italy seismic sequences; the site B (41°N, 17°E) belongs to an area with sparse and sporadic seismicity in the last 40 years, after the very strong earthquake of Irpinia (M_w 6.9 23/11/1980) that occurred at a distance less than 100km.

As expected, the variability of the MS-GWR model tends to that of ITA18 in cases where densely sampled sites are considered (site A): in general, the uncertainty associated with the prediction must be larger than ITA18, because, in the new functional (Eq. 2), additional explanatory variables (the coordinates of event and station) are included, with respect to the original functional form of ITA18. The uncertainty associated with site B is, instead, on average three times larger than ITA18. As in ITA18, the largest variation of σ_μ depends on the earthquake magnitude: in all the cases considered, σ_μ increases at magnitude greater than 7.0, where the data sampling is poorer. Similar behavior is observed for $V_{S,30}$<300 m/s. Note that the range of the Joyner-Boore distance R_{JB} in Figure 9 is [0,100] km, consistent with the bandwidths h_E, h_S selected for the estimation of the MS-GWR. These bandwidths directly reflect on the range of validity of the model itself, which should not be used beyond the range of the training data – similarly as for unweighted models. Finally, T=0.1s is still the period of SA at which the higher uncertainty about the prediction is observed.

5. Cross-validation and comparison with independent events

In order to validate the model, we carry out a 10-fold cross-validation, splitting the dataset completely at random (i.e., sampling without replacement the data $(z_i, x_{ij}, \mathrm{j} \in \mathrm{C} \cup \mathrm{E} \cup \mathrm{S})$, $i = 1, \ldots, N$) in 10 folds F_1, …., F_{10} and comparing the (in-sample) mean squared error (MSE), defined as:

$$MSE_{10-fold} = \frac{1}{10}\sum_{j=1}^{10}\frac{\sum_{i \epsilon F_j}\left(z_i - \hat{z}_{-j}\right)^2}{N_j} \qquad [4]$$

where N_j is the number of data, z_i are the observations and $\hat{z}_{-j}$ are the predicted value using the proposed model error for 5 intensity measures - PGA, SA (0.1s), SA (0.3s), SA (1s), SA (3s) - using all folds except for F_j. To allow for a fair comparison with ITA18, predictions of ITA18 are calculated following the same CV procedure, by recalibrating each time the model upon the same dataset considered for MS-GWR. Note that the calibration is here based on a restriction of the dataset originally considered to calibrate ITA18 (see § 2). Regression coefficients obtained for the restricted dataset where however equivalent to those originally obtained by Lanzano et al. (2019) (not shown).

Results (Figure 10) show that MS-GWR leads to improved results with respect to ITA18 over all the considered periods, supporting the introduction of spatially varying coefficients. The improvement of the prediction of MS-GWR model with respect to ITA18 is particularly evident at high frequencies, such as for 0.1s, for which the median value of $MSE_{10-fold}$ and the associated standard deviation are reduced by 28% and 25%, respectively.

The prediction performance of the proposed model is also assessed through a spectral comparison between the predicted ground motion parameters and the observed ones at given recording sites for some independent events (*i.e.,* not included in the calibration dataset). The independent earthquakes used in this analysis are reported in Table 2. The records used for testing are taken from the ITACA database (see *Data and Resources*).

First, we make a qualitative comparison between some observed spectra of the earthquakes in Table 2 and the predictions of the ITA18 and MS-GWR models in Figure 11. The illustrative recordings are representative of three possible outcomes: a) the MS-GWR prediction is closer to the observation of ITA18 (top panel); b) the MS-GWR and ITA18 predictions are similar, although far from observation (bottom left); c) ITA18 predicts the observation better than MS-GWR (bottom right). Scenario (a) occurs in the majority of the cases: in particular, the two cases given as examples relate to an independent event that occurred in a densely sampled area of the calibration dataset. Scenario (b) is less frequent and generally occurs when the observation can be considered as an outlier for both predictive models. Scenario (c) is quite rare, but in any case, MS-GWR always returns fairly regular predicted spectra without bumps. More generally, in areas where few data are available, the MS-GWR model tends to make predictions very similar to that of the corresponding stationary model.

In order to quantify the average gain of MS-GWR compared to ITA18, Figure 12 reports the boxplot of the absolute value of the standardized residuals of the four selected seismic events for the same intensity measures of Figure 10. MS-GWR, on average, leads to either better or comparable results to ITA18 for the events of Termoli, Barletta and Muccia. Moreover, in the densely sampled areas, the residuals are characterized by a very low variability, as for the event of Muccia. No improvements are observed for the event of Siracusa, where the record sampling of the calibration dataset is still sparse and does not allow for a significant improvement in predictions and associated variabilities, compared to ITA18.

6. Discussion and Conclusions

The challenging goal of introducing the regionalization into the ground motion modelling of Italy led us to implement and test spatial regression techniques in the phase of predictive model calibration. We drew inspiration from the work of Landwehr et al. (2016) for California to develop a method that introduces spatial non-stationarity into the coefficients of the model. The method proposed here is called Multi-Source Geographically-Weighted Regression (MS-GWR) and consists of a family of local linear regression models, accounting for the variability of the parameters due to either event- or site-effects. All the statistical details of the methodology are given in Caramenti et al. (2020) where results are reported for the case of the peak ground acceleration. In this paper, we have tested this regression technique for the ground motion prediction of the shallow active crustal events in Italy and discussed its results with respect to several intensity measures of engineering interest, such as the ordinates of acceleration elastic response spectra; we also compared our main findings with those of the corresponding model with stationary coefficients, named ITA18 published by Lanzano et al. (2019). In order to carry out a homogeneous comparison between the proposed and existing models as well as to assess the improvements appropriately, we kept the functional form and the calibration dataset as invariant as possible. In addition, the spatial dependencies of the parameters have been introduced in a simplified manner, following the experience gained in the paper by Landwehr et al. (2016).

In this regard, Figure 13 returns the spatial distribution of the total residuals ($y - \hat{y}$) of the 2018/04/10 M_W 4.6 Muccia earthquake (see also Table 2 for additional information) using the ITA18 and the predictive model proposed in this paper using the MS-GWR. The ITA18 residuals show a spatial trend with highly marked azimuthal dependencies, highlighted by large positive residuals (i.e., predictions larger than the observations) at short-periods (Figure 13a) in the Eastern sectors, with respect to the epicenter; while the remaining residuals (prevailing in the Western sectors) are, on average, negative. At longer periods, ITA18 residuals are moderately positive almost in the whole investigated area (Figure 13c). For both spectral ordinates, the spatial trends are less marked when we apply the MS-GWR technique: at short-period (Figure 13b), the positive residuals in the North-Eastern sector reduce in absolute value, while, in the epicentral area, no spatial trend is visible at the plot scale; at longer periods, the negative bias observed on ITA18 is corrected and the residuals do not exhibit any significant pattern.

This simple example shows how the application of the MS-GWR method results in a significant improvement in the model predictions, which can be interpreted as a partial removal of the ergodic assumption. Nevertheless, even if the MS-GWR model is able to explain a relevant part of the spatial variability observed in the data compared to ITA18, some caveats arise with respect to the starting assumptions, when we move to spatially-variable models:

- The spatial dependence for the geometric spreading and anelastic attenuation coefficients, based only on the event coordinates, is rather simplified. In fact, these terms depend on the source-to-site path, thus on both the event and station coordinates. For instance, to account for regional effects, some authors use a spatially-independent scaling with distance and, define anelastic attenuation correctives for homogeneous zones that are based on the site-dependent propagation properties of the media (Campbell & Bozorgnia 2014; Kotha et al. 2020); other authors use grid-based approaches to group and calculate repeatable path terms, obtained from the decomposition of residuals (Dawood and Rodriguez-Marek, 2013; Abrahamson et al. 2019; Sgobba et al. 2021). The latter approach would certainly be preferable for future developments of MS-GWR model, but it faces with a lack of data that often does not allow estimating corrections for all source-site paths;
- The coefficients for geometric spreading c_2 and anelastic attenuation c_3 are affected by a strong trade-off, showing a significant degree of anti-correlation in large part of the study area. This undesirable effect is very common in GMM calibration (Boore et al., 2014; Campbell and Bozorgnia, 2014) and the starting model (ITA18) is also affected by. This evidence implies that we cannot give physically-consistent interpretation to the observed spatial trends of the MS-GWR coefficients on the basis of the geological setting at a regional scale. In this respect, there is no unique solution as this effect is also related to the way in which spatial scaling is modeled with distance: Boore et al. (2014) suggest to perform the calibration in multiple steps to better control the trade-off; other authors (e.g. Campbell & Bozorgnia, 2014) suggest to separate data for the c_2 and c_3 calibration by distance threshold (e.g. within 50km for geometrical spreading and >50km for anelastic attenuation);
- The coefficient c_3 tends to assume weakly positive values in some areas, causing, as an undesired effect, an increase of the seismic motion with distance increasing, generally beyond the limit of model validity. At long-periods, this coefficient can be set to zero since the contribution of anelastic attenuation is negligible; at short-periods, instead, this instability can be related to physical phenomena that can alter the expected attenuation

trend with distance, as it happens in the Po Plain from a certain distance onwards due to wave reflections at the Moho discontinuity. In the latter case, setting c_3 to zero means ignoring the physical phenomenon and, on the contrary, it would be more appropriate to take it into account in the modelling, as, for example, proposed by Lanzano et al. (2016);

- For short-periods, the scarcity of recorded data and the lack of recording stations in some areas could cause instabilities in the calculation of scaling with $V_{S,30}$ (coefficient k), which could take on positive values, contrary to what is expected from physics (Kamai et al. 2014). Until additional records are available, a practical solution to control this instability may be to correct *a-posteriori* the k coefficient, by setting to zero when it assumes positive values. Another solution could be to increase the kernel bandwidth h_s, in order to enlarge the sampling, but this would then make the prediction of motion less "local";
- The model proposed in this study, unlike Landwehr et al. (2016), does not introduce spatial dependencies of the offset on the geographical coordinates of the recording site or event; this modelling assumption could limit the effectiveness of the approach in fully capturing the variability of the GMM. This issue could be mitigated by extending MS-GWR to a mixed-effects framework, an approach which is commonly adopted to remove the ergodic assumption on (not-regionalized) GMM models. In this paper, we have performed *a-posteriori* estimate of the repeatable site and event terms, with the purpose to verify which of the components of the variability are more affected by the non-stationary modeling. As a result, the MS-GWR modelling mainly allows to describe the differences in the level of ground motion for source areas characterized by average stress drops due to different dynamic regimes, rather than capturing differences related to the properties of the media in which seismic waves propagate.

In conclusion, the model proposed in this article provides promising results, but the abovementioned modelling issues must be tackled to improve the predictive power of the model. The latter goal could be certainly achieved by enlarging the calibration dataset with small magnitude and broadband records and additional data from neighboring countries. This will significantly improve predictions compared to the model presented herein in areas where sampling is poor, such as Apulia and Sicily regions. In addition, the cross-correlation among different periods could be taken into account, to build a joint probabilistic model for the IMs at different periods; this would potentially allow for enhanced point predictions and joint uncertainty assessment. A geostatistical approach based on functional data analysis for spatial data (Ramsay and Silverman, 2005; Menafoglio and Secchi 2017) has been recently proposed to deal with profiles of IMs over all vibration periods (Menafoglio et al., 2020), showing promising results in the generation of shaking scenarios from the corrective terms of ITA18 (see also Sgobba et al., 2019). However, more research is needed in this setting, to develop regionalized (non-stationary) functional models to be used in the formulation of non-ergodic GMMs.

7. Data and resources

The report by Caramenti et al. (2020) is publicly available at https://mox.polimi.it/publication-results/?id=917&tipo=add_qmox. All data used in this article came from published sources listed in the references. The accelerometric waveforms used in this study are published in the following databases: i) Engineering Strong-Motion database (ESM, http://esm-db.eu) and ii) ITalian ACcelerometric Archive (ITACA, http://itaca.mi.ingv.it). The complete list of the GMMs, published in peer-reviewed papers, is made available with a short description by John Douglas at http://www.gmpe.org.uk. The coefficient tables of the MS-GWR calibration presented here are also available in a GitHub repository at https://github.com/lucaramenti/ms-gwr . All the sources are last accessed in January 2021.

The electronic supplements of this paper include: i) a table with the stationary coefficients obtained from MS-GWR regression (TableS1.csv); ii) a table with the spatially varying coefficient c_2 for a 10km equally-spaced grid (TableS2.csv); iii) a table with the spatially varying coefficient c_3 for a 10km equally-spaced grid (TableS3.csv); iv) a table with the spatially varying coefficient k for a 10km equally-spaced grid (TableS4.csv); v) Total residuals (logarithmic difference between observations and predictions) of the model MS-GWR as a function of moment magnitude (left), Joyner-Boore distance (middle) and share wave velocity, averaged in the uppermost 30 meters $V_{S,30}$ (right) for acceleration response spectra at T=0.1s (FigureS5.pdf); vi) Total residuals (logarithmic difference between observations and predictions) of the model MS-GWR as a function of moment magnitude (left), Joyner-Boore distance (middle) and share wave velocity, averaged in the uppermost 30 meters $V_{S,30}$ (right) for acceleration response spectra at T=1s (FigureS6.pdf).

8. Acknowledgments

This study is partially funded by INGV-DPC agreement B1 2019-2021, with the aim of promoting research activities in the field of seismic hazard in Italy. Francesca Pacor and Lucia Luzi are acknowledged for their support in this research and for the coordination of the activities for the accelerometric databases developments and ground motion modelling. We would also like to thank Sreeram Reddy Kotha and another anonymous reviewer of the paper for their valuable comments, that helped us in the revision phase of the manuscript.

Reference

Abrahamson, N. A., W. J Silva, and R. Kamai (2014). Summary of the ASK14 ground motion relation for active crustal regions, Earthquake Spectra 30(3) 1025-1055.

Abrahamson, N.A., Kuehn, N.M., Walling, M. and Landwehr, N., 2019. Probabilistic Seismic Hazard Analysis in California Using Nonergodic Ground-Motion Models. Bull. Seismol. Soc. Am. 109(4):1235-1249.

Akkar, S., Sandıkkaya, M.A. and Bommer, J.J., 2014. Empirical ground-motion models for point-and extended-source crustal earthquake scenarios in Europe and the Middle East. Bull. Earthq. Eng. 12(1):359-387.

Al Atik, L., N. Abrahamson, J. J. Bommer, F. Scherbaum, F. Cotton, and N. Kuehn (2010). The variability of ground-motion prediction models and its components. Seismol. Res. Lett. 81(5) 794-801.

Al Atik, L. and R.R. Youngs (2014). Epistemic uncertainty for NGA-West2 models. Earthquake Spectra 30(3) 1301-1318.

Anderson, J. G., and J. N. Brune (1999). Probability seismic hazard analysis without the ergodic assumption, Seismol. Res. Lett. 70,19–28.

Anderson, J. G. and Y. Uchiyama (2011). A Methodology to Improve Ground-Motion Prediction Equations by Including Path Corrections, Bull. Seismol. Soc. Am. 101(4), 1822–1846.

Bazzurro, P., and C. A. Cornell (2004). Nonlinear soil-site effects in probabilistic seismic-hazard analysis, Bull. Seismol. Soc. Am. 94, 2110–2123.

Bindi, D., M. Massa, L. Luzi, G. Ameri, F. Pacor, R. Puglia,and P. Augliera (2014). Pan-European ground-motion prediction equations for the average horizontal component of PGA, PGV, and 5%-damped PSA at spectral periods up to 3.0 s using the RESORCE dataset. Bull. Earthq. Eng. 12(1) 391-430.

Bommer, J. J., J. Douglas, and F. O. Strasser (2003). Style-of-faulting in ground-motion prediction equations, Bull. Earthq. Eng. 1, 171–203.

Boore, D. M., J. P. Stewart, E. Seyhan, and G. Atkinson (2014). NGA-West2 equations for predicting PGA, PGV, and 5% damped PSA for shallow crustal earthquakes. Earthquake Spectra, 30(3) 1057-1085.

Boore, D.M., 2010. Orientation-independent, nongeometric-mean measures of seismic intensity from two horizontal components of motion. Bull. Seismol. Soc. Am. 100(4) 1830-1835.

Boore, D. M., and J. J. Bommer (2005). Processing of strong-motion accelerograms: Needs, options and consequences, Soil Dynam. Earthq. Eng. 25, 93–115.

Bora, S.S., F. Scherbaum, N. Kuehn, P. Stafford, and B. Edwards (2015). Development of a response spectral ground-motion prediction equation (GMPE) for seismic-hazard analysis from empirical Fourier spectral and duration models. Bull. Seismol. Soc. Am. 105(4) 2192-2218.

Bozorgnia, Y. et al. (2014). NGA-West2 research project. Earthquake Spectra, 30(3) 973-987.

Bragato, P. L., M. Sugan, P. Augliera, M. Massa, A. Vuan, and A. Sarao (2011). Moho reflection effects in the Po Plain (northern Italy) observed from instrumental and intensity data, Bull. Seismol. Soc. Am. 10(5) 2142–2152.

Brunsdon, C., A. S. Fotheringham, and M. Charlton (1998). Geographically Weighted Regression - Modelling spatial non-stationarity, J. Royal Statistical Society: Series D (The Statistician) 47(3) 431-443.

Campbell, K.W., and Y. Bozorgnia (2014). NGA-West2 ground motion model for the average horizontal components of PGA, PGV, and 5% damped linear acceleration response spectra, Earthquake Spectra 30(3) 1087-1115.

Caramenti, L., A. Menafoglio, S. Sgobba, and G. Lanzano (2020). Multi-source mixed geographically weighted regression for seismic ground motion modelling. MOX-report 67/2020, Politecnico di Milano. https://mox.polimi.it/publication-results/?id=917&tipo=add_qmox

Cauzzi, C., E. Faccioli, M. Vanini, and A. Bianchini (2015). Updated predictive equations for broadband (0.01–10 s) horizontal response spectra and peak ground motions, based on a global dataset of digital acceleration records. Bull. Earthq. Eng. 13(6) 1587-1612.

Chao, S.H., C.M. Lin, C.H. Kuo, J.Y. Huang, K.L. Wen, and Y.H. Chen (2020). Implementing horizontal-to-vertical Fourier spectral ratios and spatial correlation in a ground-motion prediction equation to predict site effects. Earthquake Spectra, in press.

Chiou, B. S. J., and R. R. Youngs (2014). Update of the Chiou and Youngs NGA model for the average horizontal component of peak ground motion and response spectra. Earthquake Spectra, 30(3), 1117-1153.

Cramer, C. H. (2003). Site seismic-hazard analysis that is completely probabilistic, Bull. Seismol. Soc. Am. 93(4) 1841–1846.

Dawood H. M., and A. Rodriguez-Marek (2013). A Method for Including Path Effects in Ground-Motion Prediction Equations: An Example Using the Mw 9.0 Tohoku Earthquake Aftershocks, Bull. Seismol. Soc. Am. 103(2B):1360–1372.

Douglas, J., P. Suhadolc, and G. Costa (2004). On the incorporation of the effect of crustal structure into empirical strong ground motion estimation, Bull. Earthq. Eng. 2, 75–99.

Douglas, J., and B. Edwards (2016). Recent and future developments in earthquake ground motion estimation. Earth-Science Reviews 160 203-219.

Esposito, S., and I. Iervolino (2012). Spatial correlation of spectral acceleration in European data, Bull. Seismol. Soc. Am. 102, 2781–2788.

Fotheringham, S., C. Brunsdon, and M. Charlton (2002). Geographically Weighted Regression - the analysis of spatially varying relationships. John Wiley & Sons Ltd.

Goda, K, Atkinson, GM (2010) Intraevent spatial correlation of ground-motion parameters using SK-net data. Bulletin of the Seismological Society of America 100: 3055–3067.

Kamai, R., N.A. Abrahamson, and W.J. Silva (2014). Nonlinear horizontal site amplification for constraining the NGA-West2 GMPEs, Earthquake Spectra 30(3) 1223-1240.

Kotha, S. R., D. Bindi, and F. Cotton (2016). Partially non-ergodic region specific GMPE for Europe and Middle-East. Bull. Earthq. Eng. 14(4) 1245-1263.

Kotha, S. R., G. Weatherill, D. Bindi, and F. Cotton (2020). A regionally-adaptable ground-motion model for shallow crustal earthquakes in Europe. Bull. Earthq. Eng. 18 4091–4125.

Kuehn, N. M., and N. Abrahamson (2020). Spatial correlations of ground motion for non-ergodic seismic hazard analysis, Earthq. Eng. Struct. Dyn. 49 4–23.

Landwehr, N., N. M. Kuehn, T. Scheffer, and N. Abrahamson (2016). A nonergodic ground-motion model for California with spatially varying coefficients. Bull. Seismol. Soc. Am. 106(6) 2574-2583.

Lanzano G., L. Luzi, F. Pacor, C. Felicetta, R. Puglia, S. Sgobba, and M. D’Amico (2019). A revised ground motion prediction model for shallow crustal earthquakes in Italy, Bull. Seismol. Soc. Am. 109(2) 525-540.

Lanzano, G., F. Pacor, L. Luzi, M. D'Amico, R. Puglia, and C. Felicetta (2017). Systematic source, path and site effects on ground motion variability: The case study of Northern Italy, Bull. Earthq. Eng. 15(11) 4563–4583.

Lanzano, G., M. D’Amico, C. Felicetta, R. Puglia, L. Luzi, F. Pacor, and D. Bindi (2016). Ground-motion prediction equations for region-specific probabilistic seismic-hazard analysis. Bull. Seismol. Soc. Am. 106(1) 73-92.

Lin, P.-S., B. Chiou, N. Abrahamson, M. Walling, C.-T. Lee, C.-T. Cheng (2011) Repeatable source, site, and path effects on standard deviation for empirical ground-motion prediction models. Bull. Seismol. Soc. Am. 101(5) 2281–2295.

Luzi, L., D. Bindi, R. Puglia, F. Pacor, and A. Oth (2014). Single-station sigma for italian strong-motion stations. Bull. Seismol. Soc. Am. 104(1) 467–483.

Luzi, L., F. Pacor, R. Puglia, G. Lanzano, C. Felicetta, M. D'Amico, A. Michelini, L. Faenza, V. Lauciani, I. Iervolino, and G. Baltzopoulos (2017). The central Italy seismic sequence between August and December 2016: Analysis of strong-motion observations, Seismol. Res. Lett. 88(5) 1219-1231.

Menafoglio, A., and P. Secchi (2017) Statistical analysis of complex and spatially dependent data: a review of object-oriented spatial statistics, Eur J Oper Res 258(2) 401–410.

Menafoglio, A., S. Sgobba, G. Lanzano, and F. Pacor (2020) Simulation of seismic ground motion fields via object-oriented spatial statistics with an application in Northern Italy, Stoch. Environm. Res. Risk Assess. 32(12) 3421-3437.

Park, J., P. Bazzurro, and J. W. Baker (2007). Modeling spatial correlation of ground motion intensity measures for regional seismic hazard and portfolio loss estimation, Appl. Stat. Prob. Civ. Eng. 1–8.

Ramsay, J, and B. Silverman (2005) Functional data analysis, 2nd edn. Springer, New York.

Rodriguez-Marek, A., G. A. Montalva, F. Cotton, and F. Bonilla (2011). Analysis of single-station standard deviation using the KiK-net data. Bull. Seismol. Soc. Am. 101(3) 1242–1258.

Sabetta, F., and A. Pugliese (1987). Attenuation of peak horizontal acceleration and velocity from Italian strong-motion records, Bull. Seismol. Soc. Am. 77(5) 1491-1513.

Sabetta, F., and A. Pugliese (1996). Estimation of response spectra and simulation of nonstationary earthquake ground motions, Bull. Seismol. Soc. Am. 86(2) 337-352.

Sahakian, V.J., A. Baltay, T.C. Hanks, J. Buehler, F.L. Vernon, D. Kilb, and N.A. Abrahamson (2019). Ground motion residuals, path effects, and crustal properties: A pilot study in Southern California, J. Geophys. Res. Solid Earth, 124(6):5738-5753.

Scasserra, G., J. P. Stewart, P. Bazzurro, G. Lanzo, and F. Mollaioli (2009). A comparison of NGA ground-motion prediction equations to Italian data, Bull. Seismol. Soc. Am. 99, no. 5, 2961–2978.

Schiappapietra, E., and J. Douglas (2020). Modelling the spatial correlation of earthquake ground motion: insights from the literature, data from the 2016-2017 central Italy earthquake sequence and ground-motion simulations, Earth- Science Reviews 203.

Sgobba, S., G. Lanzano, F. Pacor, R. Puglia, M. D'Amico, C. Felicetta, and L. Luzi (2019). Spatial correlation models of systematic site and path effects for Ground-Motion fields in Northern Italy, Bull. Seismol. Soc. Am. 109(4) 1419–1434.

Sgobba S., L. Lanzano, and F. Pacor (2021). Empirical non-ergodic shaking scenarios based on spatial correlation models: an application to central Italy. Earthq. Eng. Struct. Dyn. 50 60-80.

Sokolov, V, Wenzel, F (2011) Influence of spatial correlation of strong ground motion on uncertainty in earthquake loss estimation. Earthquake Engineering and Structural Dynamics 40: 993–1009.

Stafford, P. J. (2014). Crossed and nested mixed-effects approaches for enhanced model development and removal of the ergodic assumption in empirical ground-motion models, Bull. Seismol. Soc. Am. 104(2) 702-719.

Stucchi, M., C. Meletti, V. Montaldo, H. Crowley, G. M. Calvi, and E. Boschi (2011). Seismic hazard assessment (2003–2009) for the Italian building code, Bull. Seismol. Soc. Am. 101(4) 1885-1911.

Villani, M., and N. A. Abrahamson (2015) Repeatable site and path effects on the ground-motion sigma based on empirical data from Southern California and simulated waveforms from the CyberShake platform, Bull. Seismol. Soc. Am. 105(5) 2681–2695.

Wasserstein, R. L., and N. A. Lazar (2016). The ASA's statement on p-values: Context, process, and purpose, Am. Stat. 70, no. 2, 129–133.

Woessner, J. et al. (2015). The 2013 European seismic hazard model: key components and results, Bull. Earthq. Eng. 13(12) 3553-3596.

Full mailing address of each author

1. **Giovanni Lanzano**, Istituto Nazionale di Geofisica e Vulcanologia, Via Alfonso Corti 12, 20133 Milano, Italy, giovanni.lanzano@ingv.it;
2. **Sara Sgobba**, Istituto Nazionale di Geofisica e Vulcanologia, Via Alfonso Corti 12, 20133 Milano, Italy, sara.sgobba@ingv.it;
3. **Luca Caramenti**, MOX, Department of Mathematics, Politecnico di Milano, Via Bonardi 9, Milano, Italy, luca.caramenti@mail.polimi.it;
4. **Alessandra Menafoglio**, MOX, Department of Mathematics, Politecnico di Milano, Via Bonardi 9, Milano, Italy, alessandra.menafoglio@polimi.it

Tables

Table 1. P-Values obtained from the model regression.

Coefficients	SA-T=0.1s		SA-T=1s	
	ITA18	**MS-GWR**	**ITA18**	**MS-GWR**
a	<< 0.05	<< 0.05	<< 0.05	<< 0.05
b_1	< 0.05	<< 0.05	<< 0.05	<< 0.05
b_2	0.137	0.133	< 0.05	0.149
c_1	<< 0.05	<< 0.05	<< 0.05	<< 0.05
f_1	< 0.05	< 0.05	0.586	< 0.05
f_2	0.526	0.118	0.935	0.103

Table 2. List of independent events for model validation. In italics the ITACA event ID.

Municipality name ***ITACA event ID***	**Event Date**	**Moment magnitude (Mw)**	**Epicenter latitude [°]**	**Epicenter longitude [°]**	**Number of records**
Muccia, MC *EMSC-20180410_0000011*	2018-04-10 03:11:31	4.6	43.0687	13.03650	174
Termoli, CB *EMSC-20180816_0000090*	2018-08-16 18:19:06	5.1	41.87420	14.86480	167
Barletta, BT *EMSC-20190521_0000022*	2019-05-21 08:13:32	4.0	41.29920	16.30030	51
Siracusa, SR *IT-1990-0003*	1990-12-13 00:24:26	5.6	37.19500	15.46800	7

List of figure captions

Figure 1. Calibration dataset: a) location of earthquake events and recording stations; b) moment magnitude M_w vs Joyner-Boore distance scatter plot.

Figure 2. Stationary coefficients of ITA18 vs ITA18_MS-GWR: a) offset a; b) magnitude scaling coefficient b_1; c) magnitude scaling coefficient b_2; d) strike-slip coefficient f_1; e) thrust fault coefficient f_2; f) magnitude-dependent geometrical spreading coefficient c_1.

Figure 3. Maps of the spatially variable coefficients for the distance scaling: a) geometrical spreading coefficient c_2 for SA-T=0.1s; b) geometrical spreading coefficient c_2 for SA-T=1s; c) anelastic attenuation coefficient c_3 for SA-T=0.1s; d) anelastic attenuation coefficient c_3 for SA-T=1s. The values of stationary coefficients obtained by ITA18 calibration are given in the plot.

Figure 4. Maps of the Pearson correlation index between c_2 and c_3 coefficients ($\rho_{c2,c3}$): a) SA T=0.1s; b) SA T=1s.

Figure 5. Maps of the spatially variable coefficients for $V_{S,30}$ scaling coefficient k at: a) SA-T=0.1s; b) SA-T=1s. The values of stationary coefficients obtained by ITA18 calibration are given in the plot.

Figure 6. Mean site amplification ($\delta S2S_{ref}$) with respect to ITA18 predictions at $V_{S,30}$=800m/s as a function of $V_{S,30}$/800 for selected station in south-eastern Sicily.

Figure 7. Standard deviation components vs. period: a) total (σ); b) between-event (τ); c) site-to-site (ϕ_{S2S}); d) event- and site- corrected residuals (ϕ_0).

Figure 8. Maps of the median predictions $\hat{y}$ and associated epistemic uncertainty SD($\hat{y}$) for the scenario M_w=6.0, R_{JB}=10km, $V_{S,30}$=300m/s and normal faults: a) $\hat{y}$ of $\log_{10}$SA at T=0.1s; b) SD($\hat{y}$) of $\log_{10}$SA at T=0.1s; c) $\hat{y}$ of $\log_{10}$SA at T=1s;d) SD($\hat{y}$) of $\log_{10}$SA at T=1s.

Figure 9. Epistemic uncertainty of MS-GWR model and ITA18 as a function of the predictive variables for the sites A and B in Figure 6: a) period; b) moment magnitude M_w; c) Joyner-Boore distance R_{JB}; d) $V_{S,30}$.

Figure 10. Boxplot of MSE by 10-fold cross validation at several periods: comparison between ITA18 model (light-colored error bars) and MS-GWR model (dark-colored error bars).

Figure 11. Observed vs predicted spectra.

Figure 12. Boxplot of the standardized residuals for the selected independent events of Table 1: M_W 4.6 2018/04/10 Muccia (a), M_W 5.1 2018/08/16 Termoli (b), M_W 4.0 2019/05/21 Barletta (c) and M_W 5.6 1990/12/13 Siracusa (d). The predictions by ITA18 model (light-colored error bars) and MS-GWR model (dark-colored error bars) are compared.

Figure 13. Total residuals of the 2018/04/10 M_W 4.6 Muccia earthquake: a) ITA18, SA-T=0.1s; b) MS-GWR, SA-T=0.1s; c) ITA18, SA-T=1s; b) MS-GWR, SA-T=1s.

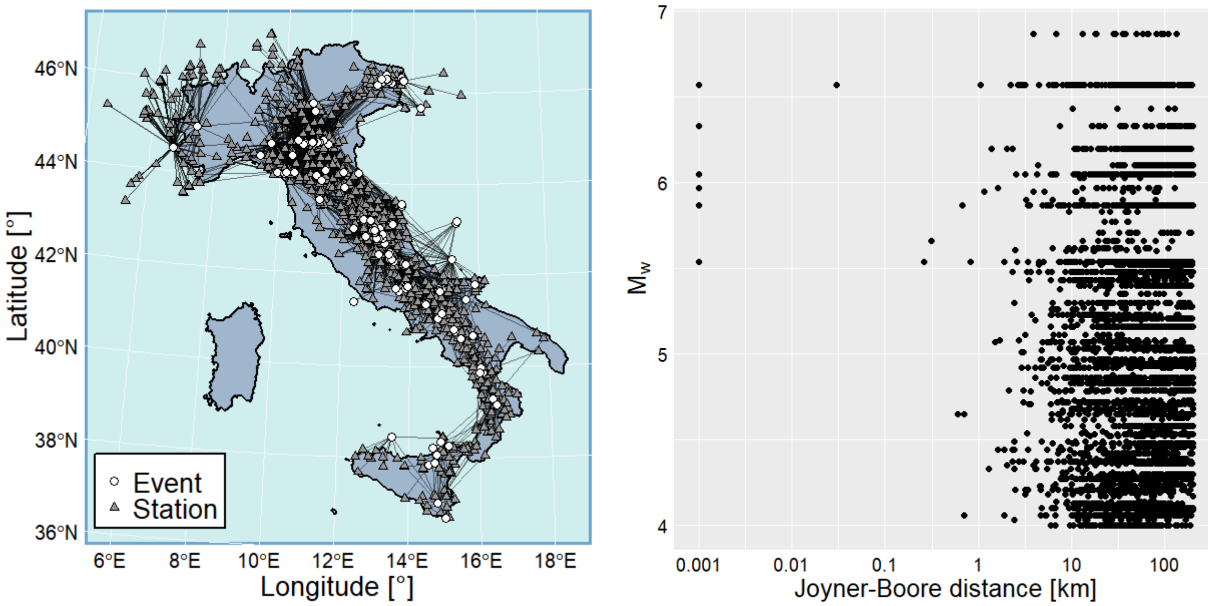

(a) (b)

Figure 1. Calibration dataset: a) location of earthquake events and recording stations; b) moment magnitude M_w vs Joyner-Boore distance scatter plot.

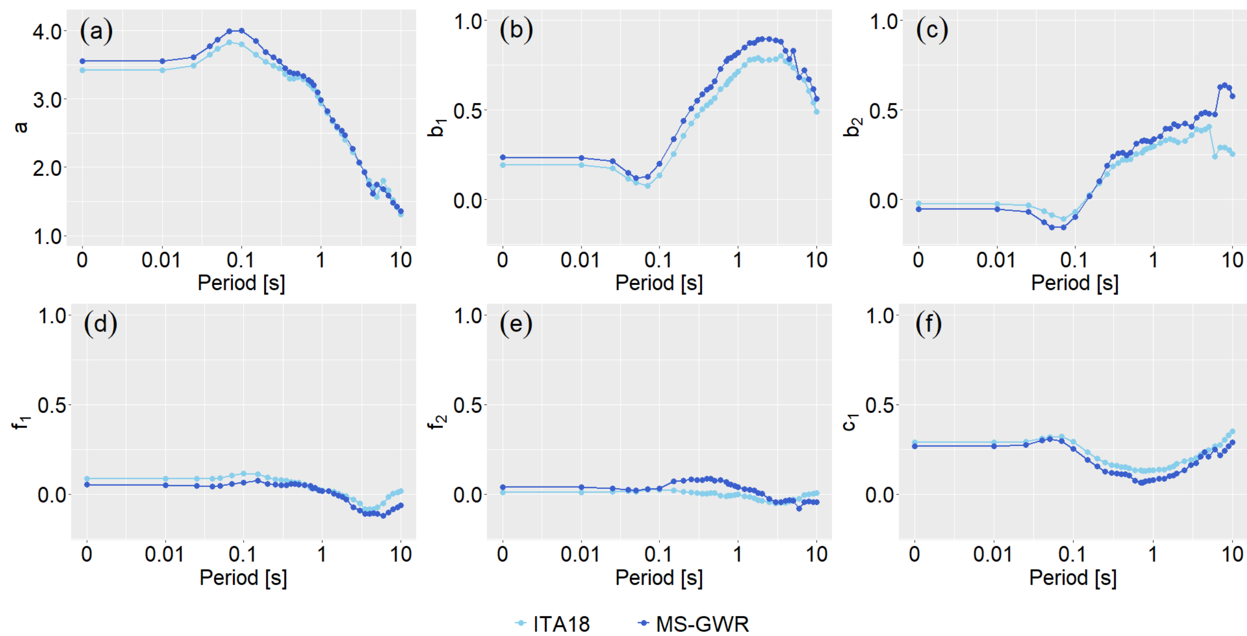

Figure 2. Stationary coefficients of ITA18 vs ITA18_MS-GWR: a) offset a; b) magnitude scaling coefficient b_1; c) magnitude scaling coefficient b_2; d) strike-slip coefficient f_1; e) thrust fault coefficient f_2; f) magnitude-dependent geometrical spreading coefficient c_1.

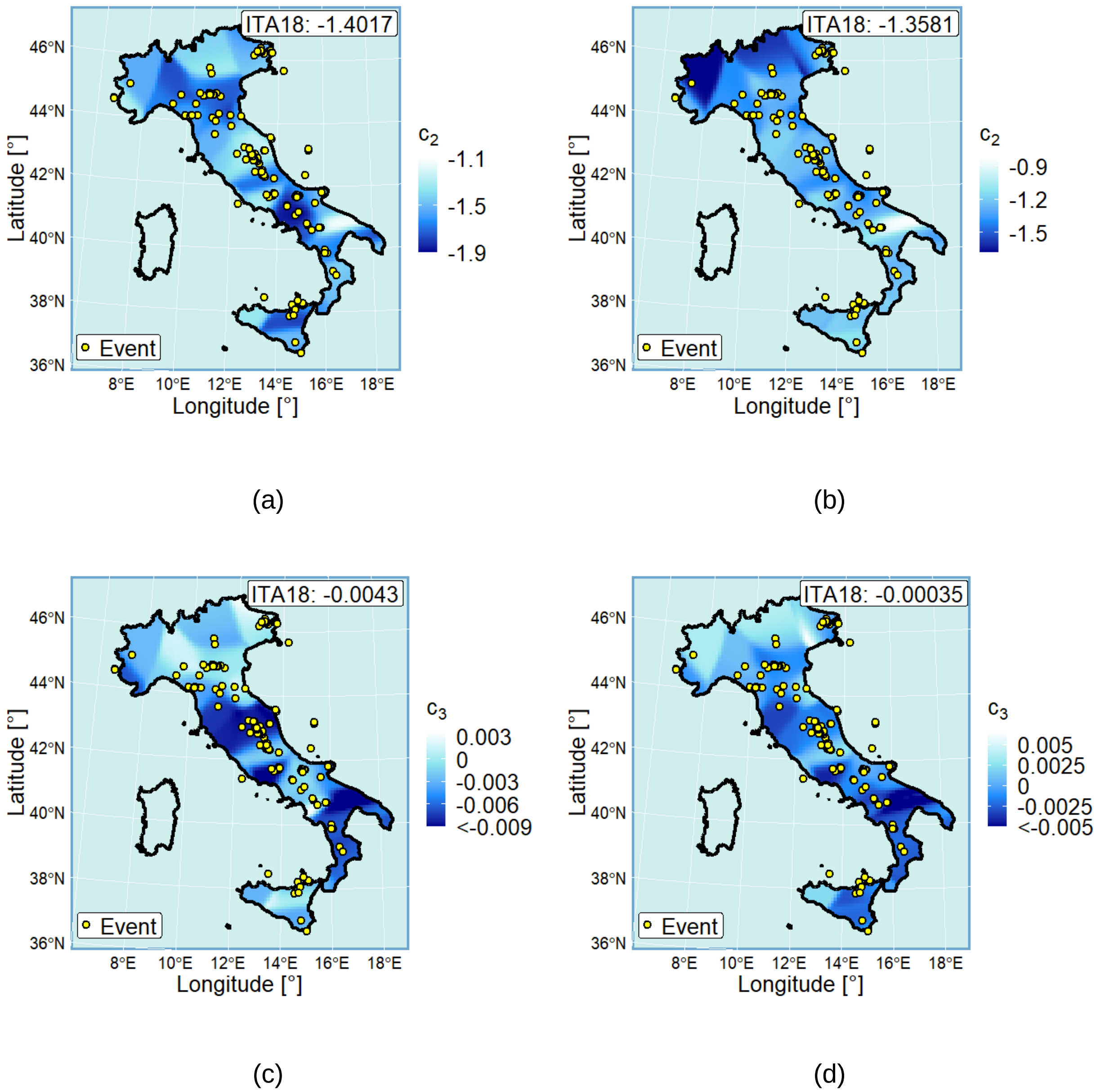

Figure 3. Maps of the spatially variable coefficients for the distance scaling: a) geometrical spreading coefficient c_2 for SA-T=0.1s; b) geometrical spreading coefficient c_2 for SA-T=1s; c) anelastic attenuation coefficient c_3 for SA-T=0.1s; d) anelastic attenuation coefficient c_3 for SA-T=1s. The values of stationary coefficients obtained by ITA18 calibration are given in the plot.

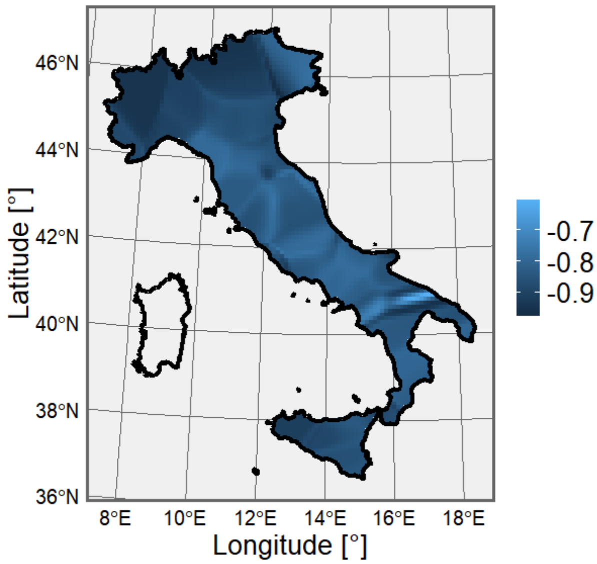

(a)

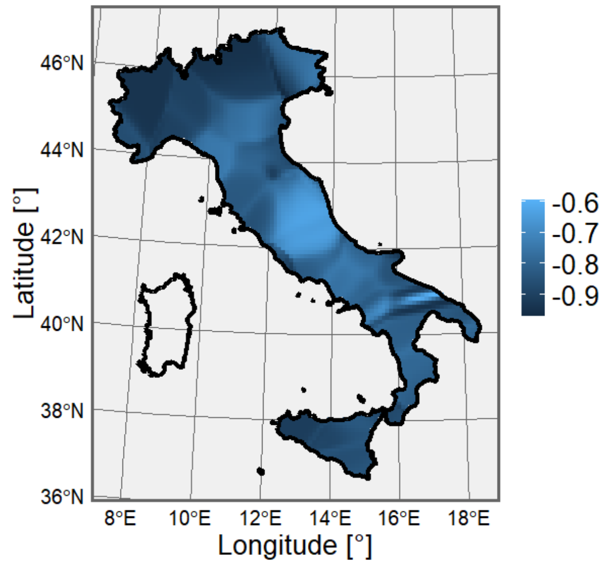

(b)

824 **Figure 4.** Maps of the Pearson correlation index between c_2 and c_3 coefficients ($\rho_{c2,c3}$): a) SA
825 T=0.1s; b) SA T=1s.

826

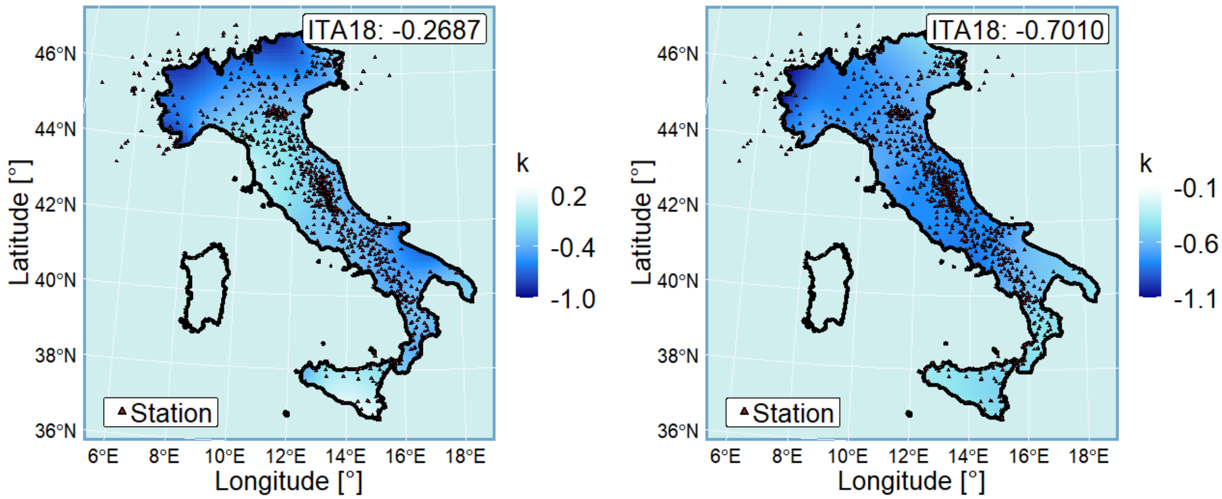

(a) (b)

Figure 5. Maps of the spatially variable coefficients for $V_{S,30}$ scaling coefficient k at: a) SA-T=0.1s; b) SA-T=1s. The values of stationary coefficients obtained by ITA18 calibration are given in the plot.

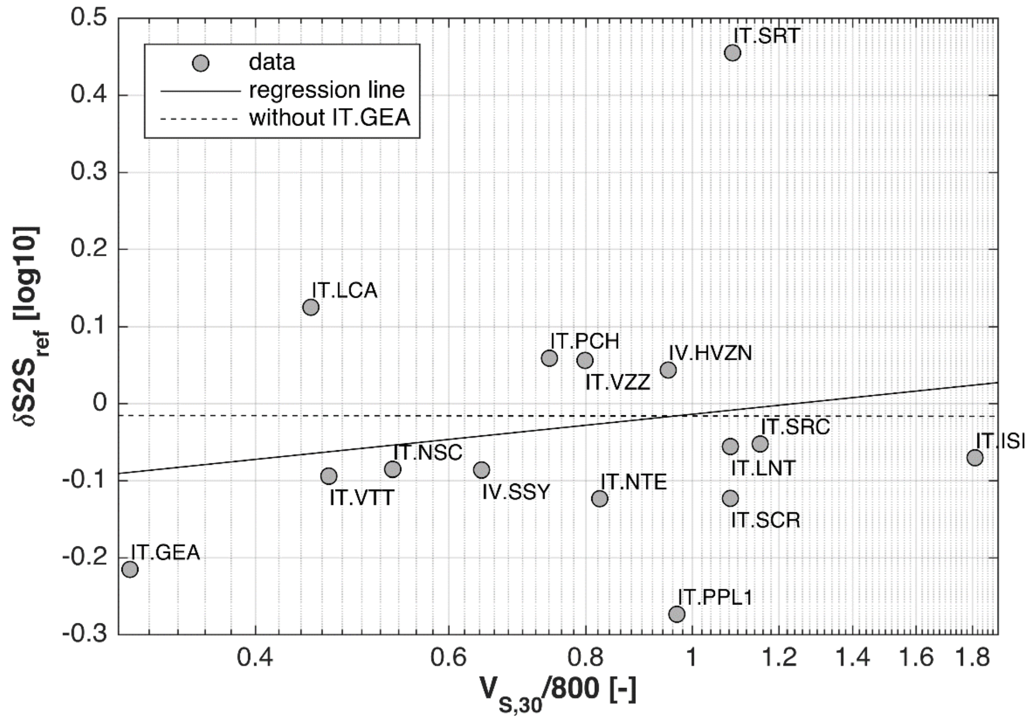

Figure 6. Mean site amplification ($\delta S2S_{ref}$) with respect to ITA18 predictions at $V_{S,30}$=800m/s as a function of $V_{S,30}$/800 for selected station in south-eastern Sicily.

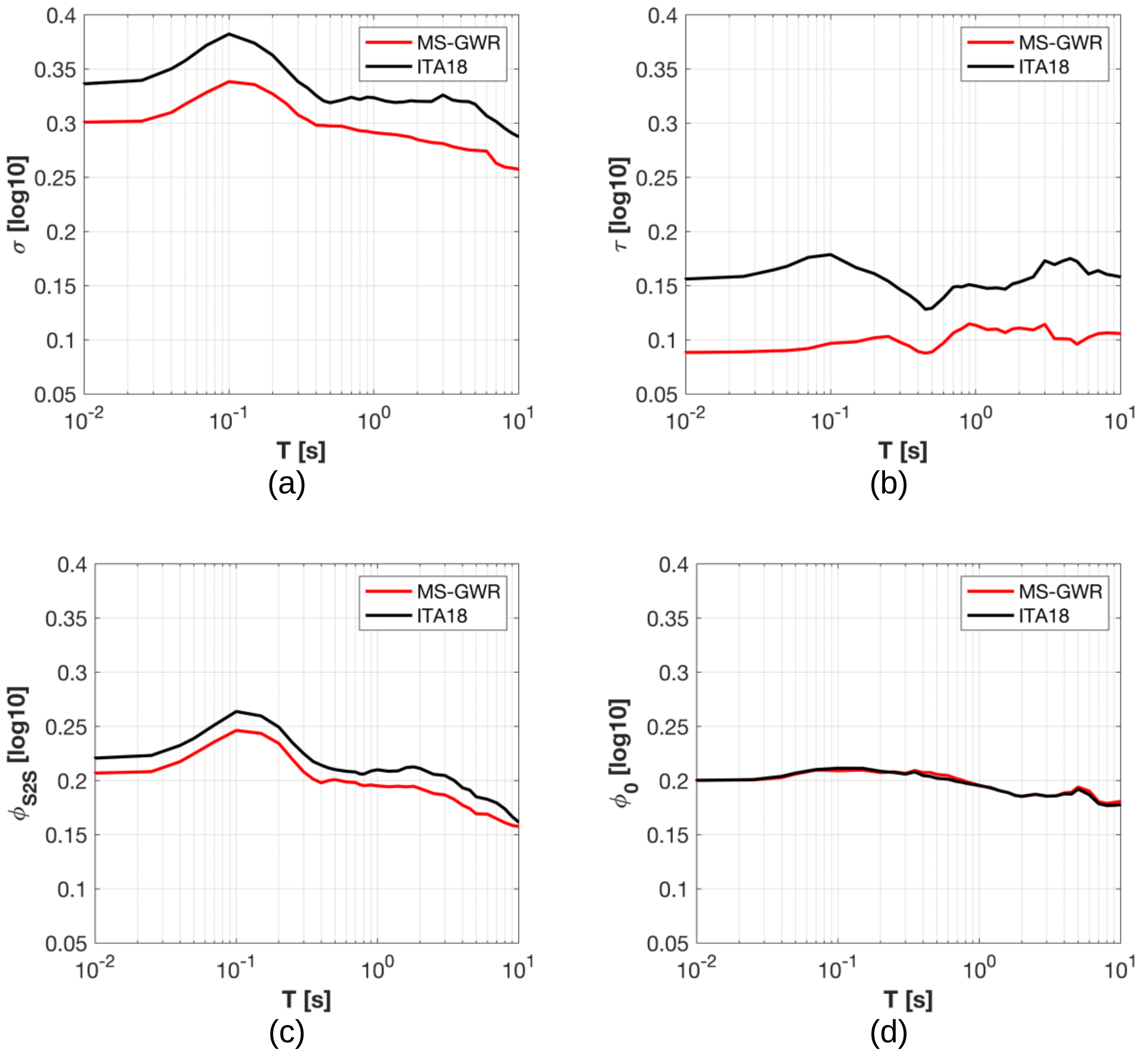

Figure 7. Standard deviation components vs. period: a) total (σ); b) between-event (τ); c) site-to-site (ϕ_{S2S}); d) event- and site- corrected residuals (ϕ_0).

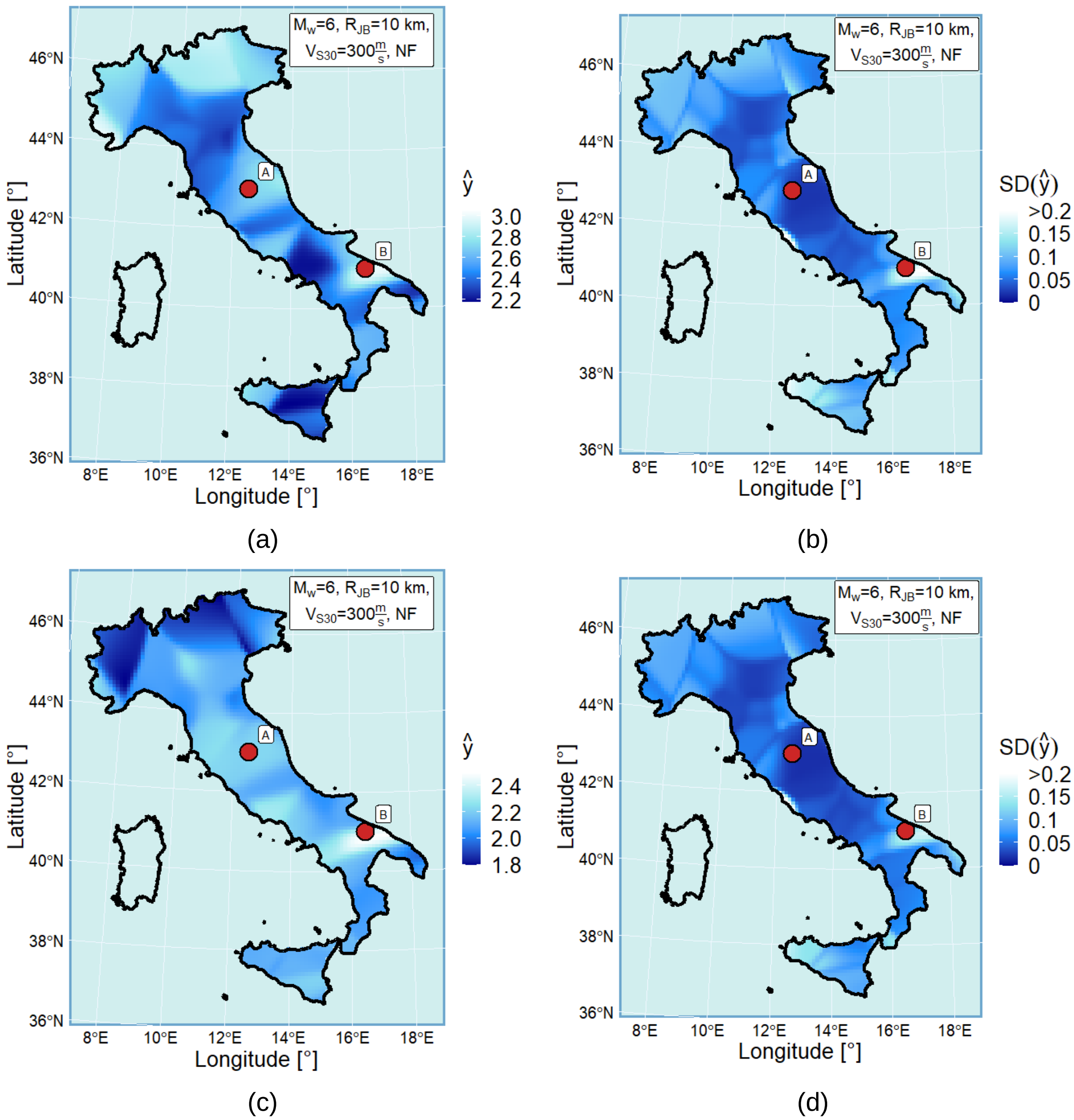

Figure 8. Maps of the median predictions $\hat{y}$ and associated epistemic uncertainty SD($\hat{y}$) for the scenario M_w=6.0, R_{JB}=10km, $V_{S,30}$=300m/s and normal faults: a) $\hat{y}$ of $\log_{10}$SA at T=0.1s; b) SD($\hat{y}$) of $\log_{10}$SA at T=0.1s; c) $\hat{y}$ of $\log_{10}$SA at T=1s;d) SD($\hat{y}$) of $\log_{10}$SA at T=1s.

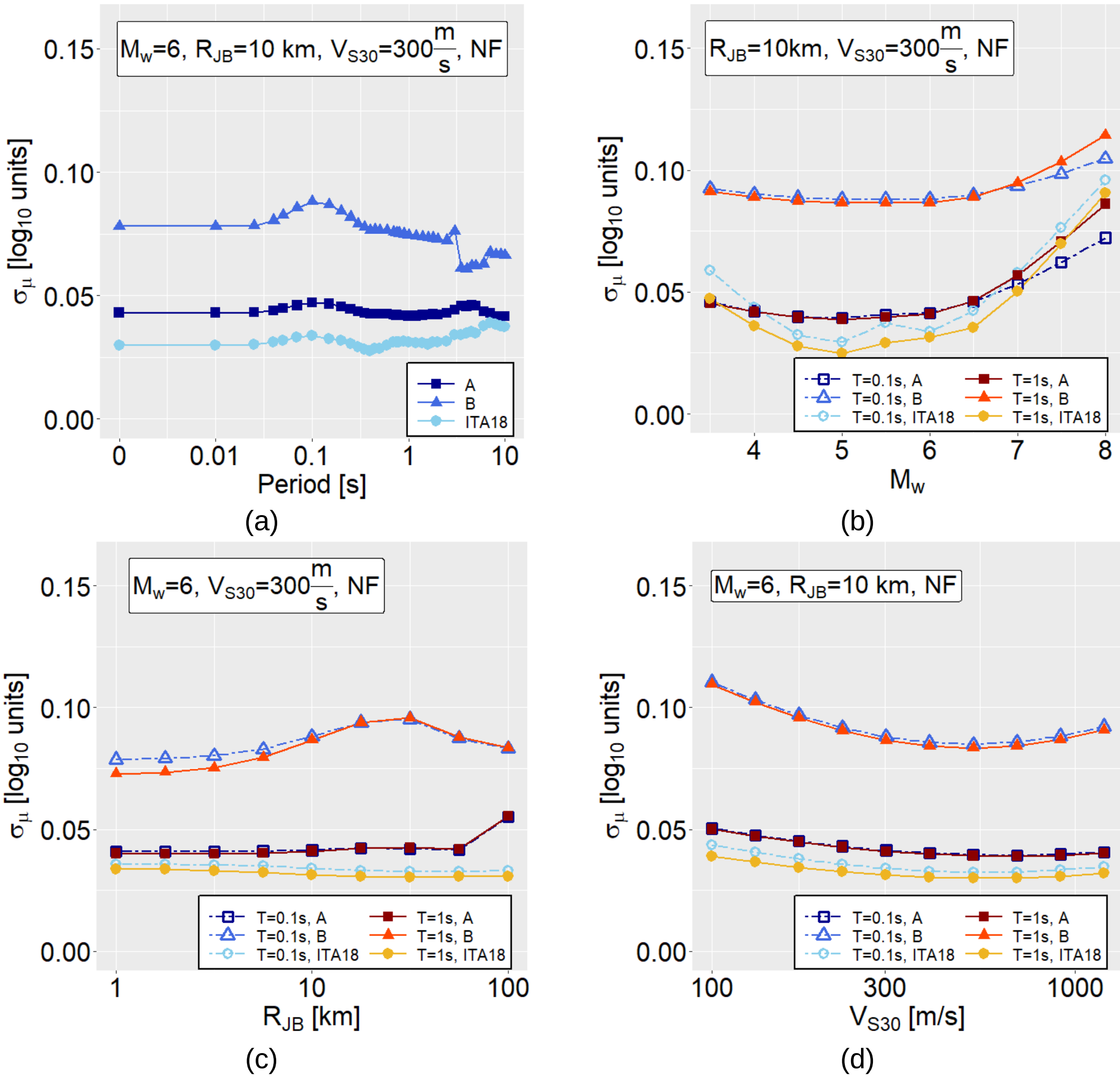

Figure 9. Epistemic uncertainty of MS-GWR model and ITA18 as a function of the predictive variables for the sites A and B in Figure 6: a) period; b) moment magnitude M_w; c) Joyner-Boore distance R_{JB}; d) $V_{S,30}$.

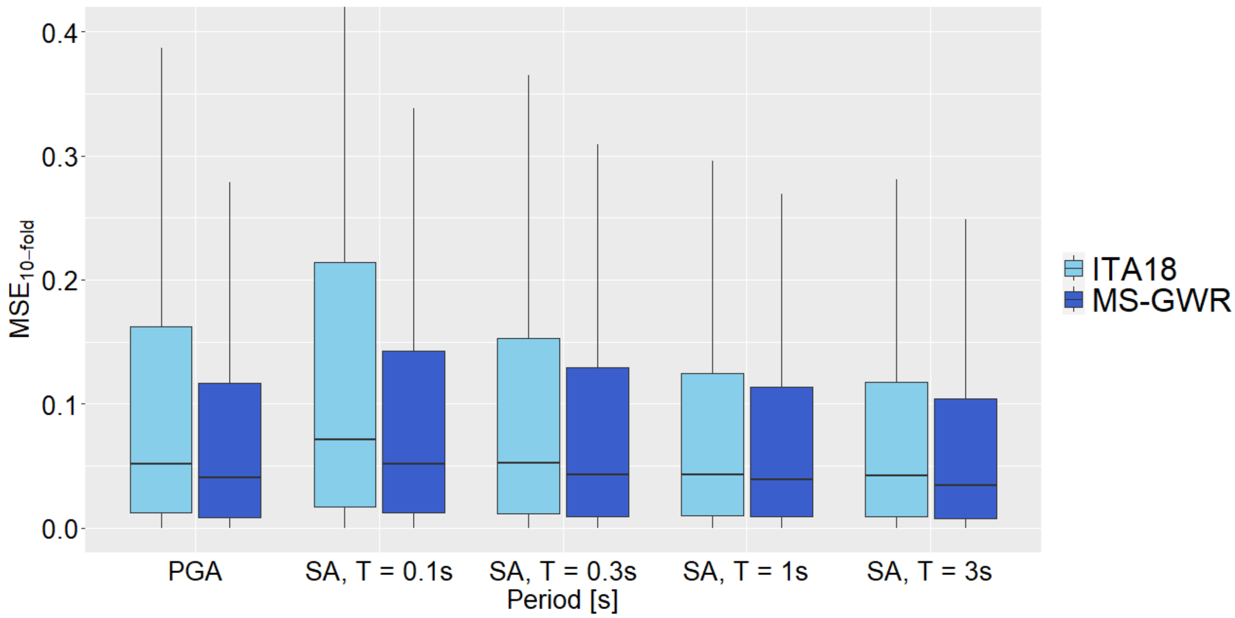

Figure 10. Boxplot of MSE by 10-fold cross validation at several periods: comparison between ITA18 model (light-colored error bars) and MS-GWR model (dark-colored error bars).

854

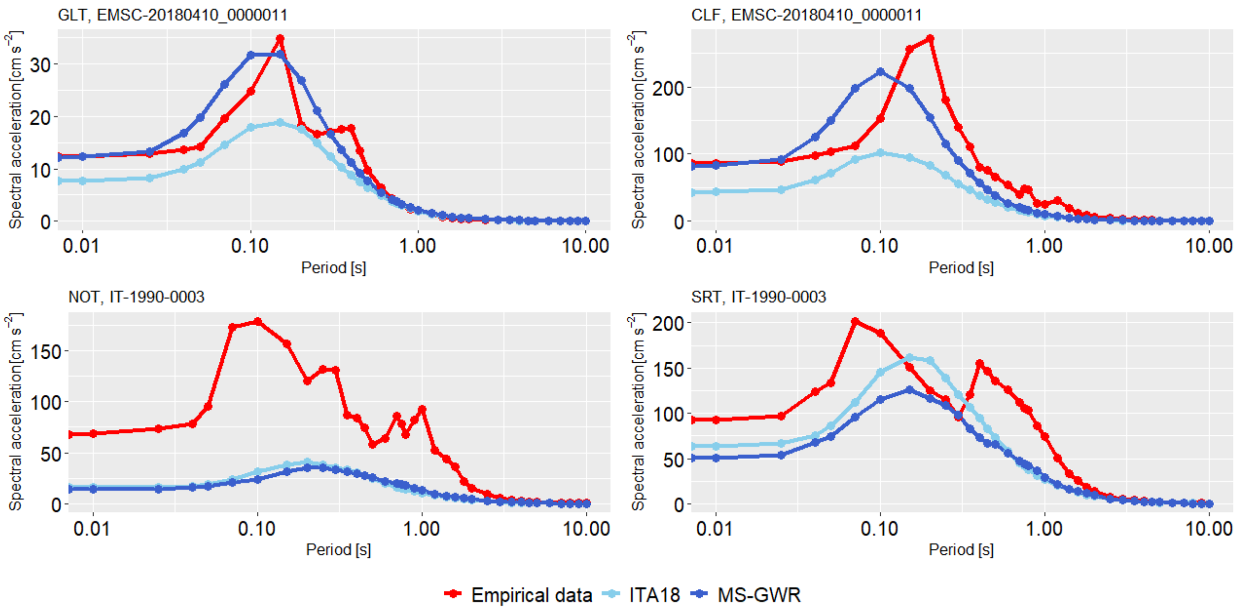

855 **Figure 11**. Observed vs predicted spectra.

856

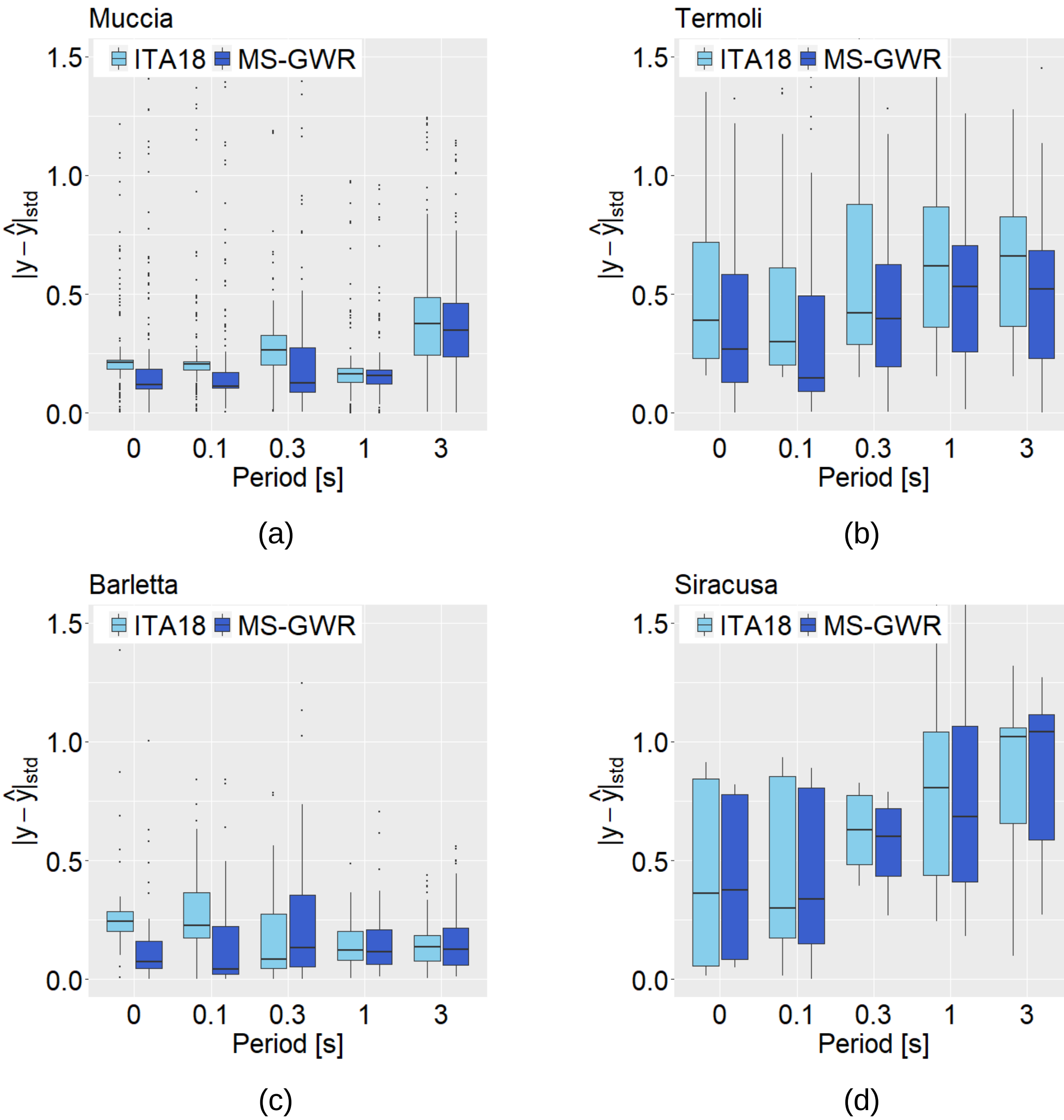

Figure 12. Boxplot of the standardized residuals for the selected independent events of Table 1: M_W 4.6 2018/04/10 Muccia (a), M_W 5.1 2018/08/16 Termoli (b), M_W 4.0 2019/05/21 Barletta (c) and M_W 5.6 1990/12/13 Siracusa (d). The predictions by ITA18 model (light-colored error bars) and MS-GWR model (dark-colored error bars) are compared.

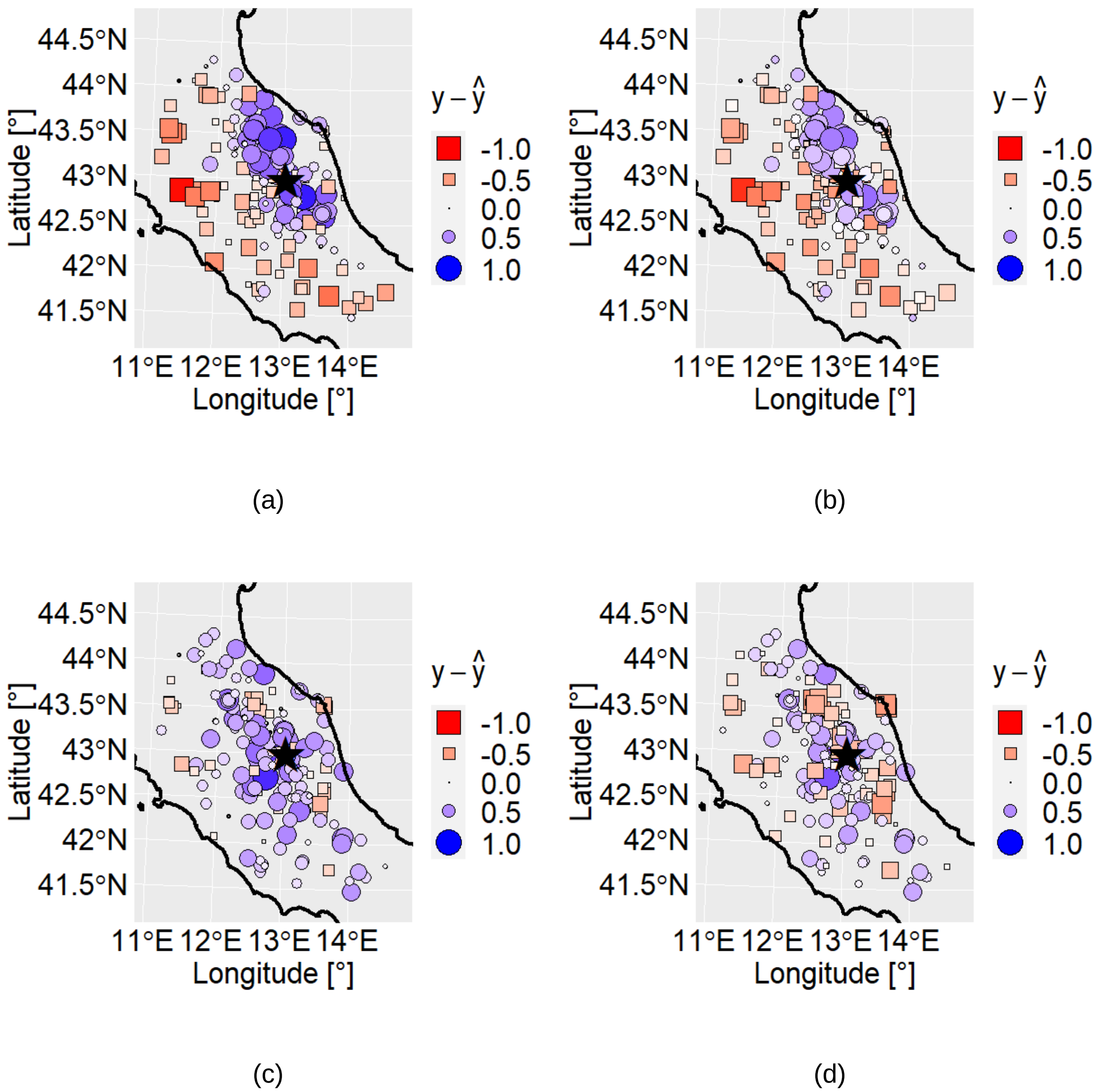

Figure 13. Total residuals of the 2018/04/10 M_W 4.6 Muccia earthquake: a) ITA18, SA-T=0.1s; b) MS-GWR, SA-T=0.1s; c) ITA18, SA-T=1s; b) MS-GWR, SA-T=1s.

Click here to access/download;Figure;figure1a.pdf

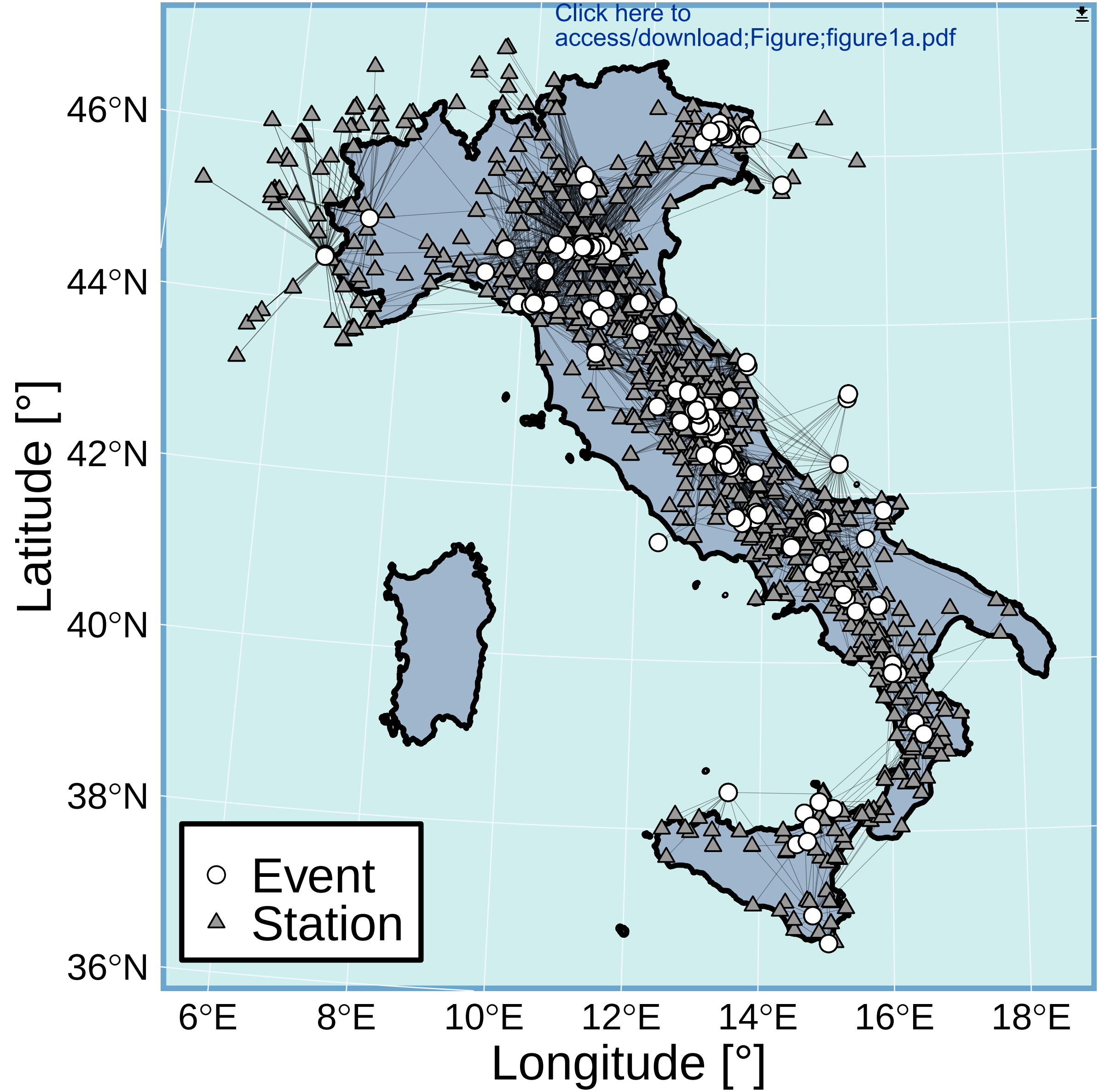

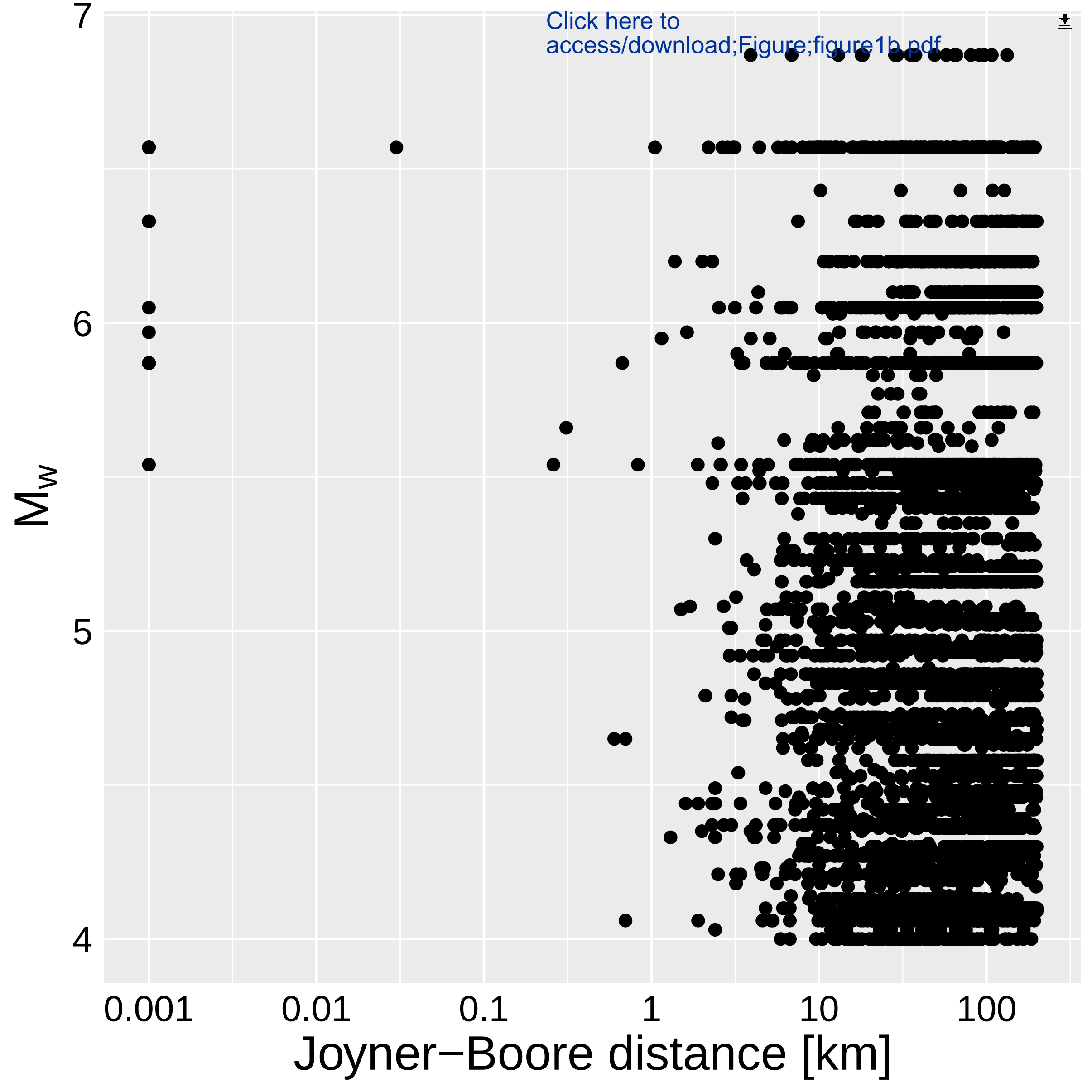

Click here to access/download;Figure;figure1b.pdf
7
6
5
4
Mw
0.001
0.01
0.1
1
10
100
Joyner−Boore distance [km]

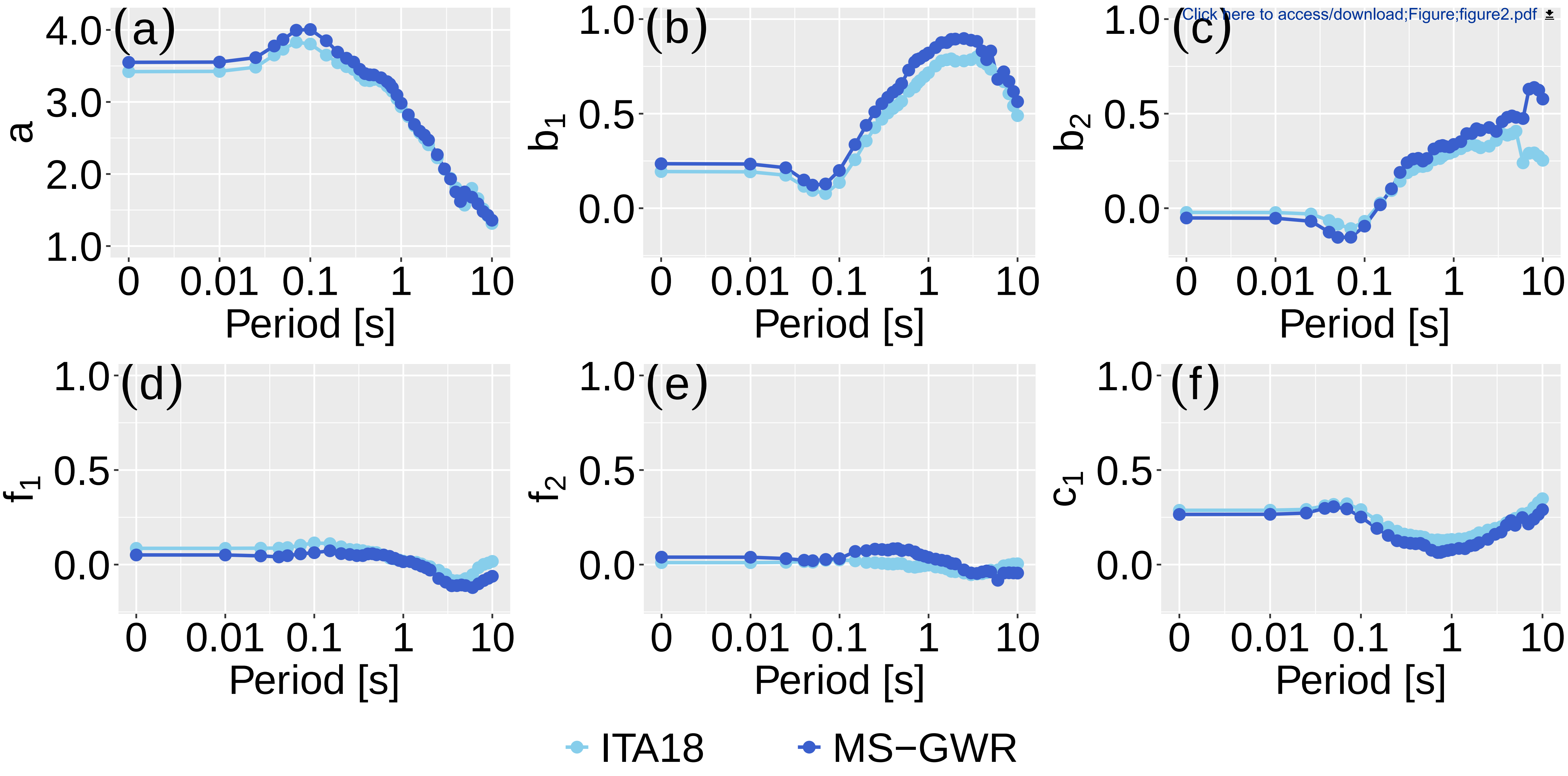
(a)
(b)
(c)
(d)
(e)
(f)
a
b1
b2
f1
f2
c1
Period [s]
0
0.01
0.1
1
10
1.0
2.0
3.0
4.0
0.0
0.5
1.0
ITA18
MS−GWR

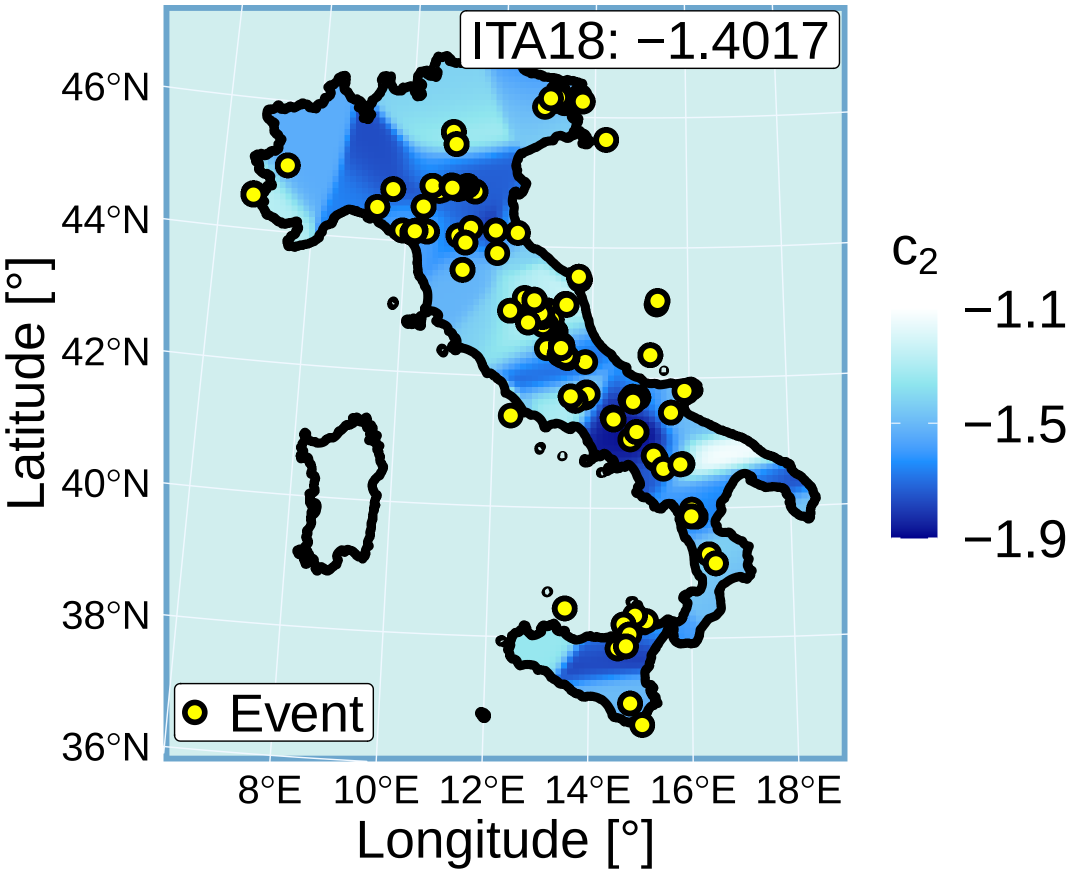
ITA18: −1.4017
46°N
44°N
42°N
40°N
38°N
36°N
Latitude [°]
8°E
10°E
12°E
14°E
16°E
18°E
Longitude [°]
Event
c_2
−1.1
−1.5
−1.9

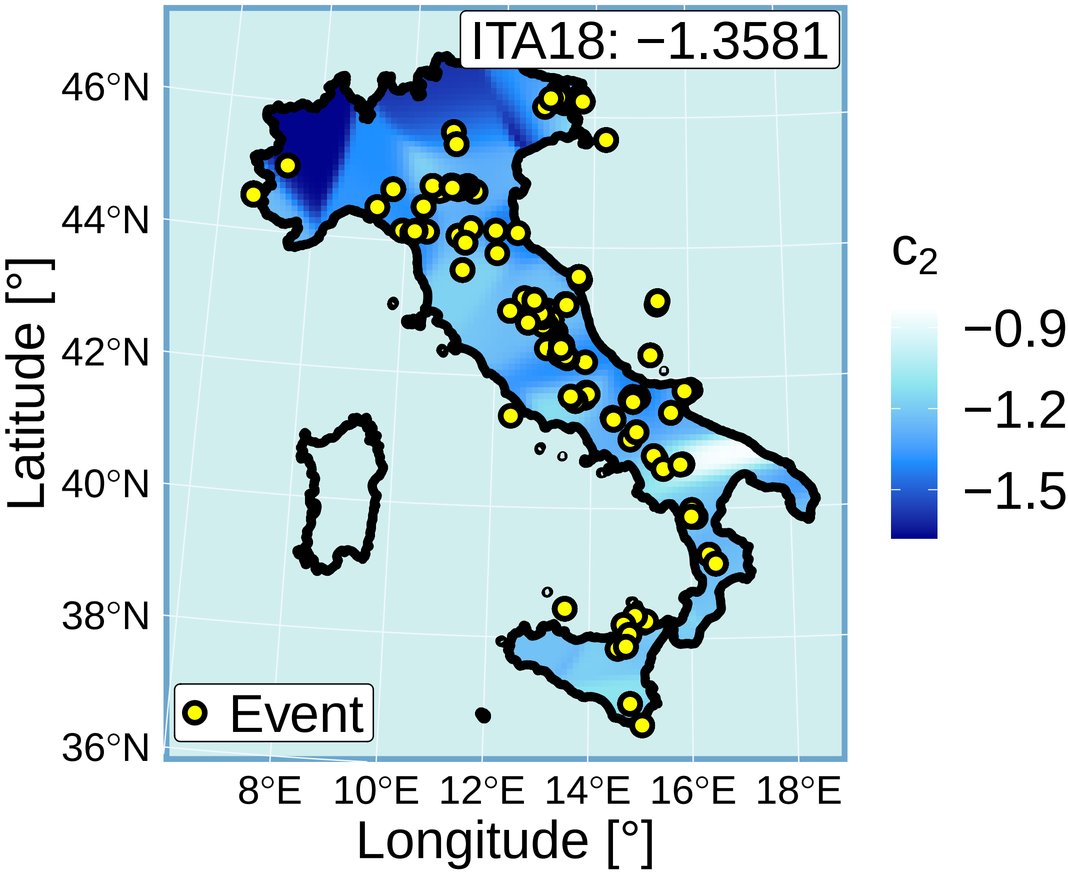
ITA18: −1.3581
46°N
44°N
42°N
40°N
38°N
36°N
Latitude [°]
8°E
10°E
12°E
14°E
16°E
18°E
Longitude [°]
Event
c_2
−0.9
−1.2
−1.5

Click here to access/download;Figure;figure3c.pdf

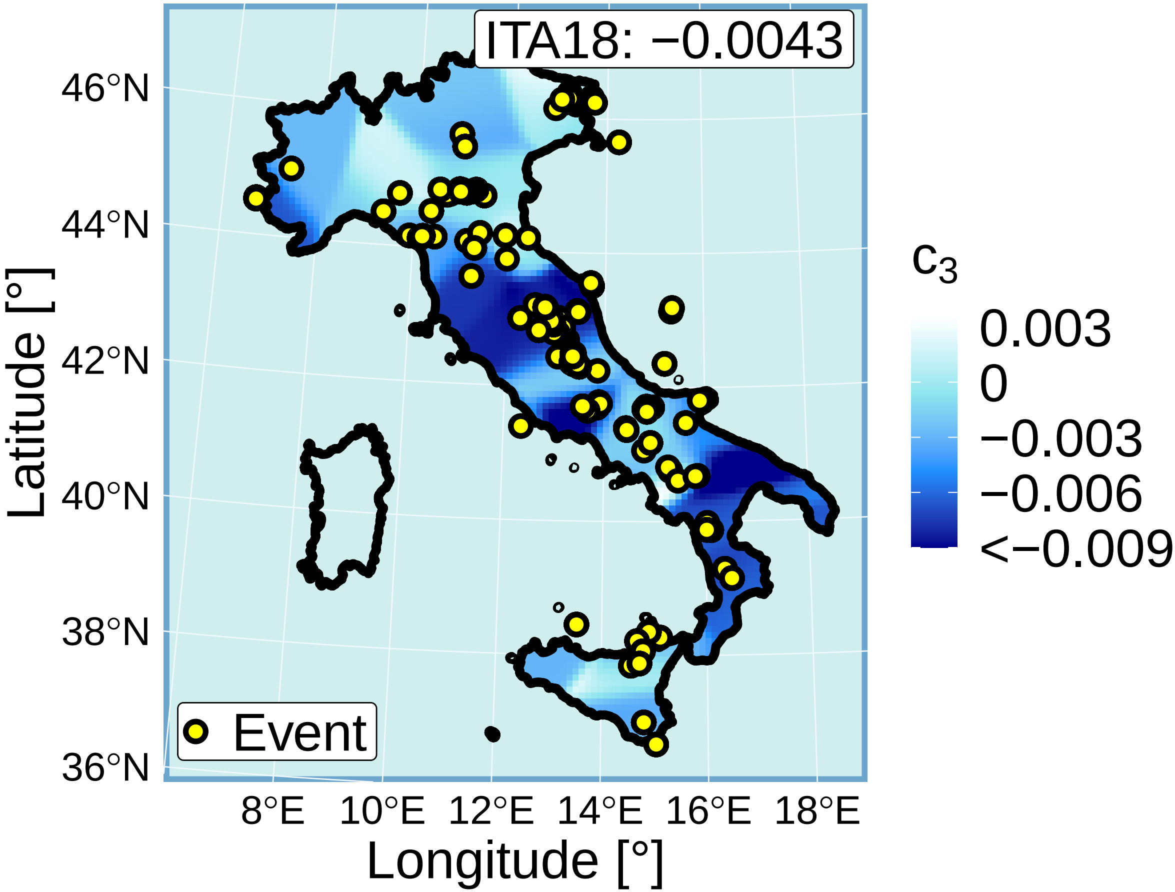

Click here to access/download;Figure;figure3d.pdf

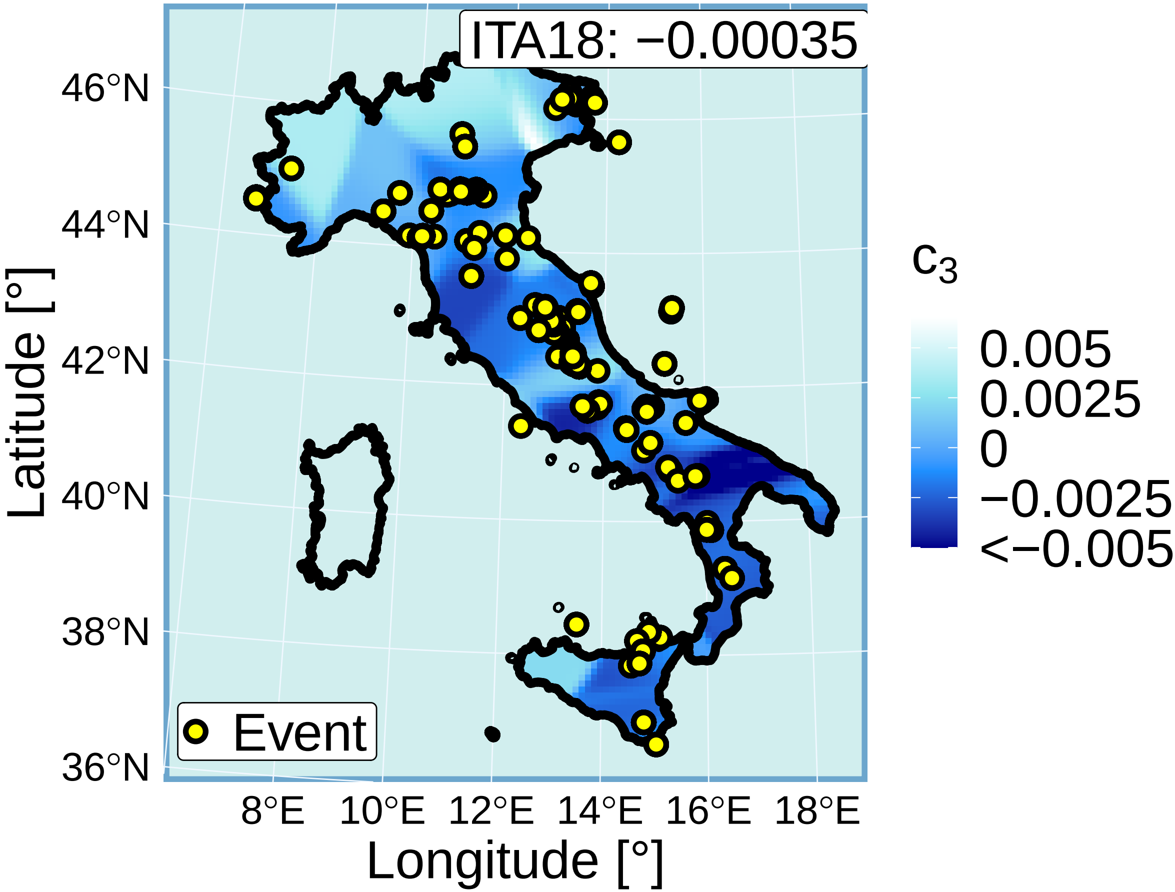

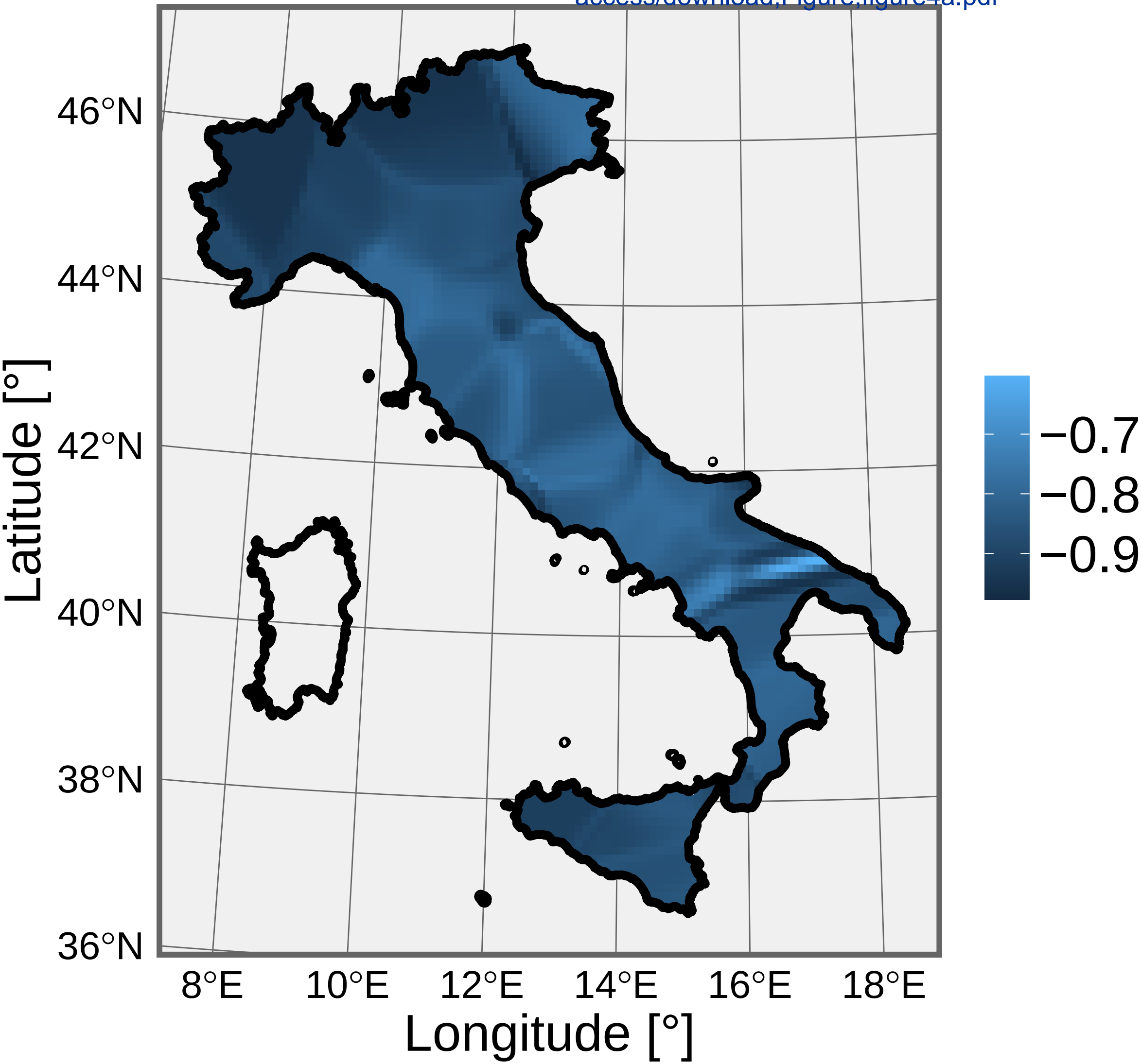
46°N
44°N
42°N
40°N
38°N
36°N
Latitude [°]
8°E
10°E
12°E
14°E
16°E
18°E
Longitude [°]
−0.7
−0.8
−0.9

Click here to access/download;Figure;figure4b.pdf

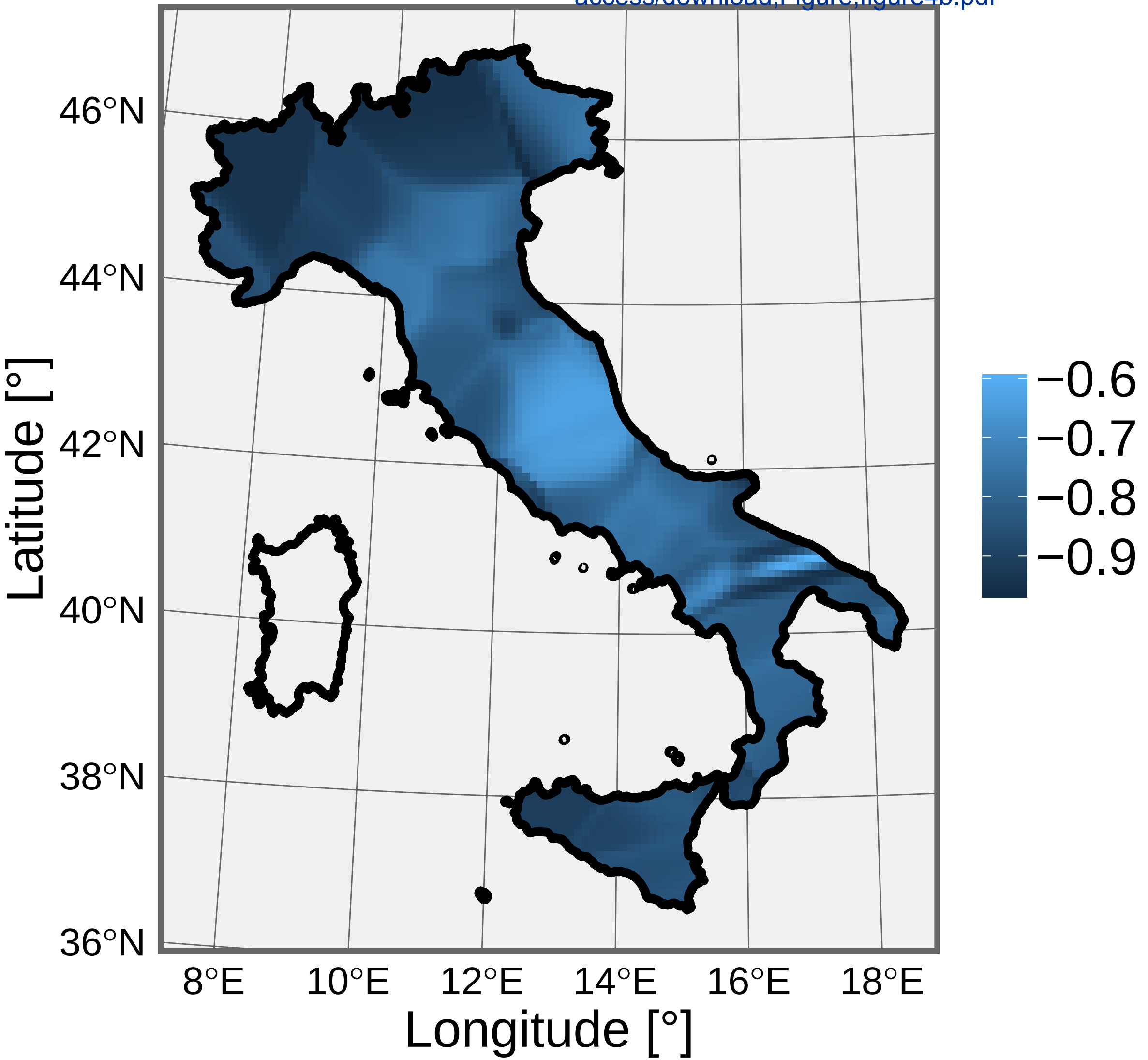

Click here to
access/download;Figure;figure5a.pdf

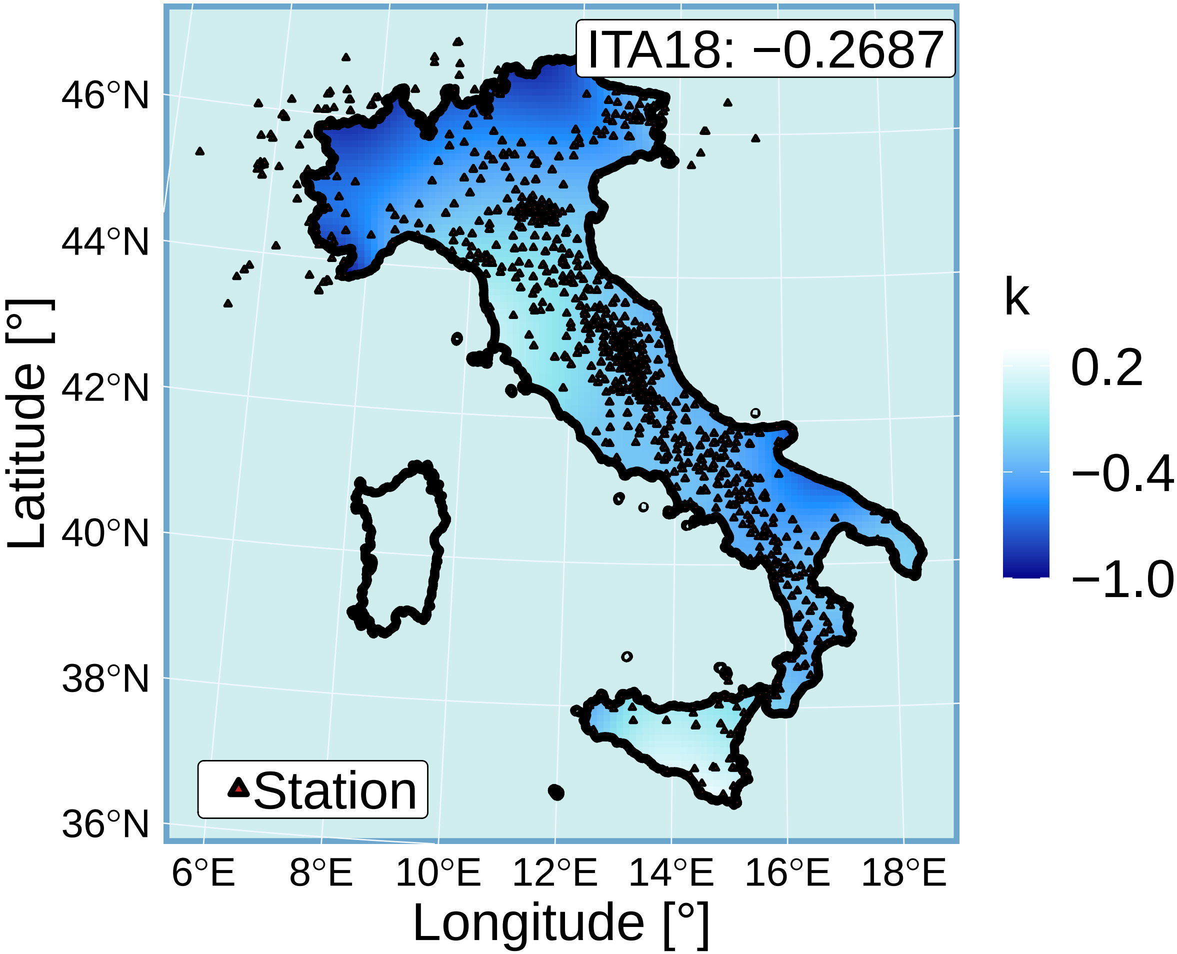

Click here to
access/download;Figure;figure5b.pdf

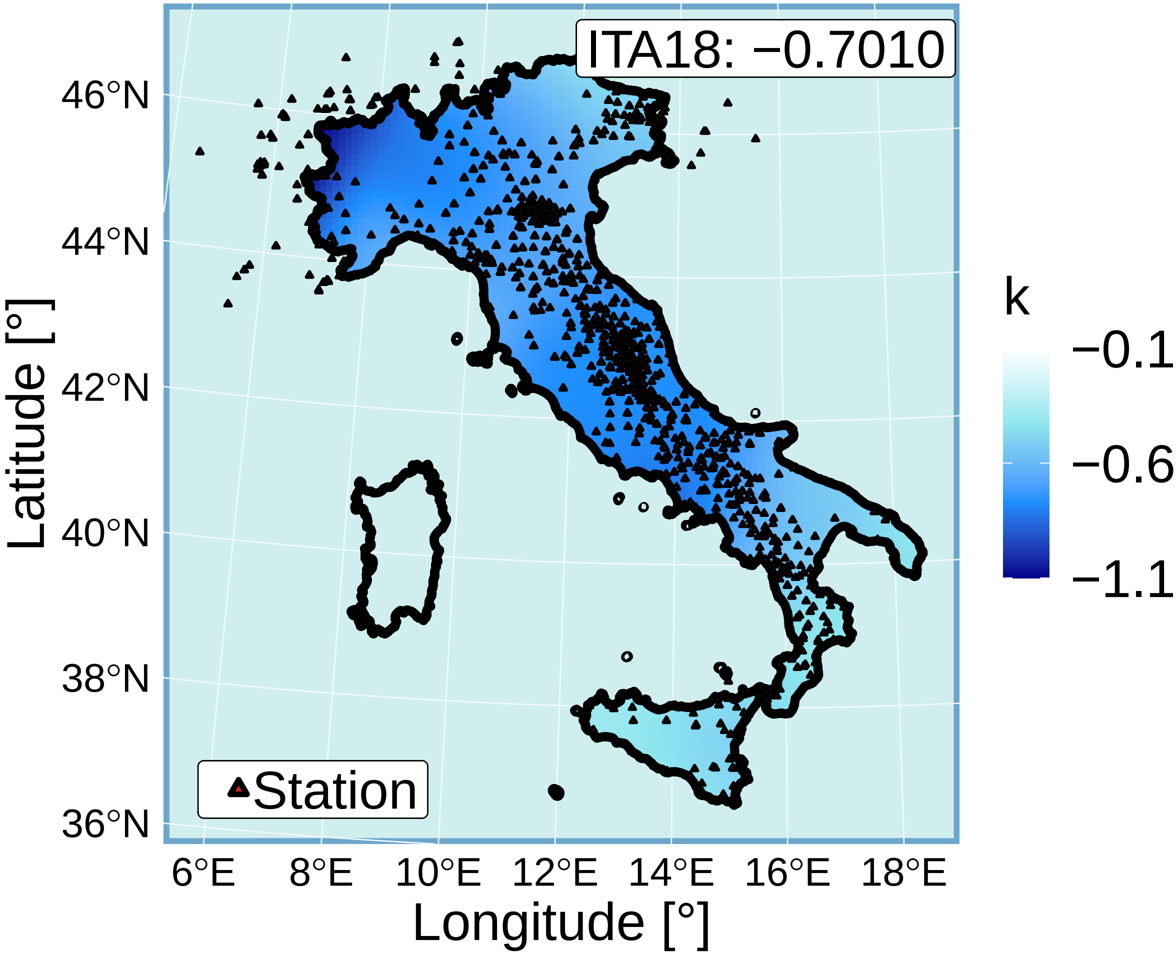

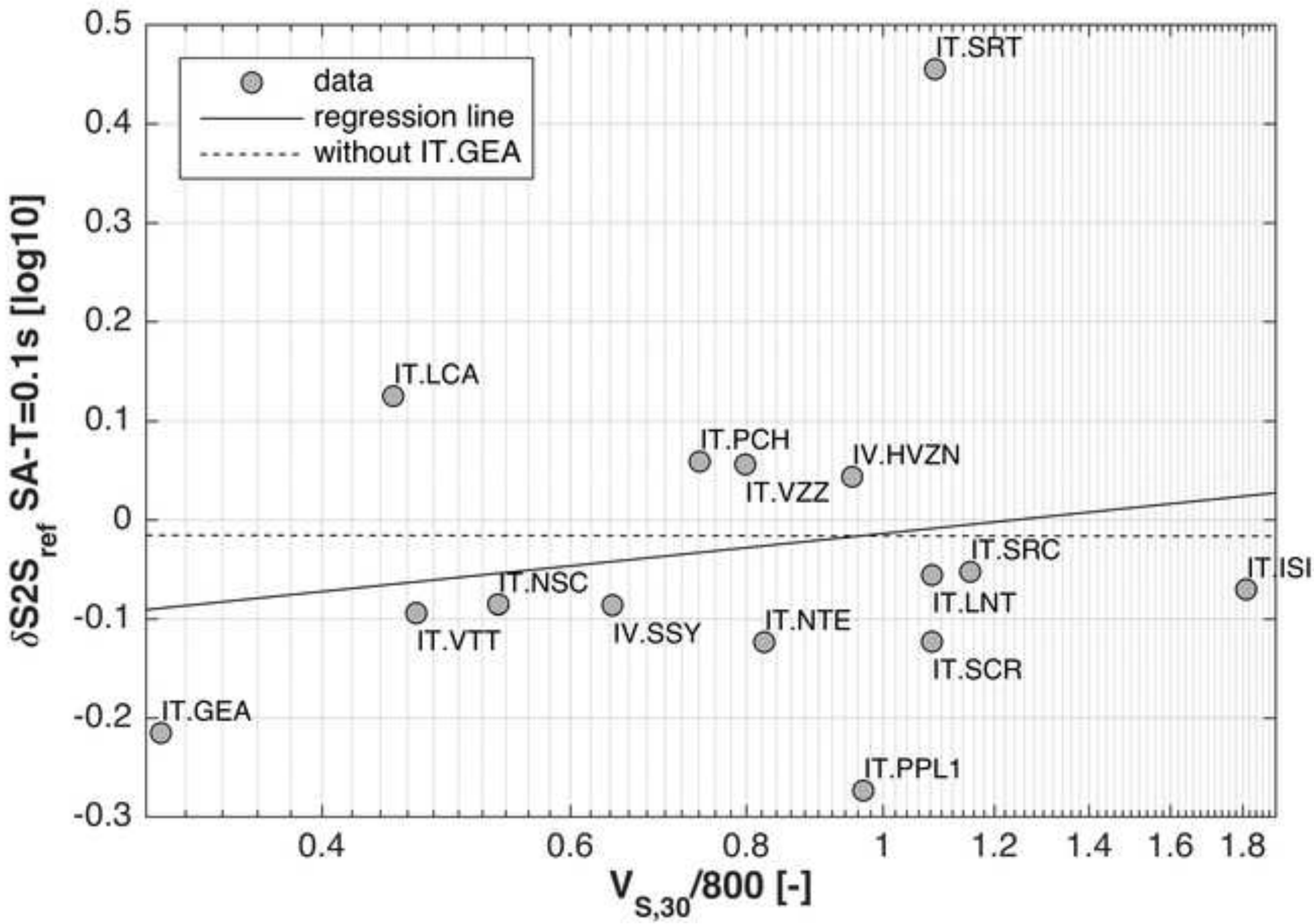
data
regression line
without IT.GEA
IT.SRT
IT.LCA
IT.PCH
IT.VZZ
IV.HVZN
IT.SRC
IT.ISI
IT.LNT
IT.NSC
IT.VTT
IV.SSY
IT.NTE
IT.SCR
IT.GEA
IT.PPL1
0.5
0.4
0.3
0.2
0.1
0
-0.1
-0.2
-0.3
0.4
0.6
0.8
1
1.2
1.4
1.6
1.8
$\delta S2S_{ref}$ SA-T=0.1s [log10]
$V_{S,30}$/800 [-]

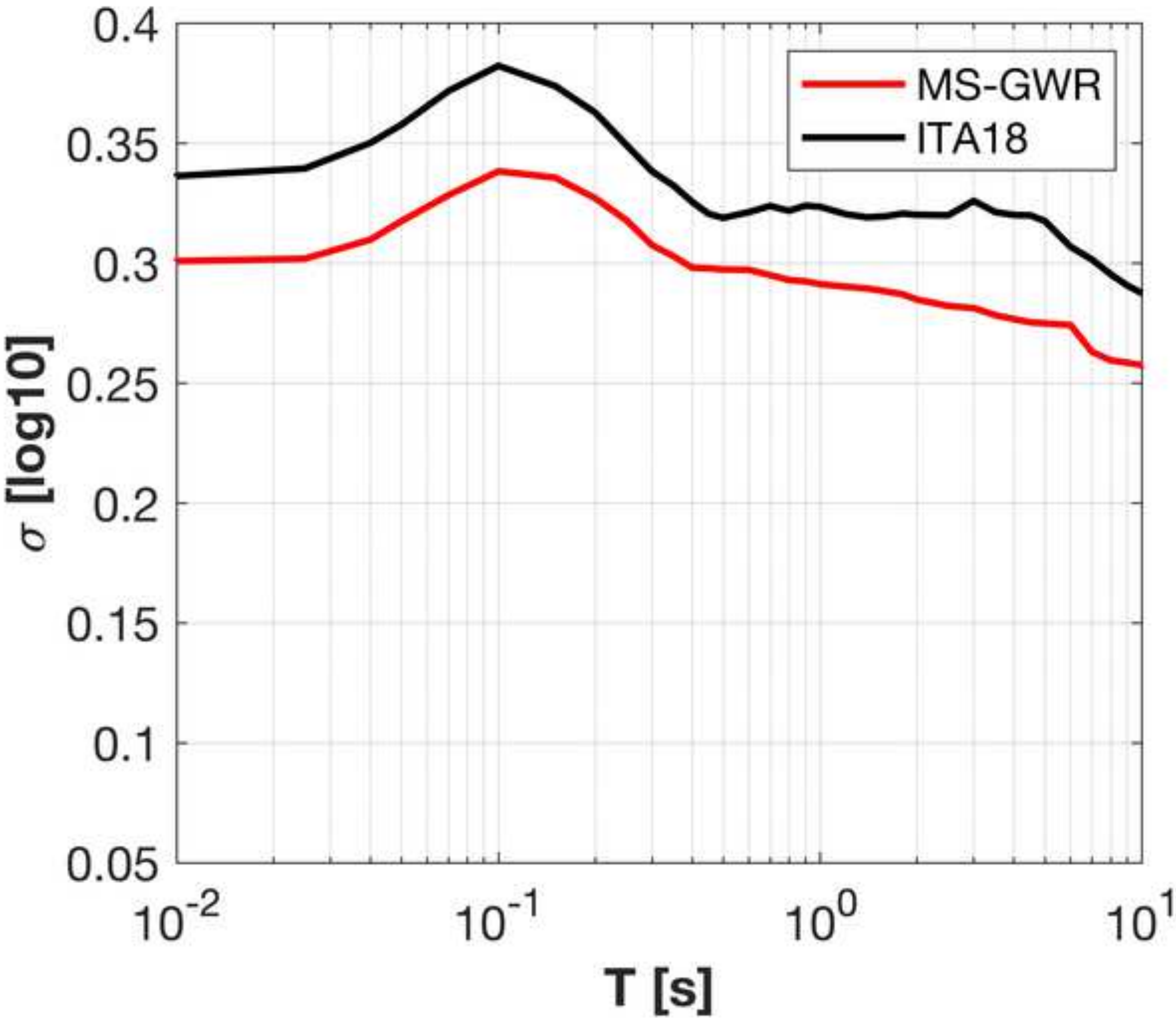
0.4
0.35
0.3
0.25
0.2
0.15
0.1
0.05
σ [log10]
10^-2
10^-1
10^0
10^1
T [s]
MS-GWR
ITA18

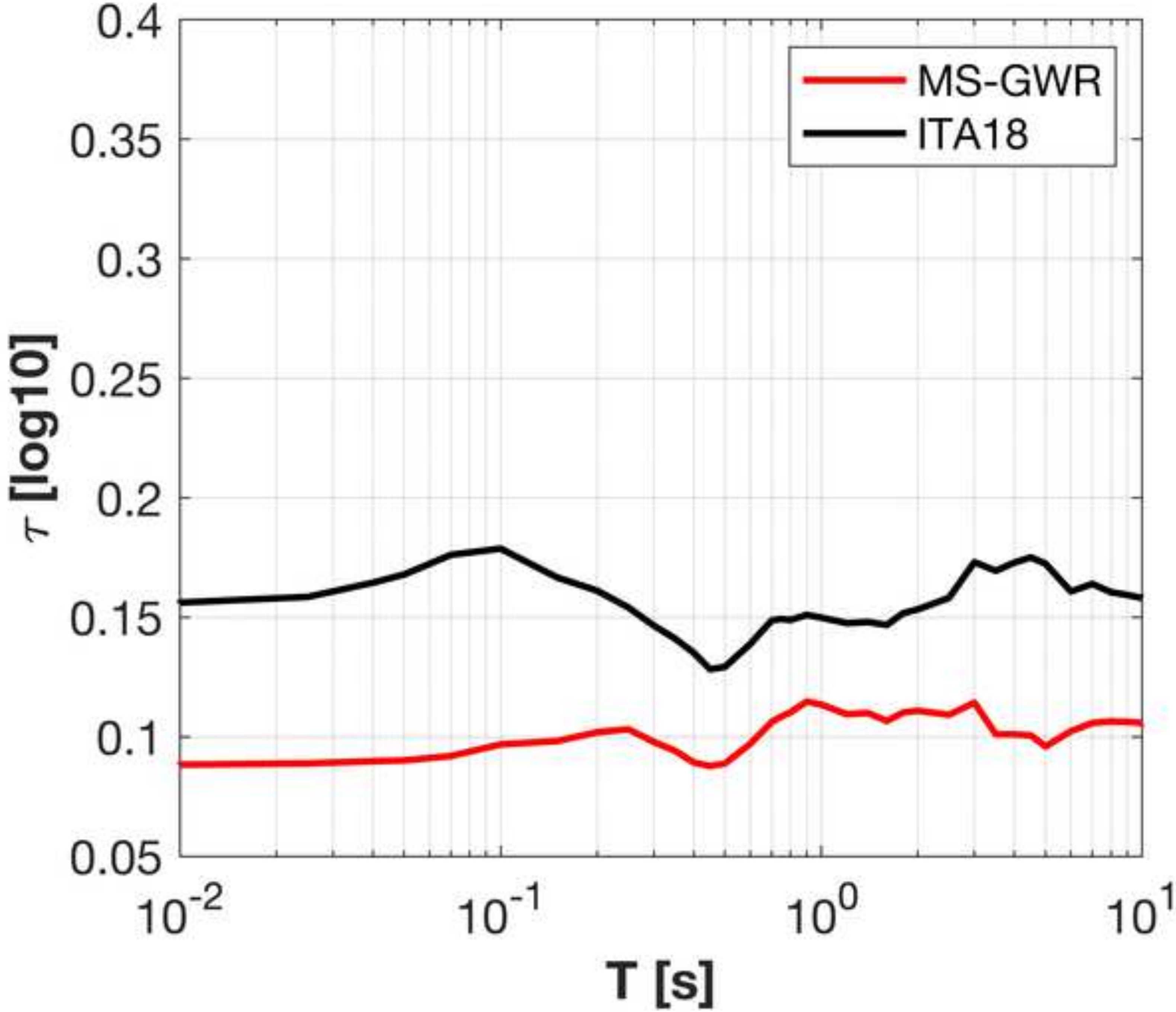
MS-GWR
ITA18
0.4
0.35
0.3
0.25
0.2
0.15
0.1
0.05
τ [log10]
10^{-2}
10^{-1}
10^{0}
10^{1}
T [s]

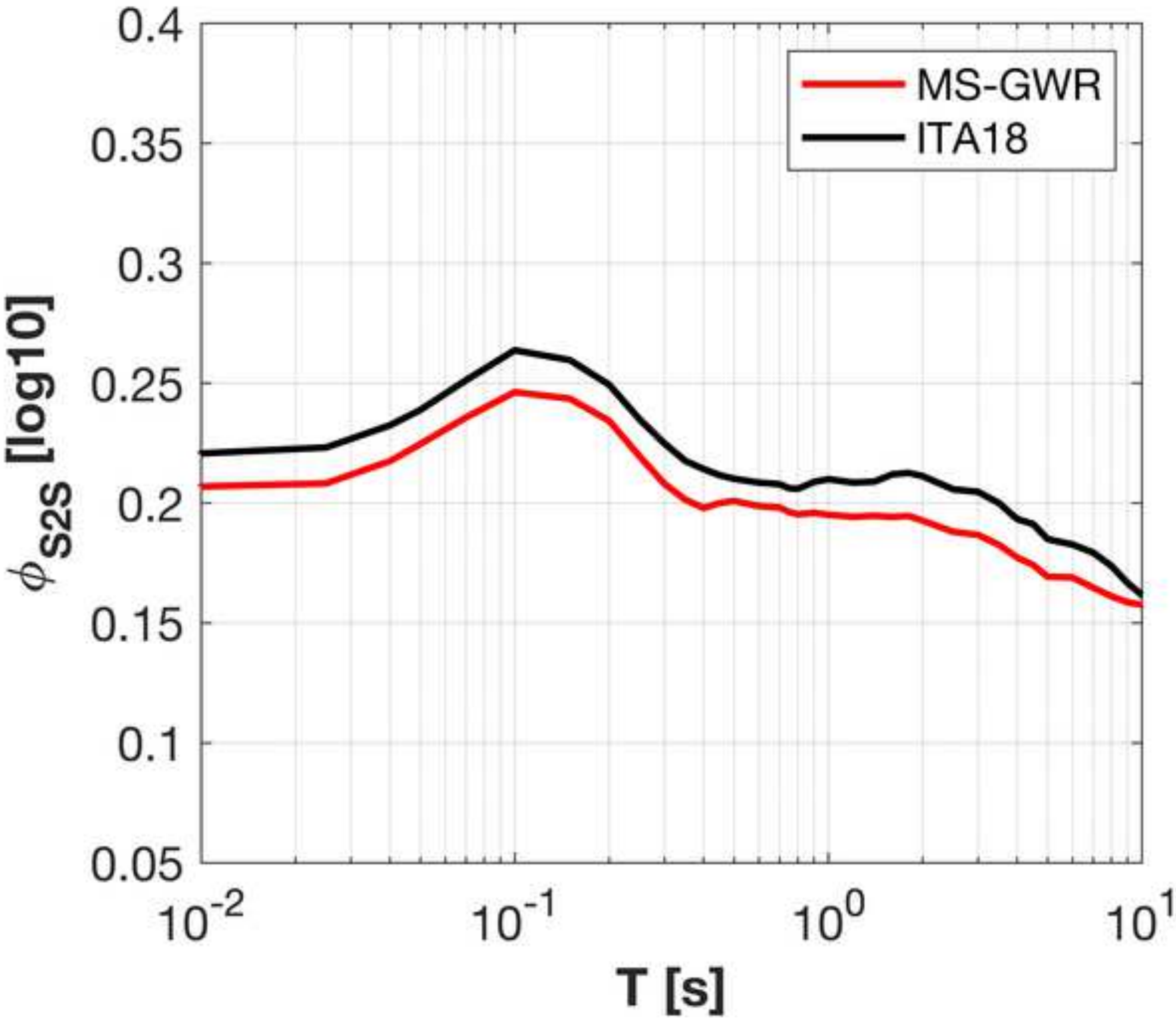
MS-GWR
ITA18
0.4
0.35
0.3
0.25
0.2
0.15
0.1
0.05
ϕ_{S2S} [log10]
10^{-2}
10^{-1}
10^{0}
10^{1}
T [s]

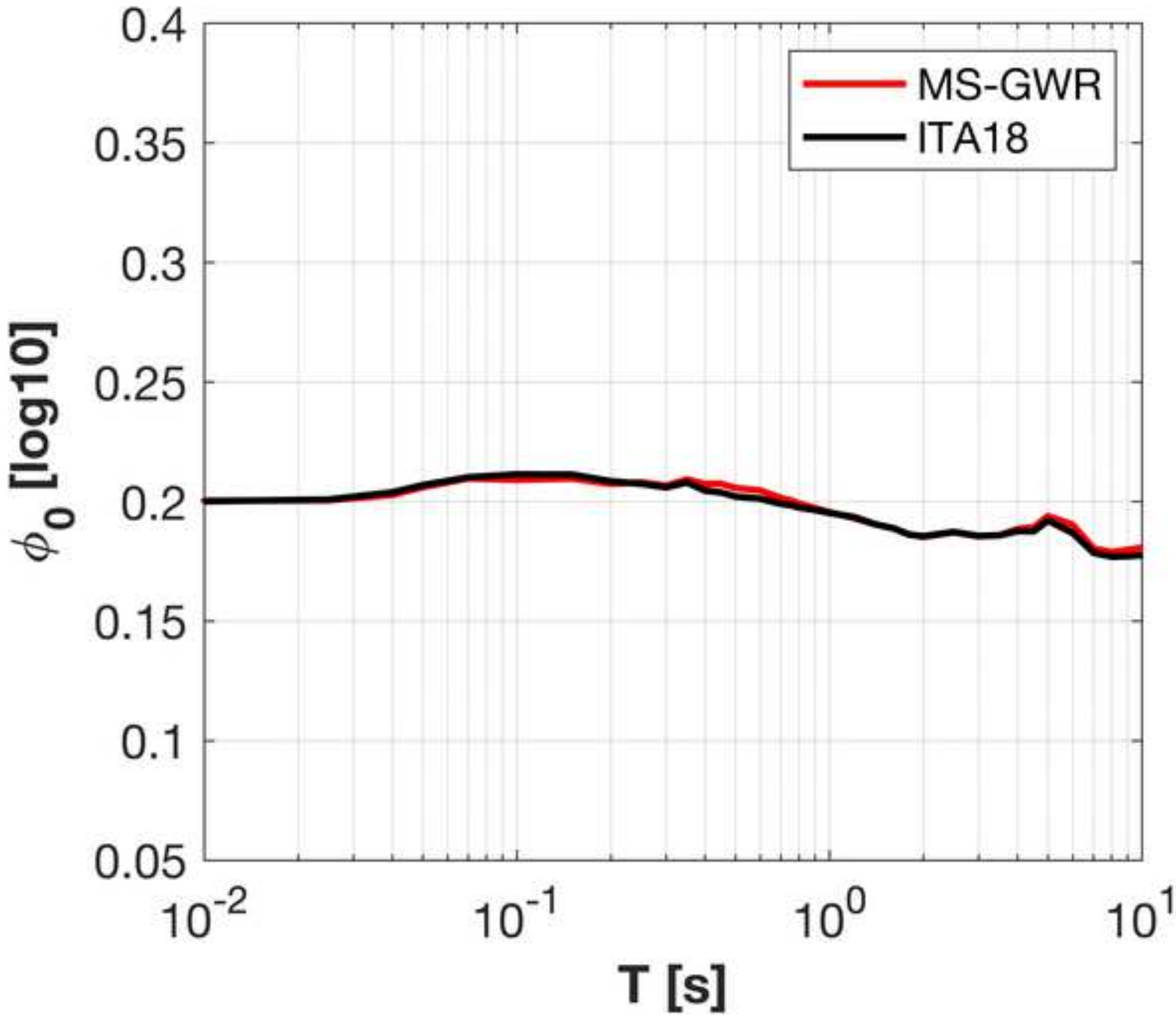
MS-GWR
ITA18
0.4
0.35
0.3
0.25
0.2
0.15
0.1
0.05
ϕ_0 [log10]
10^{-2}
10^{-1}
10^{0}
10^{1}
T [s]

Click here to access/download;Figure;figure8a.pdf

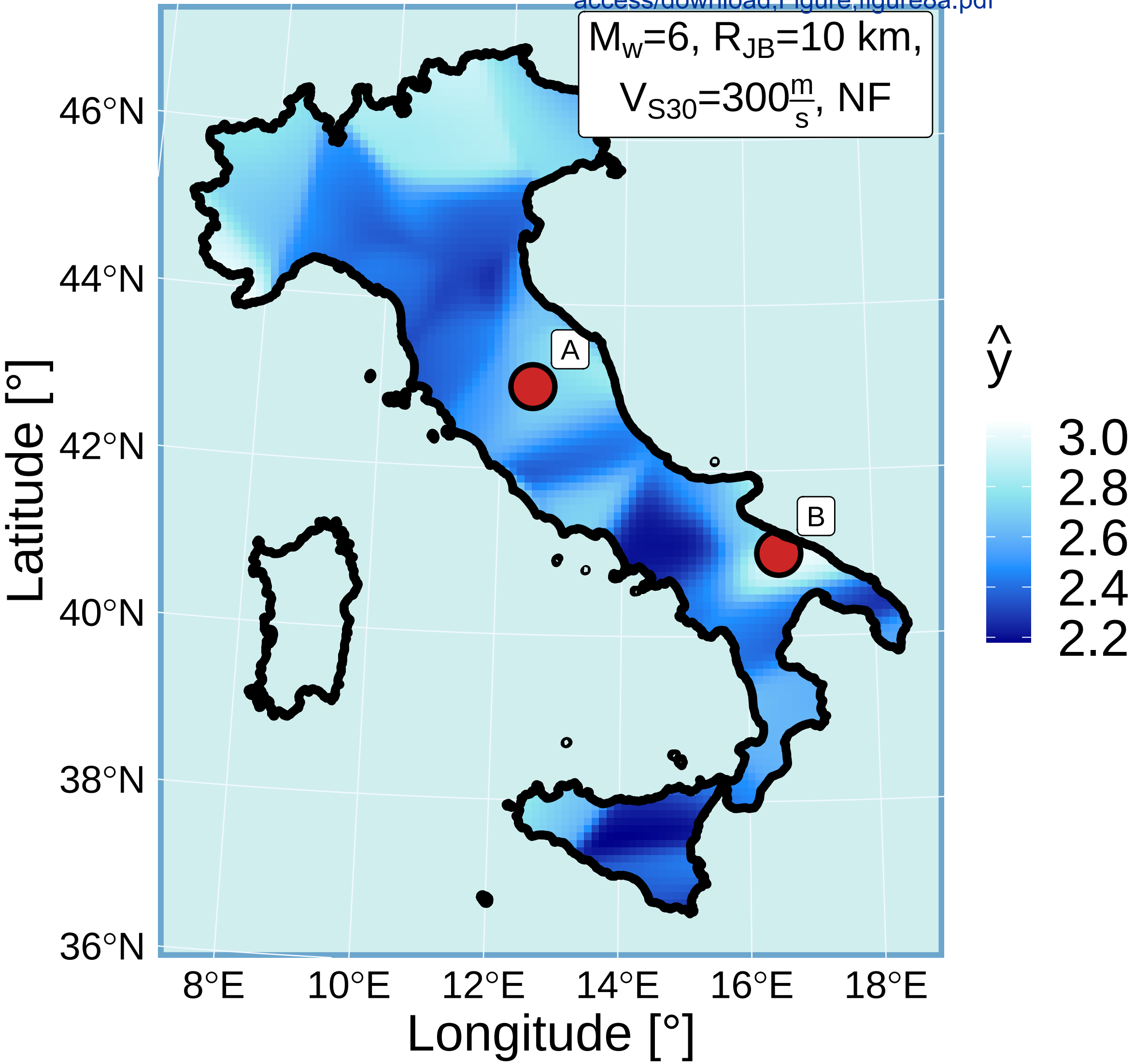

Click here to access/download;Figure;figure8b.pdf

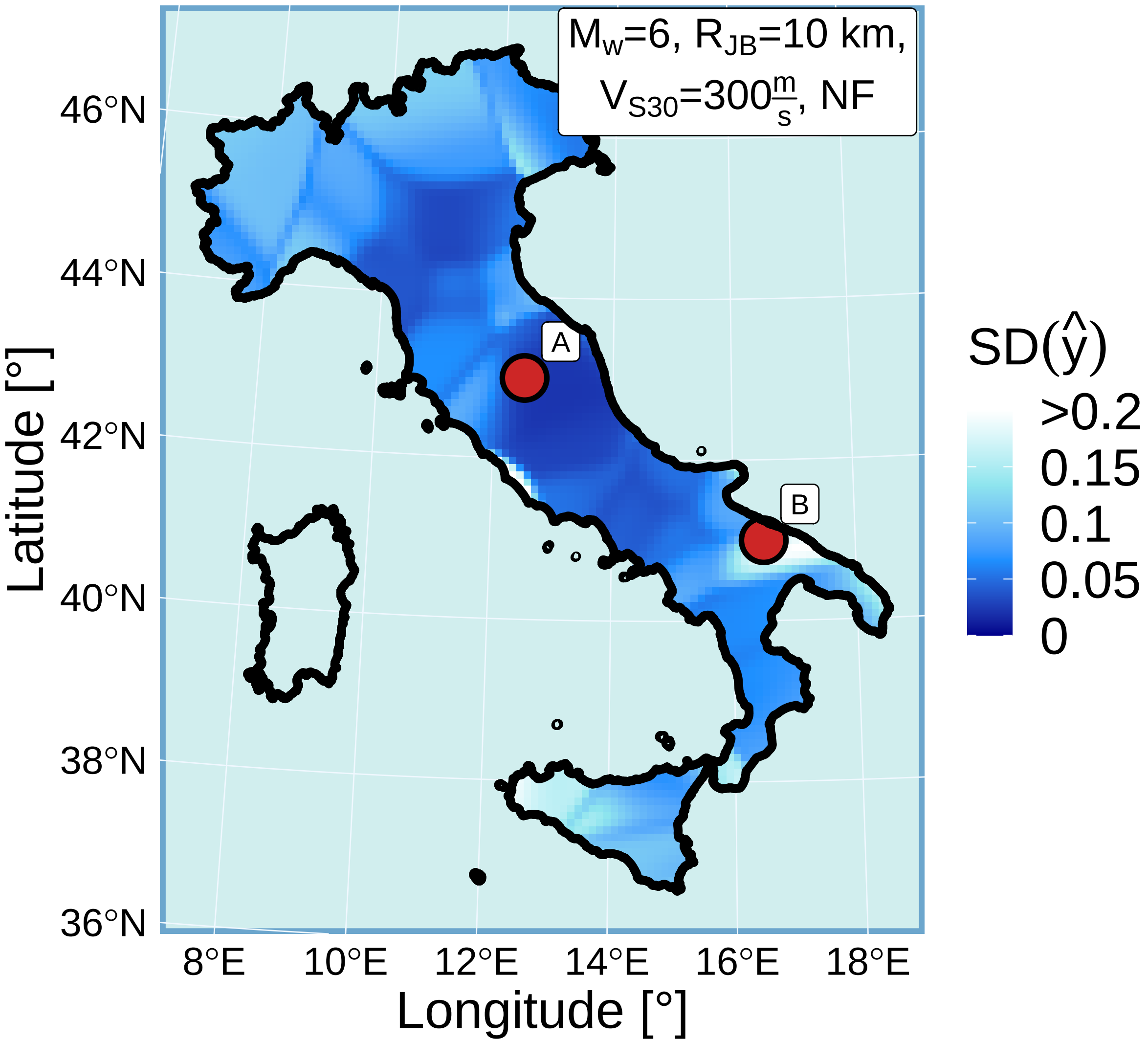

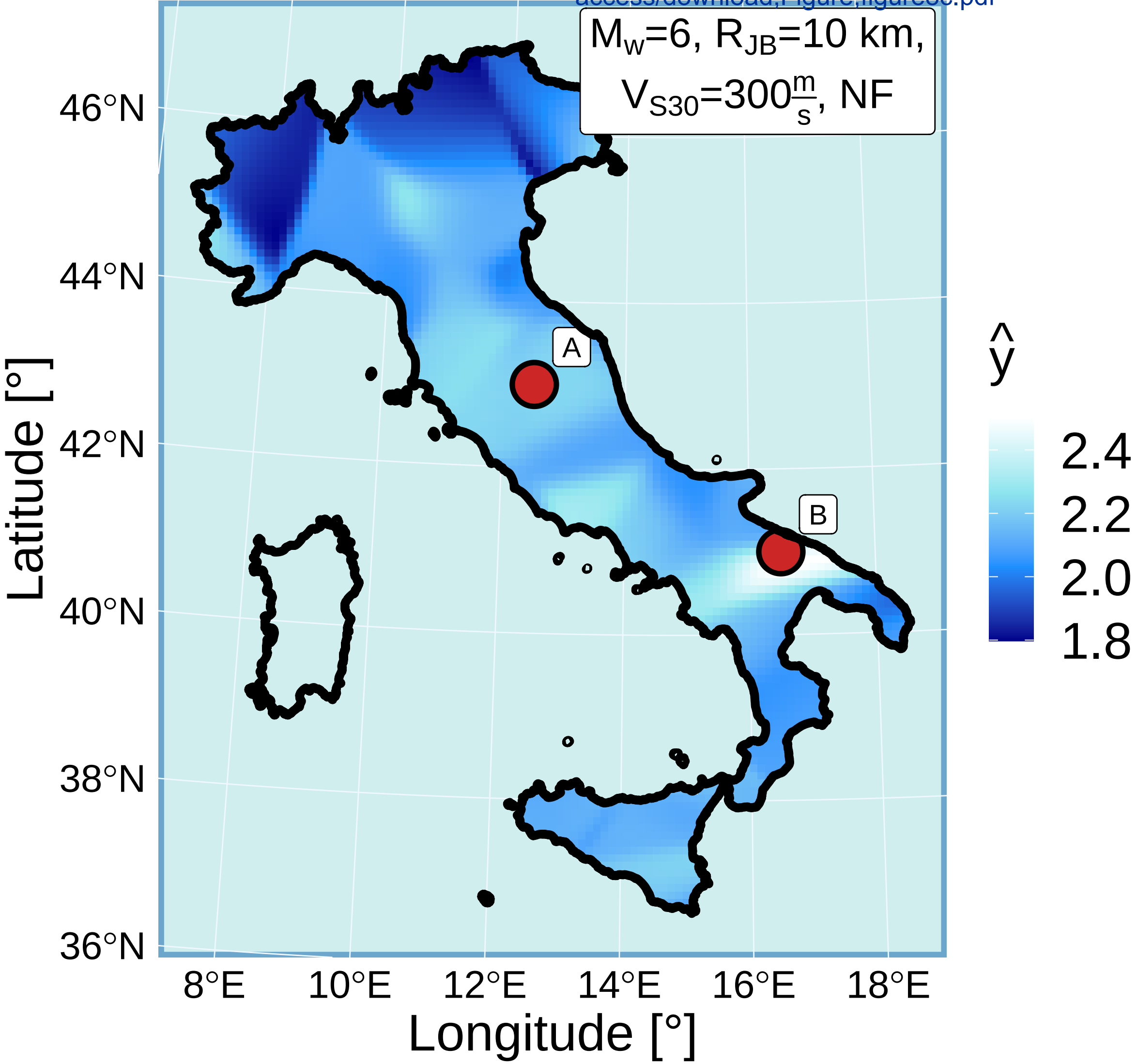
M_w=6, R_{JB}=10 km,
V_{S30}=300$\frac{m}{s}$, NF
A
B
46°N
44°N
42°N
40°N
38°N
36°N
8°E
10°E
12°E
14°E
16°E
18°E
Latitude [°]
Longitude [°]
$\hat{y}$
2.4
2.2
2.0
1.8

Click here to access/download;Figure;figure8d.pdf

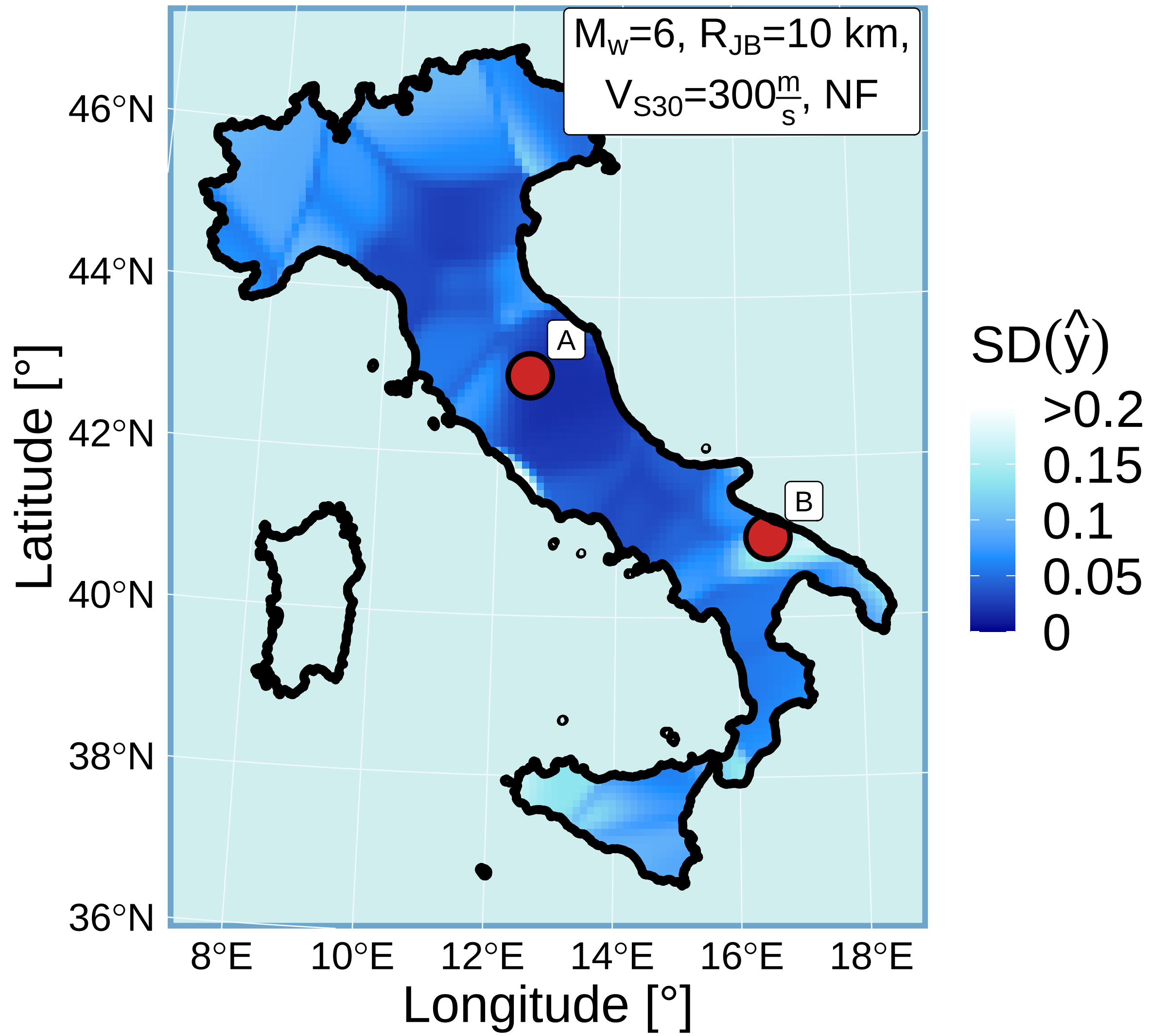

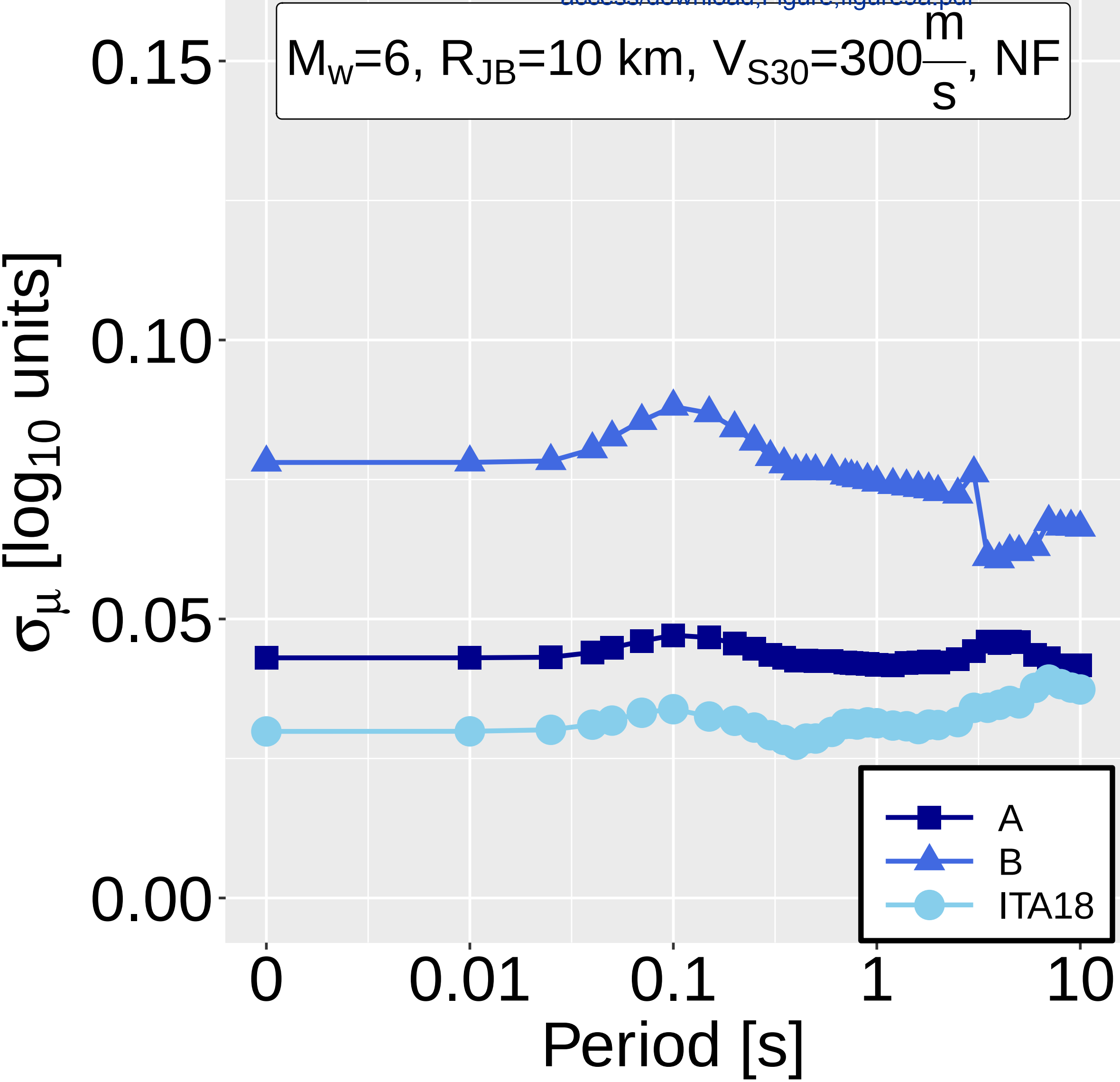
M_W=6, R_{JB}=10 km, V_{S30}=300$\frac{m}{s}$, NF
0.15
0.10
0.05
0.00
σ_μ [$\log_{10}$ units]
0
0.01
0.1
1
10
Period [s]
A
B
ITA18

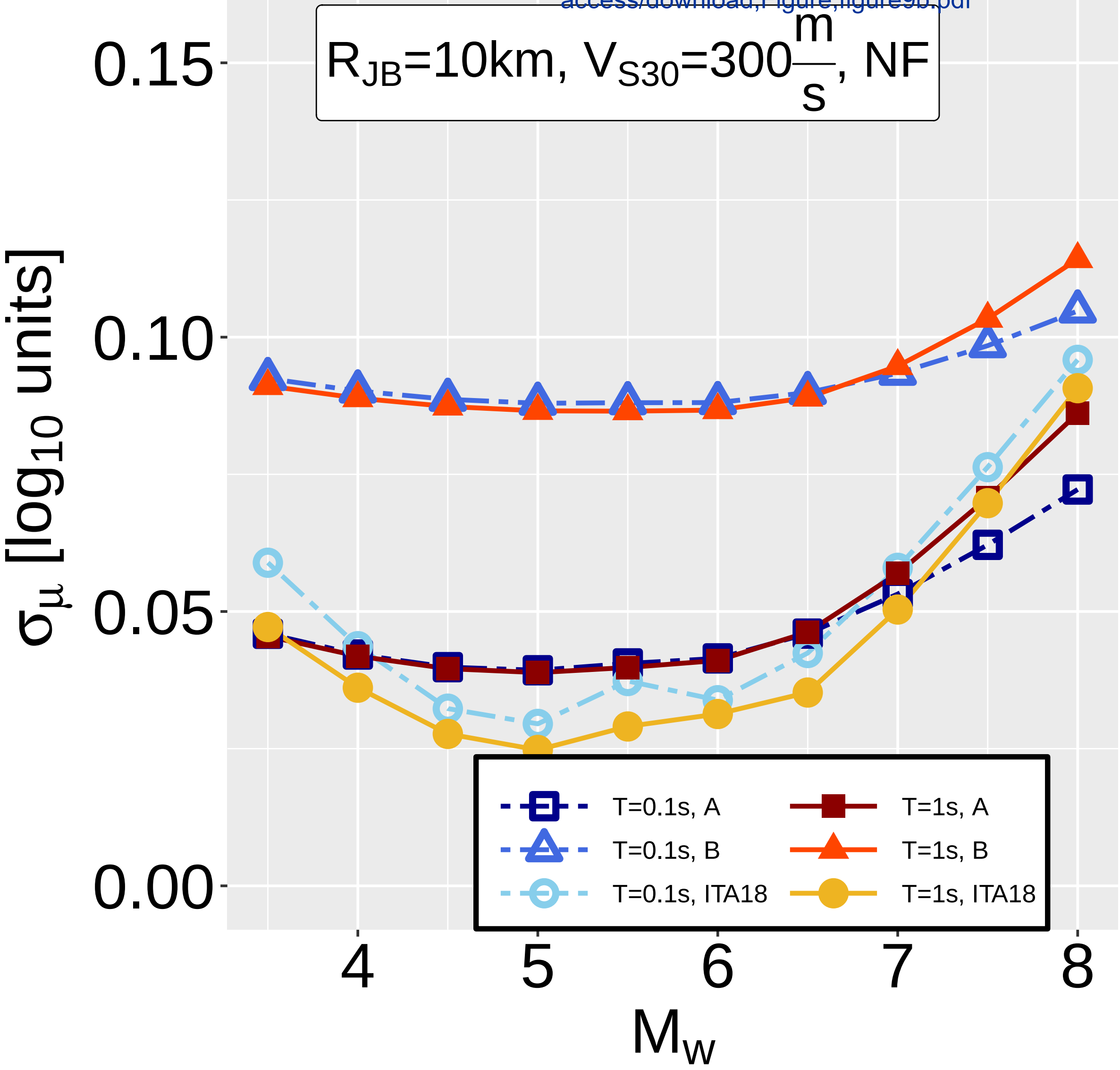
R_{JB}=10km, V_{S30}=300$\frac{m}{s}$, NF
0.15
0.10
0.05
0.00
σ_μ [$\log_{10}$ units]
4
5
6
7
8
M_W
T=0.1s, A
T=0.1s, B
T=0.1s, ITA18
T=1s, A
T=1s, B
T=1s, ITA18

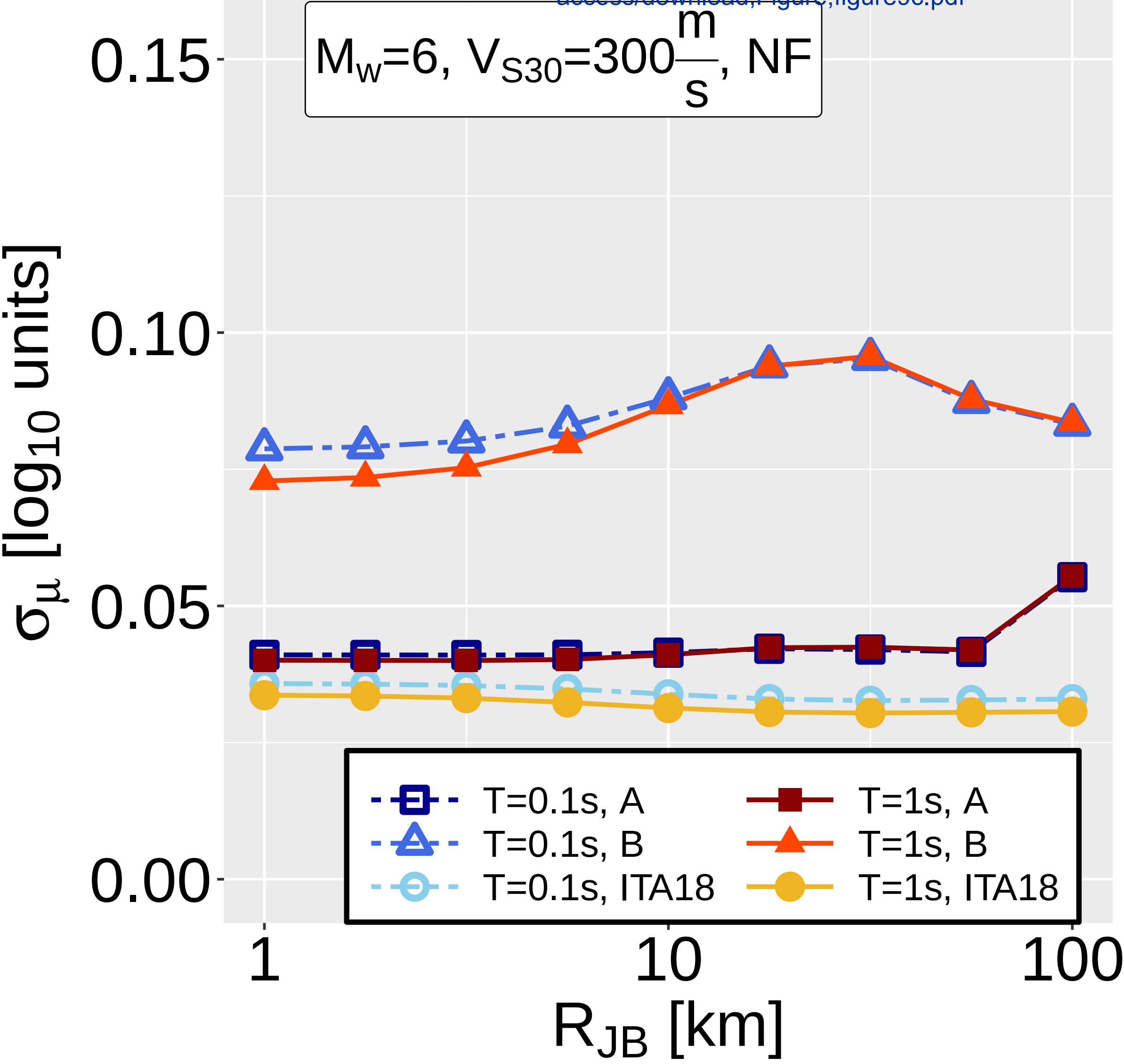
M_w=6, V_{S30}=300$\frac{m}{s}$, NF
0.15
0.10
0.05
0.00
σ_μ [$\log_{10}$ units]
1
10
100
R_{JB} [km]
T=0.1s, A
T=0.1s, B
T=0.1s, ITA18
T=1s, A
T=1s, B
T=1s, ITA18

Click here to access/download;Figure;figure9d.pdf

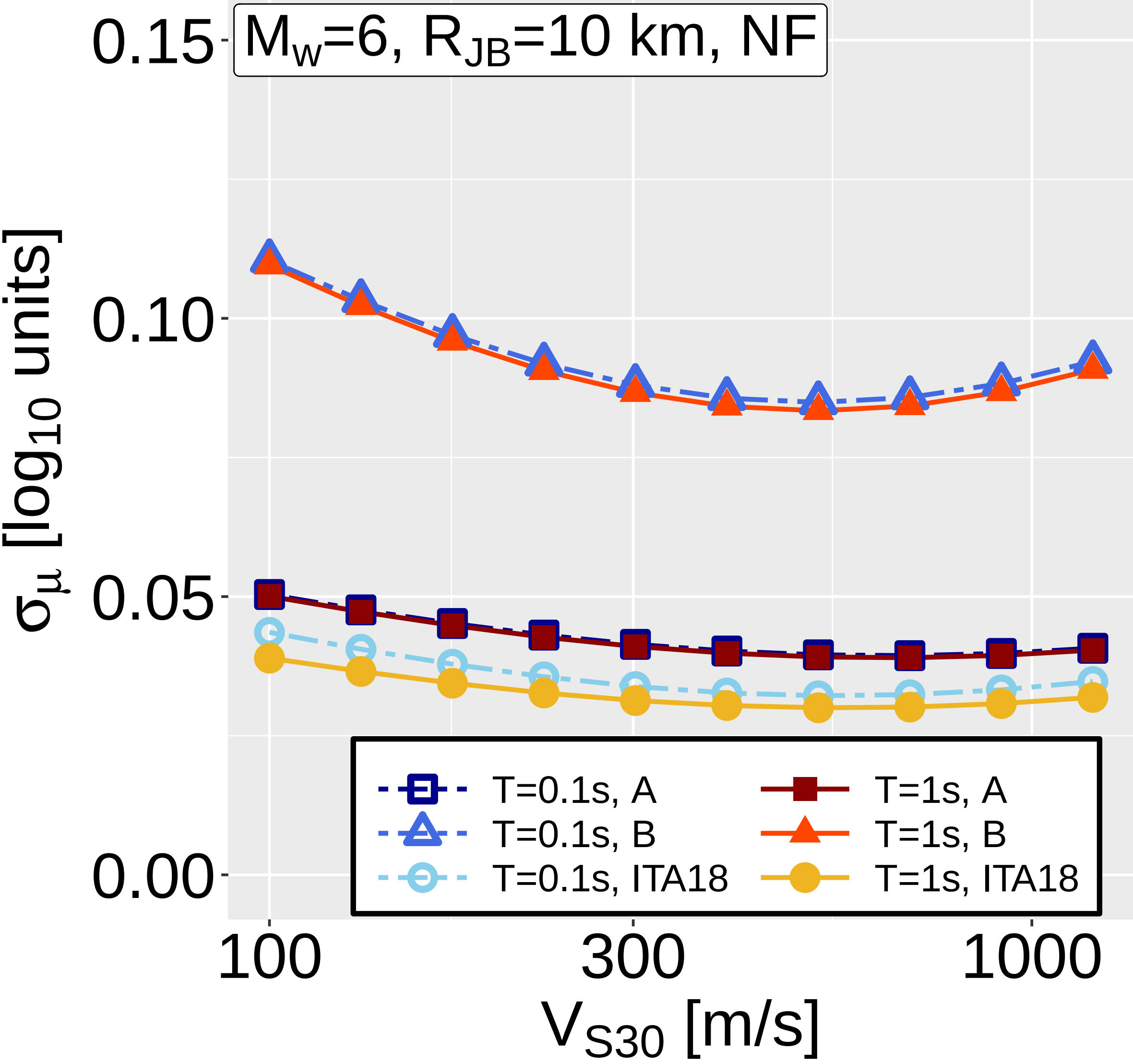

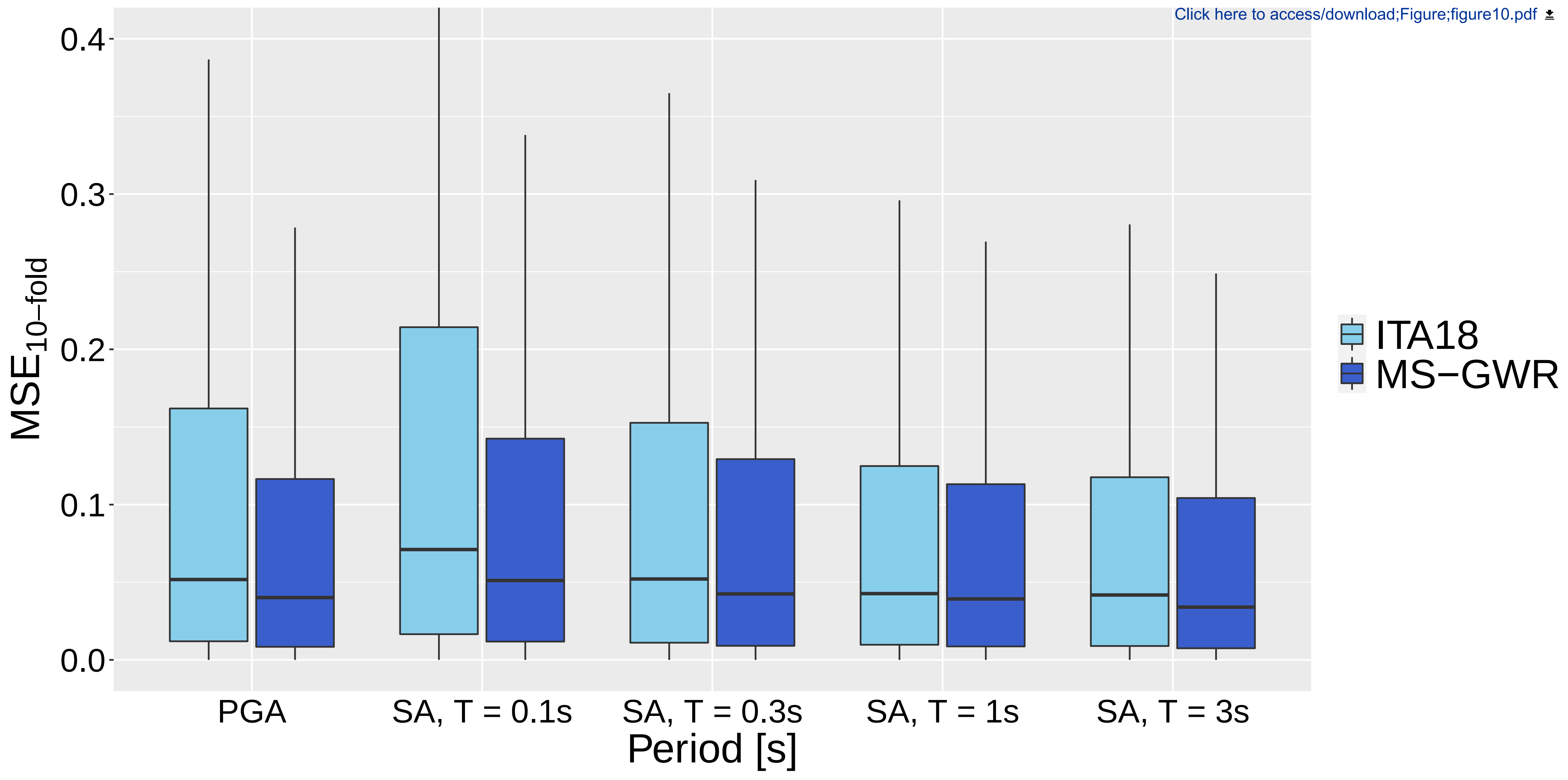
MSE$_{10\text{-fold}}$
0.4
0.3
0.2
0.1
0.0
PGA
SA, T = 0.1s
SA, T = 0.3s
SA, T = 1s
SA, T = 3s
Period [s]
ITA18
MS−GWR

Click here to access/download;Figure;figure11.pdf

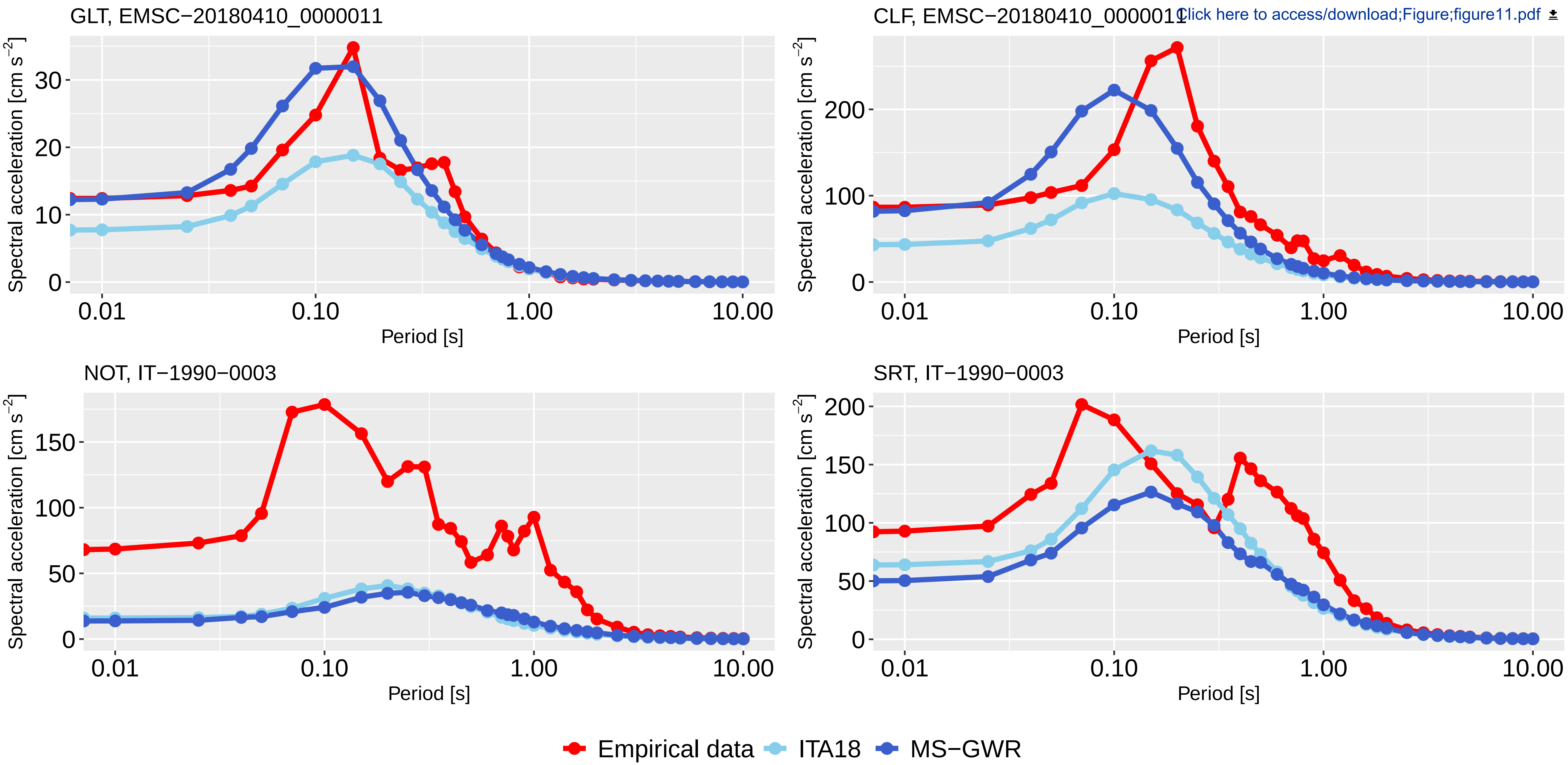

Click here to access/download;Figure;figure12a.pdf

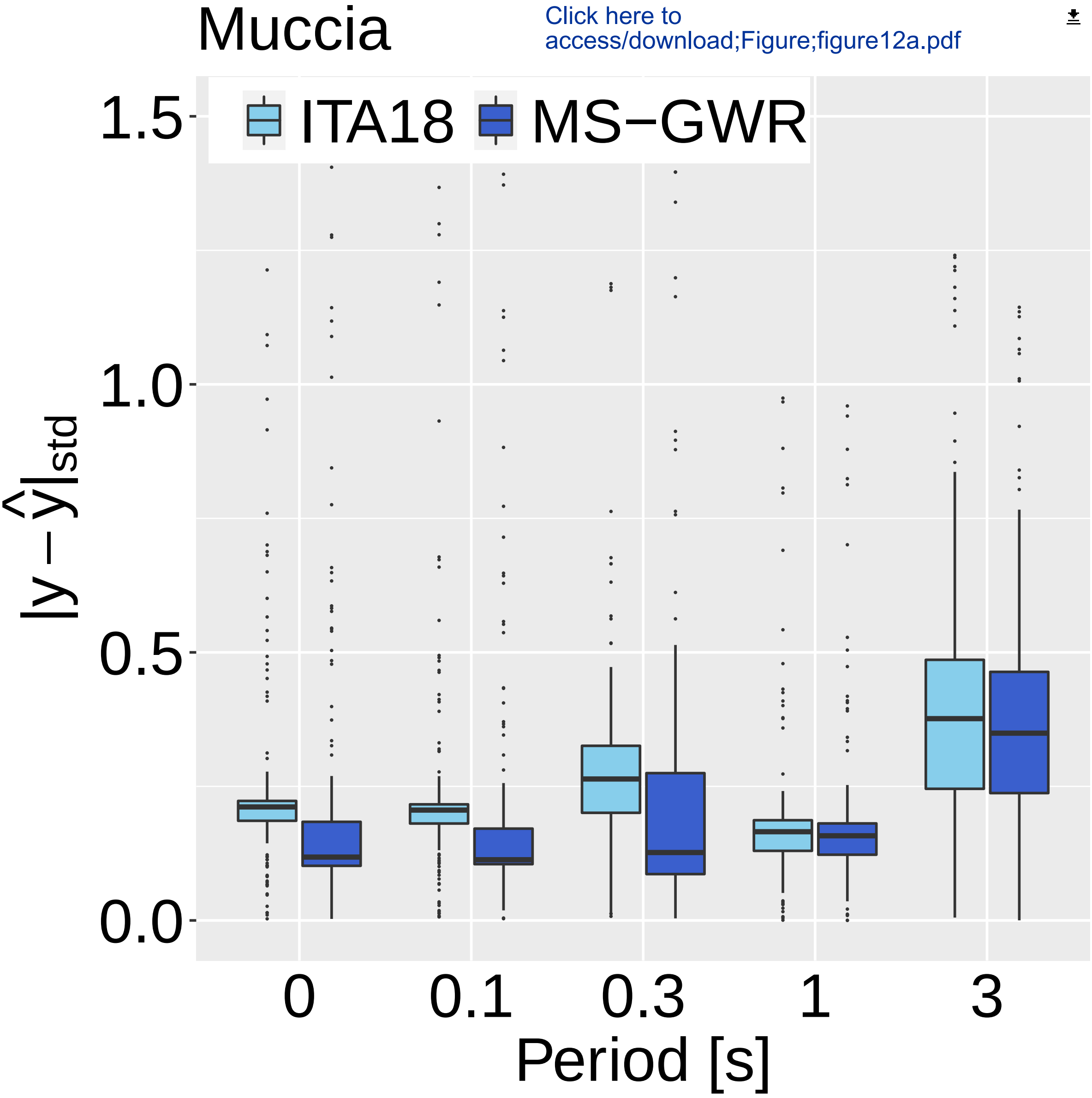

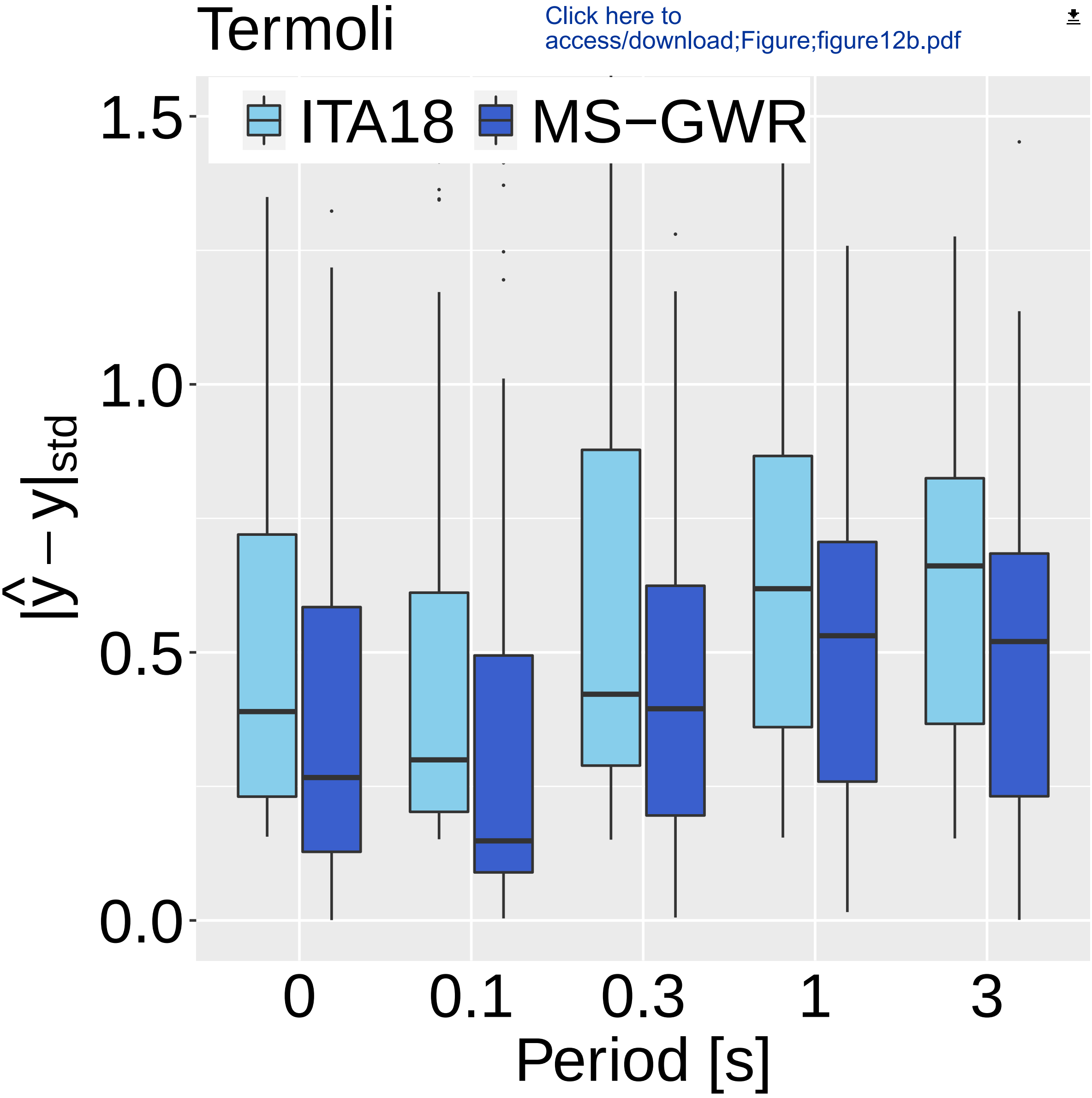
Termoli
ITA18
MS−GWR
1.5
1.0
0.5
0.0
$|\hat{y} - y|_{std}$
0
0.1
0.3
1
3
Period [s]

Click here to access/download;Figure;figure12c.pdf

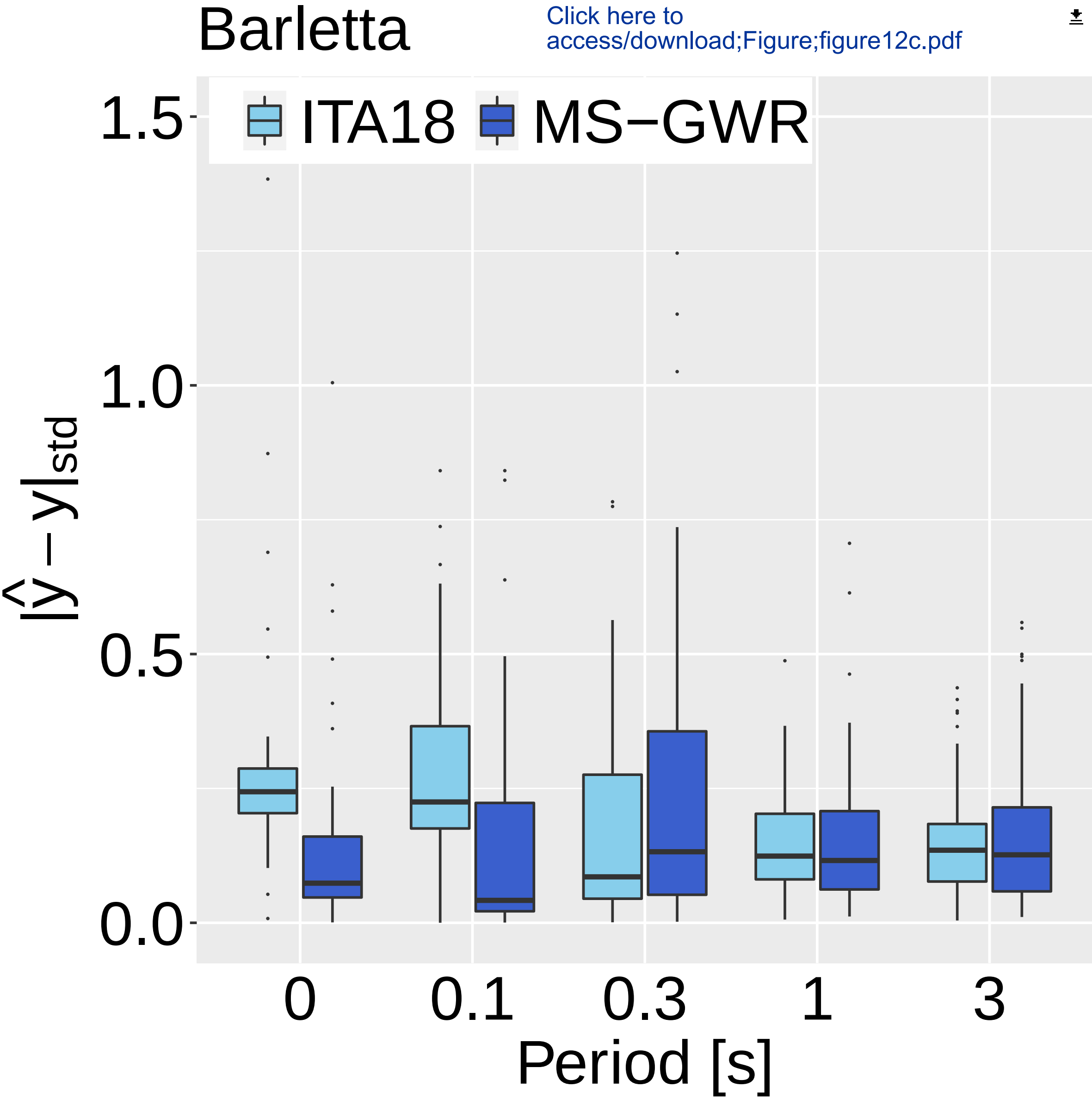

Click here to access/download;Figure;figure12d.pdf

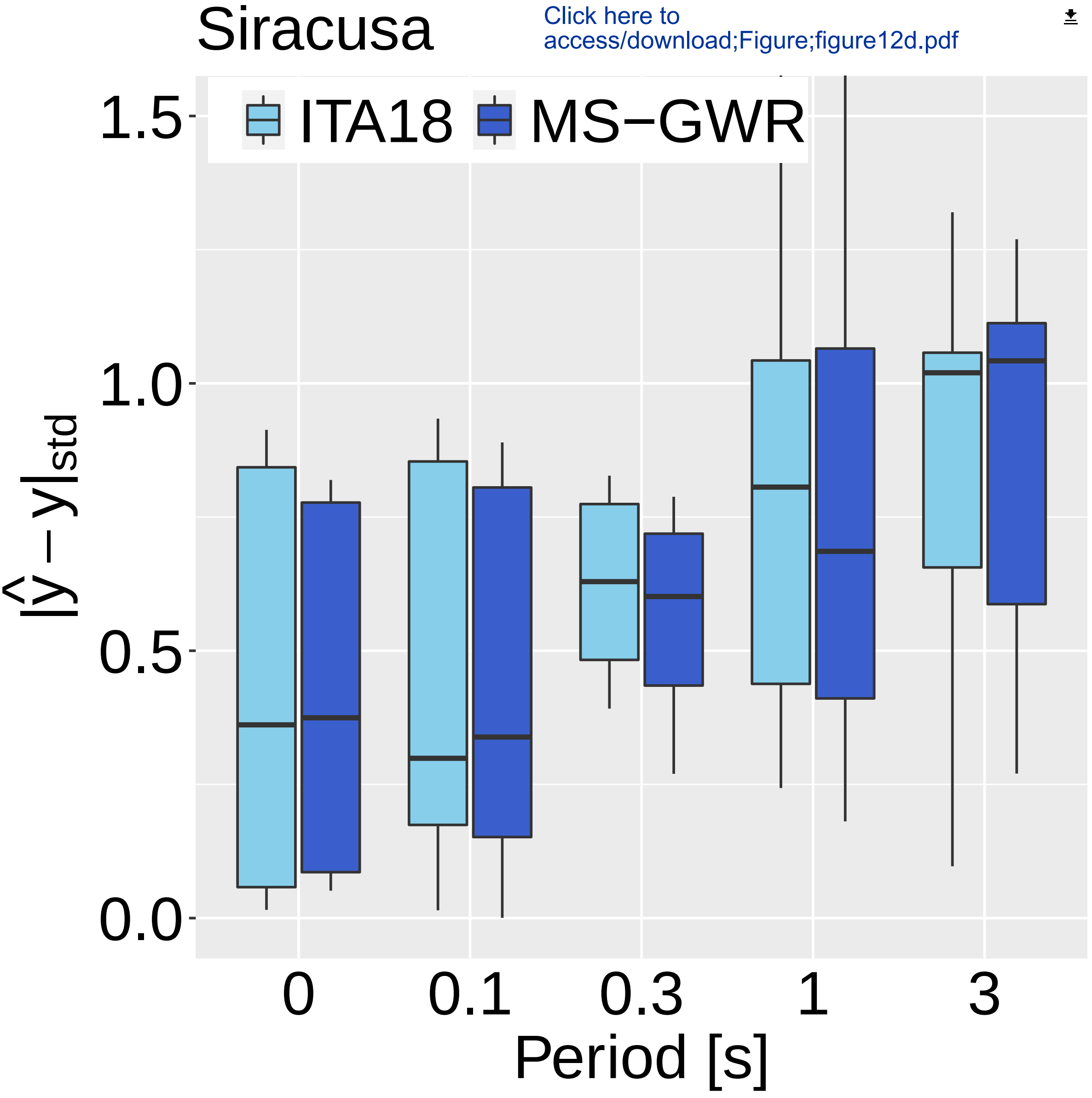

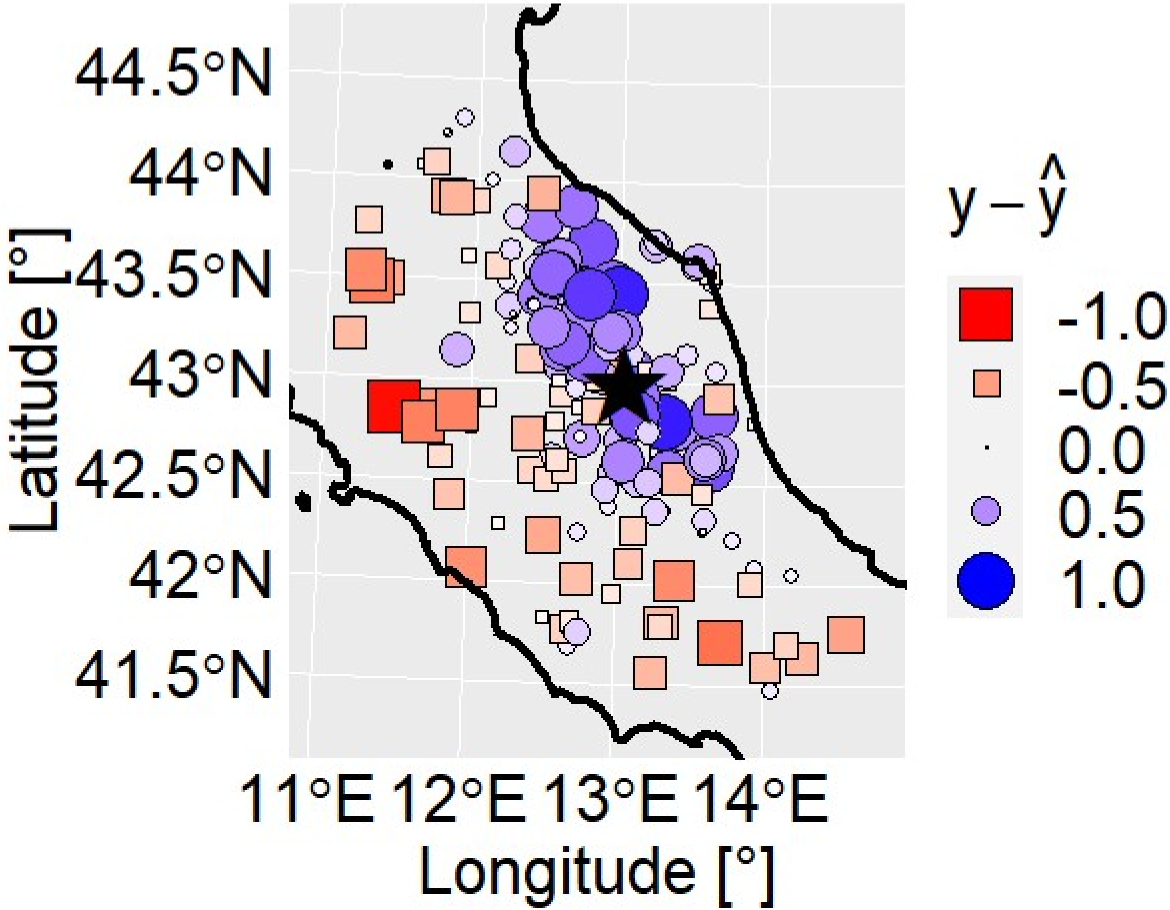
44.5°N
44°N
43.5°N
43°N
42.5°N
42°N
41.5°N
Latitude [°]
11°E 12°E 13°E 14°E
Longitude [°]
$y - \hat{y}$
-1.0
-0.5
0.0
0.5
1.0

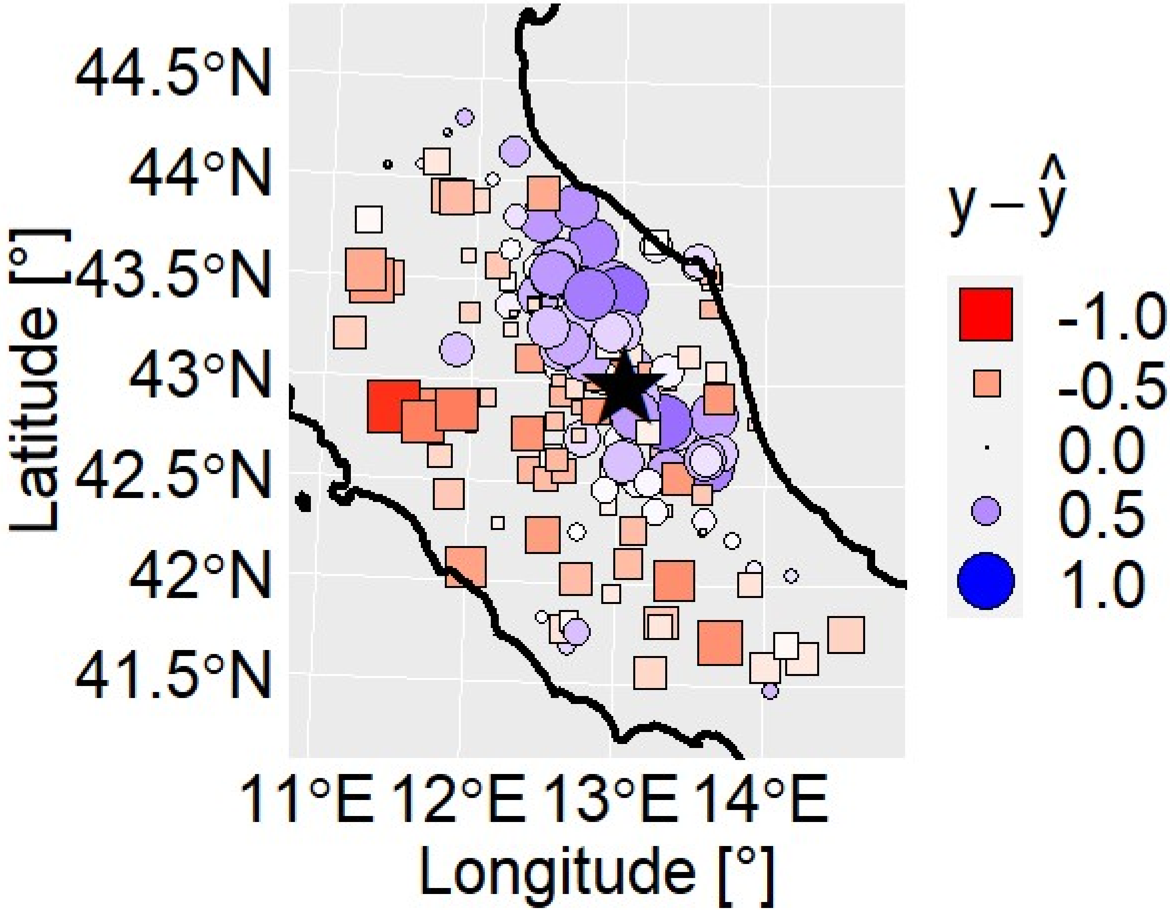

44.5°N
44°N
43.5°N
43°N
42.5°N
42°N
41.5°N
Latitude [°]
11°E 12°E 13°E 14°E
Longitude [°]
$y - \hat{y}$
-1.0
-0.5
0.0
0.5
1.0

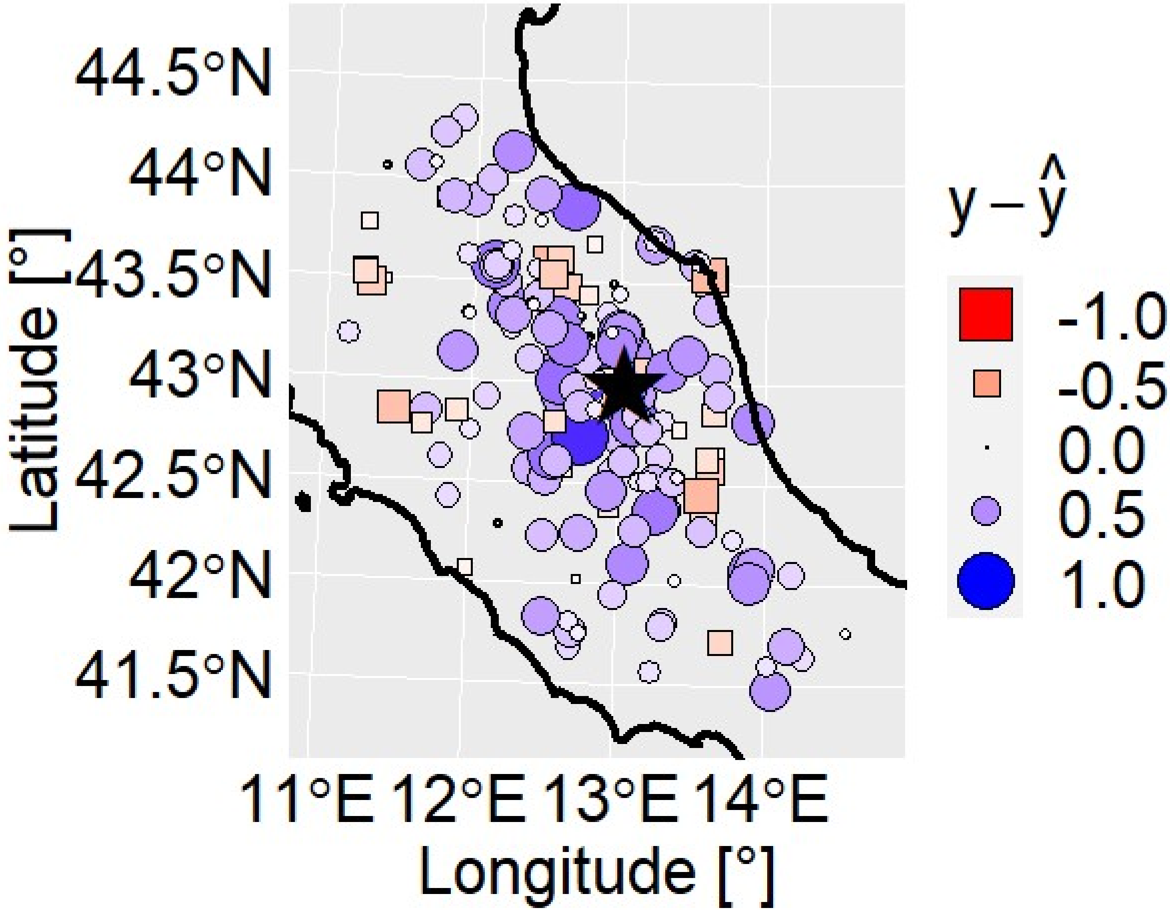

44.5°N
44°N
43.5°N
43°N
42.5°N
42°N
41.5°N
Latitude [°]
11°E
12°E
13°E
14°E
Longitude [°]
$y - \hat{y}$
-1.0
-0.5
0.0
0.5
1.0

Click here to access/download;Figure;figure13d.pdf

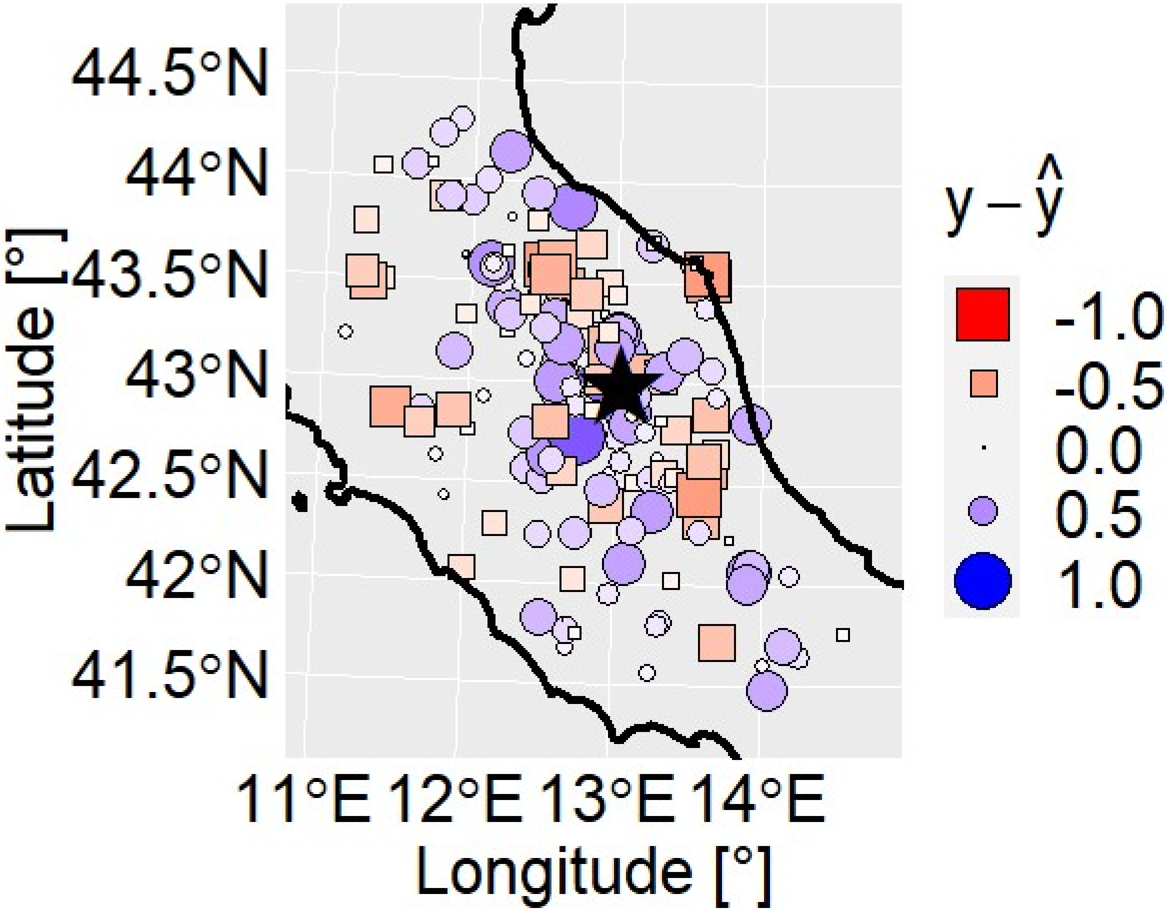

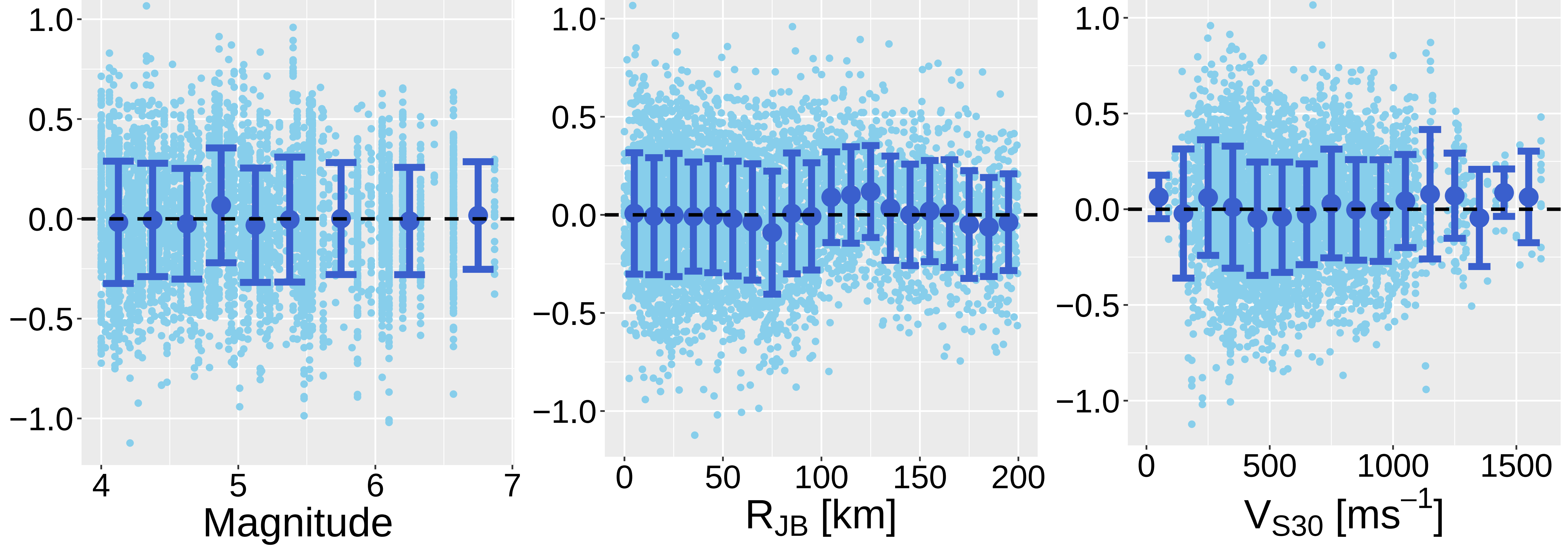
1.0
0.5
0.0
−0.5
−1.0
4
5
6
7
Magnitude
0
50
100
150
200
R_JB [km]
0
500
1000
1500
V_S30 [ms^−1]

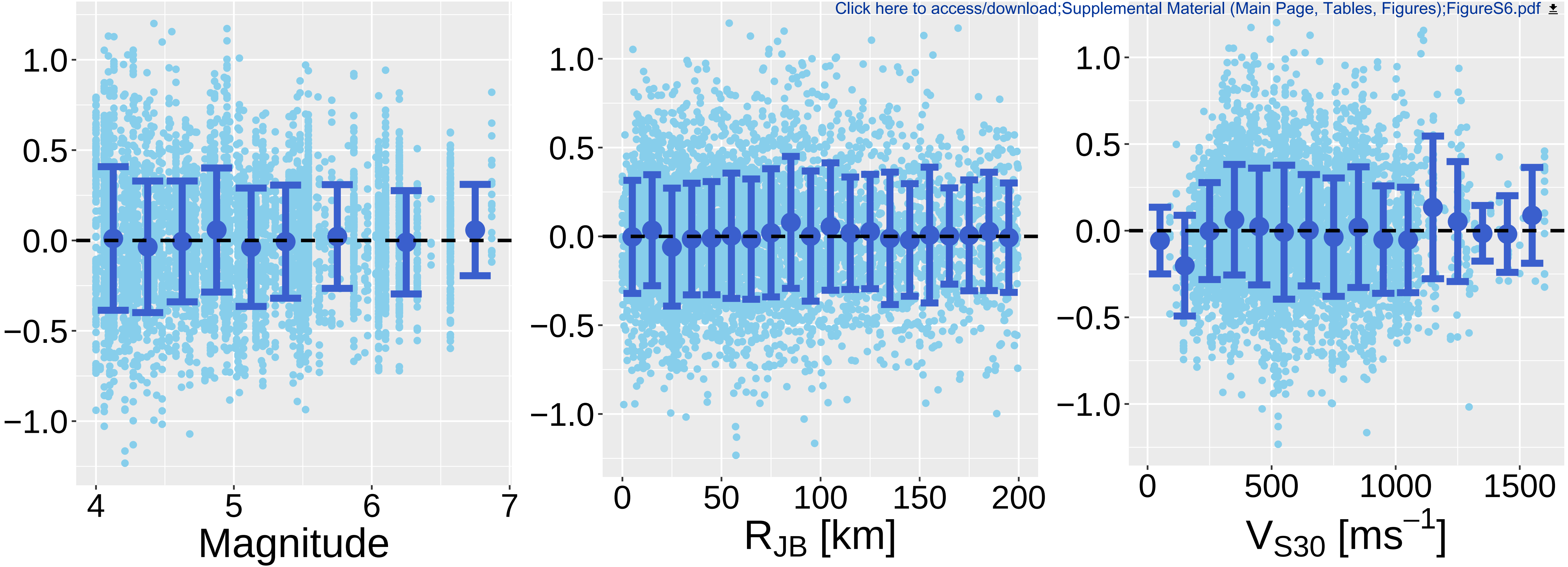
1.0
0.5
0.0
−0.5
−1.0
4
5
6
7
Magnitude
0
50
100
150
200
R_{JB} [km]
0
500
1000
1500
V_{S30} [ms^{-1}]

Click here to access/download

Supplemental Material (All Other Files, i.e. Movie, Zip, tar, csv)

TableS1.csv

Click here to access/download
Supplemental Material (All Other Files, i.e. Movie, Zip, tar, csv)
TableS2.csv

Click here to access/download
Supplemental Material (All Other Files, i.e. Movie, Zip, tar, csv)
TableS3.csv

Click here to access/download
Supplemental Material (All Other Files, i.e. Movie, Zip, tar, csv)
TableS4.csv